Huygens Close-out activities

Final technical report

Issue 2.1 - 15 June 2020

ESA Contract No. 4000121841/17/ES/JD with CNRS-LPC2E

LAB-REA-EER-CT-028-LPC2E

Authors :

Jean-Pierre LEBRETON (CNRS Orléans, LPC2E)

Annie LEROY (University of Orleans, Lab. PRISME and Ecole de l'Air et de l'Espace, Salon-de-provence Air)

Summary

Huygens, the ESA-provided element of the Cassini-Huygens mission, is an atmospheric probe that descended under parachute through the atmosphere and landed on the surface of Titan, one of the several natural satellites of Saturn, on January 14th, 2005. The goal of the mission is to study the physical properties and chemical composition of the atmosphere and the surface of Titan. The bottom of the probe was equipped with a set of vanes to control its spin profile (magnitude and direction) under parachute, in the same direction as the one imparted at release from the Orbiter, namely an anti-clockwise -positive- spin direction as seen in the separation velocity direction. Although the probe was released from its carrier Cassini with the correct spin direction, the spin rate started to decrease and eventually reversed (clockwise –negative- spin direction as seen in the velocity direction) during the descent (Lebreton, 2005) (Pérez-Ayucar, et al. 2005). The probe spin was controlled by an overall torque of the opposite sign to the one provided by the vanes. It should also be noted that the Huygens drop-test model (SM2) that was released at an altitude of 35 km from a stratospheric balloon above Kiruna in 1995 (Jäkel, et al. 1996) also spun under parachute in a direction contrary to the expected one. This SM2 behaviour, which went unnoticed during the performance evaluation of the flight data, was only found when a comparative study of the performances of the flight probe and of the SM2 drop test was undertaken in early 2005 (Sarlette, et al. 2005). Post-flight engineering evaluation of the anomalous spin investigated a couple of reasons for the reversed spin, but were not conclusive. The further evaluation of the spin behavior of both the flight probe and of the SM2 was one of the subjects of an industrial study led by Vorticity carried out in 2014-2015 (Ltd VORTICITY 2015). The study concluded that the vanes torque was not strong enough to control the spin, and hypothesized that the spin profile of the flight probe could be explained by the fact that one of the two HASI instrument booms did not deploy during the whole descent. No definitive explanation was reached as to the reasons for the SM2 spin anomaly. The study recommended that further studies be made to ascertain the reasons for the reversed spin profile for both vehicles.

The present report deals with results obtained in the framework of the Huygens close-out activities under an ESA Contract with CNRS No. 4000121841/17/ES/JD, a 2-year study, that was started in October 2017, in order to provide new insights into this spin anomaly. The Huygens probe is composed of a main body with numerous fixed appendages, and two deployable booms (the HASI instrument booms), all mounted on its external circumference. As a result of its shape, the Huygens probe generates separated flows over a substantial part of its surface, and from the point of view of aerodynamics, it is therefore considered as a bluff body because, over a wide range of Reynolds numbers, the drag is dominated by the pressure losses in the wake. The larger the wake, the smaller is the pressure recovery and the greater the pressure drag. It became clear that these different appendages and protuberances can interfere with the dynamics of the rotational movement around the probe's axis. The main objective of the work, the subject of this report, was therefore to provide additional data aiming at characterizing the individual torques applied by the spin vanes, by each of the fixed appendages, and the ones applied by each of the two HASI instrument booms in different deployment configurations. The work mainly relied on the testing of a mock-up of the Huygens probe in a subsonic wind tunnel, which could be equipped with different configurations of the fixed appendages and of the booms in different deployment states. It consisted in characterizing the aerodynamic properties of the vanes, of each appendage individually, and of different combinations of them when mounted on the probe mock-up. We also studied the effect of the Angle of Attack in the range ± 15°with the DISR camera head in 4 difference azimuthal positions. These additional data, together with scientific measurements, should make possible to inform the deployment scenario of the booms and to propose new possible scenarii of the spin anomaly. This is the subject of an on-going study that will follow-up after the closure of the present contract.

Two research laboratories were involved: the *Laboratoire de Physique et Chimie de l'Environnement et de l'Espace* (LPC2E, CNRS-University of Orléans) and the Laboratory *Pluridisciplinaire de Recherche en Ingénierie des Systèmes, Mécaniques et Energétiques* (PRISME) of the University of Orléans. The work was implemented as part of academic projects. Students in master courses were recruited, mainly coming from POLYTECH ORLEANS, the engineering school in which PRISME is located. They were interns at the PRISME laboratory to conduct the work. The 2-year study started formally in November 2017. Four series of wind tunnel tests campaigns were carried out in the frame of the contract (Feb 2018, May-July 2018, Feb 2019, May-July 2019). All wind-tunnel test campaigns were carried out in the subsonic wind tunnel of PRISME Laboratory at the University of Orléans. In addition to experimental work, an analytical modeling tool was developed that was intended to model the spin history during the whole descent of both the Flight probe and the SM2. The

tool parameters were adjusted to match the experimental results acquired under conditions corresponding to the Huygens flight parameters under the stabilizer chute for one set of conditions in the descent (50-60 km altitude, descent speed 50-60 m/s, spin rate about 5-10 rpm). The development of the modeling tool in the framework of internships proved to be more complex than anticipated and could not be fully validated within the frame of the contract.

We summarize all the tests performed and the main results obtained. The external environment of Huygens and its descent speed profile varied considerably during the whole descent in Titan's atmosphere. It is important to note that all the wind tunnel tests could only be carried out under a narrow range of representative conditions of the Huygens descent.

This report provides a description of all tests carried out during the two campaigns and their detailed analysis. The torque provided by the vanes alone was characterized for different vane angles. We covered a range of angles (0 to 6°) that encompassed the vane angle of the SM2 (2.2°) of the flight probe (2.8°) and to validate the measurements. It is confirmed that the vanes provided a positive torque as per the design. Our wind test results clearly demonstrated that the two sets of the main fixed appendages, the SEPS and the Radar Altimeter Antennae, produce a torque opposite to the one produced by the vanes. The negative effect of the appendages is augmented by the fact that the gas flow around them is deviated by the vanes, hence enhancing their negative effect that resulted in an overall negative torque, at least for the conditions tested in the wind tunnel. The effect of the HASI booms in three different configurations (stowed, deployed, half-deployed) were investigated. As per design, one boom produces a positive torque, while the other one produces a negative torque, but of the same magnitude. The torque produced by each of the boom (one positive, one negative) is of a magnitude slightly higher that the one created by the vanes. The fully deployed booms were expected to be neutral in terms of torque. The amplitude of the negative torque created by the fixed appendages (enhanced by the flow deviation by vanes) turned out to be larger than the torque created by the vanes.

A first attempt was made to compare the results obtained in the PRISME Wind Tunnel and those obtained during the previous industry-led study that included tests in the Von Karman Institute Wind Tunnel facility. We found it quite difficult to do a proper comparison, as some of the tests were carried out in the VKI facility with a non-flight SEPS configuration. None of the Vorticity tests fully replicated the flight configuration of neither the SM2, nor of the flight probe.

It is clear that the fixed appendages created a torque opposite to the one created by the vanes. This may explain the negative spin experienced by the SM2, which was not equipped with the HASI deployable booms. The fixed appendages also contributed to the negative torque during the descent on Titan. However, we cannot conclude with certainty on the integrated effects of the HASI booms, as their deployment history is uncertain. However, some experimental evidence exists that the HASI boom configuration changed after the stabilizer chute deployed. Work was initiated during the contract to cross-correlate the inference of the boom deploy state from the HASI measurements and other measurements on board the probe and their aerodynamic effects during the descent. This work is being pursued following the end of the contract (R. Lorenz, private communication, 2020).

Although the objectives of the contract have been fulfilled, further work should be pursued in order to validate our findings and to further investigate the deployment history of the HASI booms. Although it seems clear that one HASI boom did not deploy nominally at the beginning of the descent, the study is not conclusive on the issue of boom configuration changes later in the descent. The Huygens probe spin was clearly controlled by subtle effects that were not easy to model, neither easy to test. We believe that a proper quantitative validation of the reasons why the two probes (SM2 and flight probe) spun in the reversed direction would require a dynamic wind tunnel test, that would be done with a mock-up whose size would be adapted to the wind tunnel capability, with both the SM2 configuration (2.2° vanes, 3 SEPS, 4 Radar Altimeter antennas, representative cabling, no HASI booms, representative SEPS cables), and the flight probe configuration (2.8° vanes, 3 SEPS, 4 radar altimeter antennae, two reconfigurable HASI booms, proper representation of the DISR camera, representative external SEPS cables). A potential facility to perform such tests has been identified at ONERA, Lille, France, but no quotation has been requested.

Some results of this work were presented in oral communications (Leroy, Lebreton, et al. 2018) (Couche, et al., 2019) and posters (Thébault, et al. 2018) (Leroy, Lebreton, et al. 2019). A publication is under preparation for submission in the peer review literature (A. Leroy et al., to be submitted in 2020).

Table of Contents

Appendices

Table of illustrations

Acronyms and Abbreviations

a-c/w	anti-clockwise
ACP	Aerosol Collector and Pyrolyzer
B1,B2	HASI deployable booms
CAD	Computer Aided Design
CFD	Computational Fluid Dynamics
CNRS	Centre National de la Recherche Scientifique
c/w	clockwise
DISR	Descent Imager and Spectral Radiometer
ESA	European Space Agency
GCMS	Gas Chromatograph and Mass spectrometer
HASI	Huygens Atmospheric Structure Instrument
NASA	National Aeronautics and Space Administration
PIV	Particle Imaging Velocimetry
RAA	Radar Altimeter Antennae
rpm	Rotation per minutes
SEPS	Separation mechanisms
SM2	Special Model 2 designed for drop tests
SSP	Surface Science Package
WP	Workpackages
WT	Wind Tunnel

1 Introduction

Huygens, the ESA-provided element of the Cassini-Huygens mission, is an atmospheric probe that descended under parachute through the atmosphere and landed on the surface of Titan, one of the several natural satellites of Saturn, on January 14th, 2005. The goal of the mission was to study the physical properties and chemical composition of the atmosphere and the surface of Titan. The bottom of the probe descent module was equipped with a set of vanes to control its spin profile (magnitude and direction) under parachute, in the same direction as the one imparted at release from the Orbiter, namely an anti-clockwise- we refer to it as positive in this report- spin direction as seen in the velocity direction. The probe was released from its carrier Cassini with the correct spin direction (anticlockwise -positive- as seen in the direction of the separation velocity) and a spin amplitude of about 7.5 rpm. The spin rate kept constant during the 3-week coast to Titan and during the 3-mn entry. The spin rate decreased more rapidly than expected at the start of the descent under the main parachute and eventually reversed 10 min later (clockwise -negative- spin direction as seen in the speed direction) still under the main parachute (Lebreton, 2005) (Pérez-Ayucar, et al. 2005). For the rest of the last 5 min under the main parachute, and under the stabilizer down to the surface, the spin kept reversed. It turned out that the probe spin was controlled by an overall torque of the opposite sign to the one provided by the vanes. It should also be noted that the Huygens drop-test model (SM2) that was released at an altitude of 35 km from a stratospheric balloon above Kiruna in 1995 (Jäkel, et al. 1996) also spun under parachute in a direction contrary to the expected one. This SM2 behaviour, which went unnoticed during the performance evaluation of the test data, was only found when a comparative study of the performances of the flight probe and of the SM2 drop test was undertaken in early 2005 (Sarlette, et al. 2005). The external devices[1] accommodated on the rim of the probe contributed to the overall spin torque which was opposite to the one induced by the vanes, both for the Huygens probe on Titan, but also on the SM2. Studies undertaken by the Huygens industrial team during the post-flight evaluation of the Huygens probe performances explored several options to explain the spin anomaly, but did not come to a conclusion (Tran et al, EADS Report, HUY.EADS.MIS.TN.0006, 2005). The findings of EADS are summarized here: *"The roll rate evolution controlled by 36 spin vanes has been found to have worked improperly; spin inversion (from positive to negative) has been identified nearly 800 s after EIP (10 min under the main parachute). Currently, no firm explanation has been found. Additional tests on a more representative DM model would be required"*. 9 years later, such a study was contracted out by ESA to Industry. The evaluation of the spin behavior of both the flight probe and of the SM2 was one of the subjects of an industrial study led by Vorticity Ltd carried out in 2014-2015 (Ltd VORTICITY, 2015). During that study, wind tunnel tests were performed with the SM2 equipped with 2.2° vanes[2], the three SEPS, but no Radar Altimeter Antennae, and different configurations of the HASI booms (OFF, ON closed, ON Open). The study concluded that the vanes torque was not strong enough to control the spin, and showed that the SEPS induced a torque opposite to the one induced by the vanes. This confirmed the results of a test that was carried out in the PRISME wind tunnel facility in 2013 (unpublished results), (see appendix 5). But the study suggested that the spin profile of the flight probe could be explained by the fact that one of the two HASI instrument booms did not deploy during the whole descent. No definitive conclusion was reached as to the reason for the SM2 spin anomaly. The study recommended that further more detailed studies be made to ascertain the reasons for the reversed spin profile for both vehicles.

The present report deals with results obtained in the framework of the Huygens close-out activities under an ESA Contract with CNRS No. 4000121841/17/ES/JD, a 2-year study that was undertaken in order to provide new insights into this spin anomaly and that was started in October 2017. Two research laboratories were involved: the *Laboratoire de Physique et Chimie de l'Environnement et de l'Espace* (LPC2E, CNRS-University of Orléans-CNES, prime contractor) and the Laboratory *Pluridisciplinaire de Recherche en Ingénierie des Systèmes, Mécaniques et Energétiques* (PRISME, sub-contractor) of the University of Orléans. The work was implemented as part of Academic projects. Students in master courses were recruited as interns at the laboratory to conduct the experimental work and to develop a simulation model. They were mainly coming from Polytech Orléans, the engineering school in which the PRISME laboratory where its Wind Tunnel facility

[1] List of all external devices : SEPS (3x), Radar Altimeter Antennae (4x), HASI Pressure and Temperature Probe (1x), Electrostatic Dischargers (3x), DISR camera (1x), HASI Deployable booms (2x).
[2] The inclination of the SM2 vanes was 2.2°, while it was 2.8° for the Huygens flight probe.

is located, but also from the Grenoble University, from the Orsay University, and late during the contract period, from the Ecole de l'Air et de l'Espace, Salon De Provence.

The Huygens probe descent module is composed of a main body with numerous (12) fixed appendages, and two deployable booms (the HASI instrument booms), all mounted on its external circumference. As a result of its shape, the Huygens probe generates separated flows over a substantial part of its surface, and from the point of view of aerodynamics, it is therefore considered as a bluff body, because over a wide range of Reynolds numbers, the drag is dominated by the pressure losses in the wake. Several appendages (SEPS, RAA, TPP, HASI booms in open configuration) were in the external flow, while the DISR camera head, and the HASI booms in closed configuration, were in the separated wake flow.

The different appendages and protuberances interfere with the aerodynamics of the rotational movement around the probe's axis. The main objectives of the work, the subject of this report, were therefore to characterize the aerodynamic properties of a Huygens mock-up and more specifically, to quantify the individual torque applied by the spin vanes, by each of the fixed appendages, and the ones applied by each of the two instrument booms in different deployment configurations. Thus, the work mainly relied on testing in a subsonic wind tunnel of a 1:3 scale mock-up of the Huygens probe descent module, which could be equipped with different configurations of the various fixed appendages and of the HASI booms in different deployed configurations. The effect of the Angle of Attack in the range ± 15° with the DISR camera head in 4 different azimuthal positions was also assessed. All wind-tunnel test campaigns were carried out in the subsonic wind tunnel of the PRISME Laboratory at the University of Orléans. During the second year of the project, in addition to experimental work, a modeling tool was developed that would allow to model the spin history during the whole descent of both the Flight probe and the SM2. The tool parameters were adjusted to match the experimental results acquired under conditions corresponding to the Huygens flight parameters under the stabilizer chute for one set of conditions in the descent (50-60 km altitude, descent speed 50-60 m/s, spin rate about 5-10 rpm). The development of the modeling tool proved to be more complex than anticipated and could not be fully validated within the frame of the contract. At the very end of the contract, a simplified tool was developed by an other group of students (from Ecole de l'Air de Salon de Provence). This work evaluated the limitations of previous spin models developed by industry and developed its own model that provided a clear comparison between all model outputs for a single set of flight conditions (altitude of about 60 km in Titan's atmosphere).

The work was divided in two workpackages (WP1 and WP2).

WP1: The first workpackage was dedicated to perform wind-tunnel tests for the aerodynamic characterisation of the Huygens probe descent module 1:3 mock-up. It has to be noted that the design of this mock-up was conducted in May-July 2017 prior to the start of the contract itself, in order to benefit of the availability of a summer student knowledgeable in CAD design. The mock-up could be equipped with the vanes, the different appendages and the deployable HASI booms. The vanes were designed to be removable in order to study different mock-up configurations. The aerodynamic characterisation was achieved by aerodynamic load measurements in static configuration for the mock-up with different appendage combinations for different flow velocities and angles of attack.

→ Internships:

- *Design of the mock-up (Analysis of the possible test conditions, CAD model, 3D-printed appendages)*, Lucas METHIVIER from the University of Grenoble, (May-July 2017). Work performed prior to the contract Kick-Off.
- *Aerodynamic characterisation of the model with and without appendages at zero angle of attack*, Guillaume THEBAULT and Julien SIMIER (from POLYTECH Orléans engineering school (January-March 2018),
- *Aerodynamic characterisation of the model with and without appendages at different angles of attack*, Trong Binh VU from the University of Orsay (may-july 2018),

WP2: We found out during the WP1 activities, that the drop tests initially envisaged during the proposal would not be competitive compared to the tests carried out in the *Lucien Malavard* wind tunnel facility. Such test options were not pursued. The goal of this second workpackage was thus to go into the aerodynamic properties of the probe in depth by carrying out complementary tests in wind tunnel and by developing a simplified rotational dynamic model to help understand the probe behavior. Following the mid-term review that took place in November 2018, the mock-up was improved to be more representative of the flight probe and a new instrument (a sensitive torque meter) was installed for the work to be done. It also included a series of Particle Imaging Velocity (PIV) measurements to visualize the gas flow topology around the vanes and the appendages.

WP2 tests included:

- Tests of the new vane mock-up with four different inclinations of the vanes (0.0°, 2.2°, 2.8°, 6.8°).

- Fabrication of an intermediate position interface for the HASI booms (in addition to open and closed), and tests of its influence on the spin

- Complementary tests of the vanes mock-up with different configurations of the appendages (SEPS, RAA, DISR, TPP, SEPS cables, intermediate HASI boom positions, improved mock-up of the HASI booms) under different orientations with respect to the wind flow (Angle of Attack)

- PIV (Particle Imagery Velocimetry) measurements for selected tests in order to investigate the flow characteristics close to the vanes and the appendages

→ **Internships:**

- *Further aerodynamic characterisation of the 1/3rd mock-up of the ESA HUYGENS probe and its appendages*, Armand BERAUD, Simon COUCHE and César DE TIENDA (from POLYTECH Orléans engineering school (January-March 2019),
- *Development of a dynamic simulation for the study of the ESA HUYGENS probe*, Léo KOVACS and Rémy JOCHMANS (from POLYTECH Orléans engineering school (January-February 2019),
- *Aerodynamic study of a HUYGENS probe mock-up by PIV testing*, Maxime BOYER (from POLYTECH Orléans engineering school (April-June 2019),
- *Investigations sur l'anomalie de rotation détectée lors de la descente sous parachute de la sonde Huygens sur Titan,* Thomas MORDEC and Guillaume SERMET (from French Air force Academy), academic project (November-December 2019)[3].

The workpackage outputs are a mid-term technical report (Leroy et Lebreton 2018), the present report, a database containing the aerodynamic characterization by load balance, torquemeter and PIV measurements of many different configurations representing more than 300 tests. CAD models, pictures and video footages of the wind tunnel campaign are also provided, as well as the software of the rotational dynamic theoretical model implemented to help the understanding of the probe behavior. It also includes the student reports, but it is stressed that those reports, of academic nature, are included for completeness but should not be widely distributed as they represent the original report of the students which was not fully validated for a large dissemination beyond this project.

[3] This work was not initially foreseen as part of the contract. Report in French.

2 The Huygens mission

2.1 Mission background

The Cassini-Huygens mission is an international collaboration between the National Aeronautics and Space Administration (NASA), the European Space Agency (ESA) and the Italian Space Agency (ASI). The objective of the mission was to make an extensive survey of Saturn system including its natural satellites, among them Titan.

The NASA's Cassini orbiter, with the ESA's Huygens probe attached, was launched on October 15, 1997 heading to Saturn and its natural satellites. After a 7-year space travel, the mission reached Saturn's orbit and on December 25, 2004, Huygens was released from Cassini towards Titan, the largest satellite of Saturn. Huygens reached the surface of Titan on January 14, 2005, after a 2.5h descent under parachute, allowing the collection of a rich set of data and making it the farthest landing of a man-made object in the Solar system.

Following the Huygens mission, Cassini continued to orbit Saturn and to explore its system, until September 15, 2017, when it was deviated and burned into Saturn's atmosphere to prevent the contamination of one of the 62 known (at that time) satellites of the planet. This makes a total duration of the mission in flight of almost 20 years.

2.2 The Huygens probe

While Cassini was designed to orbit Saturn and its several satellites, the goal of Huygens was to perform measurements about the atmosphere and the surface of Titan during its entry (inside the heat shield) and its descent under parachute. The Huygens probe descent module was a 1.3 meter and 319 kilograms circular body with many devices mounted on the circumference of the probe, as shown in Figure 2.1.

The main appendages to consider as geometrical protuberances for this study are:

- Radar altimeter antennae (RAA) – x 4
- Heat-shield and back-cover separation mechanisms, or separation subsystems (SEPS) – x 3
- HASI stud with pressure and temperature sensors (Temperature and Pressure Probe, TPP) x1
- HASI (Huygens Atmospheric Structure Instrument) deployable booms – x 2
- DISR camera head - x1
- Electrostatic dischargers - x3

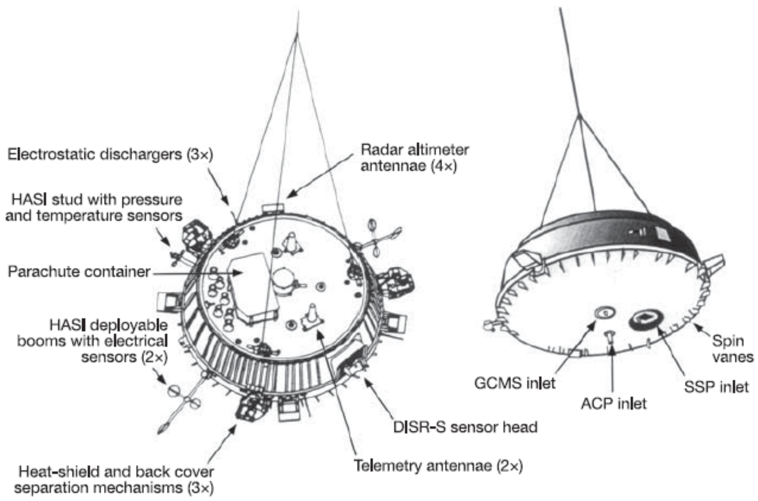

Figure 2.1: Two different views of the Huygens probe (top view on the left and bottom view on the right). Note that several external devices (including the HASI booms and the SEPS) are not represented in the figure on the right.

The three instrument apertures (GCMS, ACP, SSP) on the bottom of the foredome were also designed on the mock-up for completeness, but their effects on the drag coefficient and on the spin were not studied.

Because of the long period elapsed between the mission and this project, at the beginning of the work, there were some uncertainties about a few design probe features, notably the respective position of the two deployable HASI booms and on the angle of the vanes on the foredome of the probe.

For the HASI booms, there was some uncertainty about their accommodation, that came from a difference between the design drawing and the CAD (Computer Aided Design) file provided by ESA. The electrodes of the HASI booms are a plain disc and a ring mounted at the tips of the middle cross and a ring at the tip of the boom. In the design drawings (Figure 2.2 (a)), the disc is oriented downward while the ring is oriented upward, but the CAD (Figure 2.2 (b)) shows the opposite. An analysis of the pre-flight pictures of Huygens allowed us to determine that the flight configuration on Titan was the one stated by the drawings. A special attention has been made to this point during the wind-tunnel campaign.

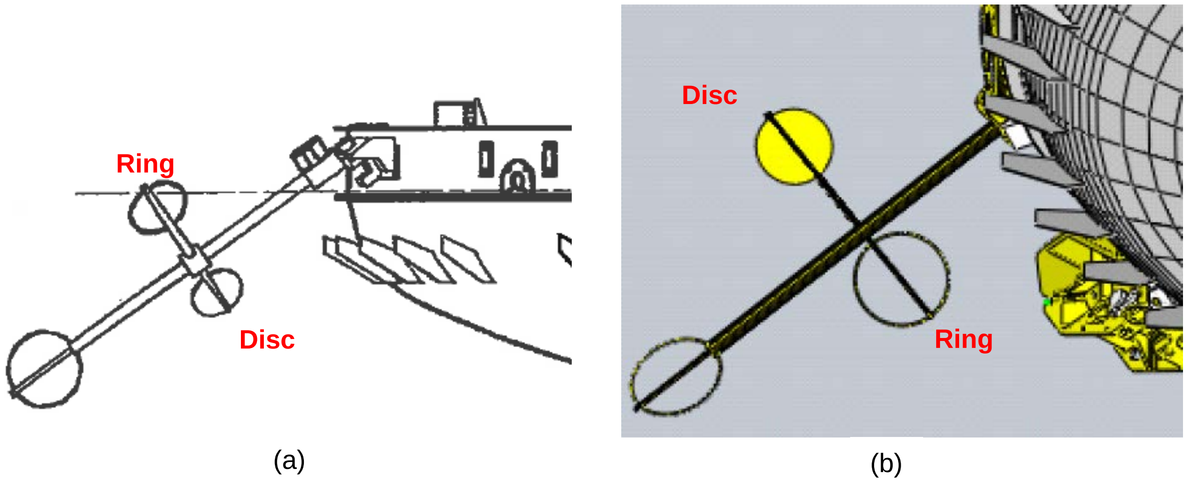

Figure 2.2: Design drawing of the HASI booms position (a) and CAD of HASI booms position (b)

During the Huygens design phase, a specific focus was placed on the geometry of the vanes because they were designed to be predominant in the spin control. They were initially set to an inclination of 2.2 degrees, but after a balloon test conducted in the Earth's atmosphere in 1995 (SM2 test, (Jäkel, et al. 1996)), it has been decided to set the inclination to 2.8°[4] for the flight probe in order to better match the amplitude of the spin near the surface (DISR requirement, which was < 15 rpm above 10 km altitude and between 1 and 3 rpm below 10 km). However, the SM2 data evaluation omitted to note that the spin was in the reversed direction (AEROSPATIALE 1996). (EADS report 2005). Hence the post-flight analysis of the SM2 data did not take full account of all torques that controlled its spin profile.

2.3 Mission sequence and spin

In order to give Huygens stability during its cruise to Titan and the correct initial speed magnitude and direction at the start of the parachute deployment sequence, when Cassini launched Huygens towards Titan, it gave the probe a spin impulse about 7.5 rotations per minute (rpm) in the anti-clockwise direction (when viewed from the orbiter). Figure 2.3 illustrates the definition of the initial and reversed spin compared to anti-clockwise (a-c/w) and clockwise (c/w) rotation respectively.

[4] The exact value of the spin vane inclination is still somewhat uncertain. An inclination angle of 3,3° is mentioned in the EADS report. A value of 2.9° is mentioned in some documents.

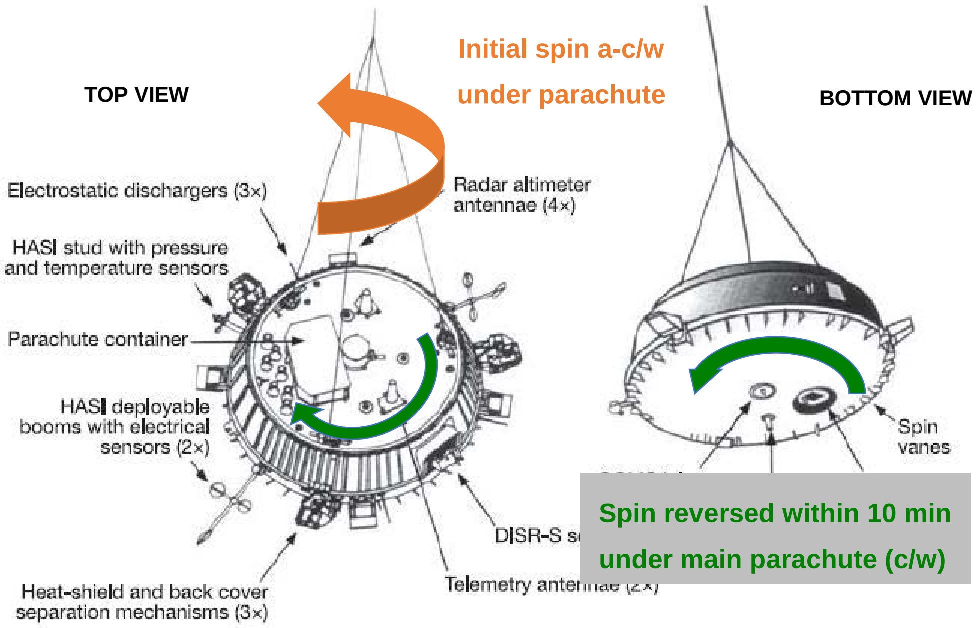

Figure 2.3: Spin direction convention (a-c/w : anti clockwise ; c/w : clockwise)

A post-mission study of the flight parameters showed that the rotation behavior under parachute was not the same as predicted before the mission (see Figure 2.4), (Lebreton 2005). In fact, as soon as the probe was under parachute, the spin rate decreased rapidly and changed from anticlockwise direction to clockwise direction after about 10 minutes of flight. Despite this change in the spin direction, the mission was successfully completed without significant impact on the science return.

However, the understanding of this unexpected spin profile and the reason for it is important for at least the following two issues: i) to explain what controlled the spin profile in addition to the spin vanes, as a lesson to be learned for future atmospheric probe missions that would require a controlled spin profile; ii) to contribute to the understanding of the HASI boom deployment history as it pertains to the interpretation of the HASI E-field measurements in Titan atmosphere and on the surface after landing. As part of the previous industrial study conducted by Vorticity under ESA contract (Ltd VORTICITY 2015), it was concluded that one cause of the reverse spin could be the fact that one of the two HASI deployable booms did not deploy during the whole descent. The conclusion that one boom did not fully deploy during the whole descent is, so far, not supported by the analysis of the performances of the HASI instrument, which concluded that one of the booms did not fully deploy early in the descent (under the main large parachute) but completely deployed under the stabilizer parachute for the rest of the descent (Hamelin, Béghin, et al. 2007), (Béghin, et al. 2007), (Hamelin 2012). The effect of a potential anomalous boom deployment was initially investigated in 2005 (Lorenz, 2005), but a non-nominal boom deployment hypothesis was not considered for the initial probe flight performances analysis (EADS 2005). This point is however being revisited (R. Lorenz et al., submitted, March 2020). In spite of this spin anomaly, the probe landed safely after a 2.5 hour descent through the atmosphere of Titan and continued to transmit data at least another 3 h 14 mn. The overall mission was a real success and confirmed the great interest of the exploration of Titan (Lebreton, 2005)

Several open points that would require further work were identified during the Vorticity study. It recommended studying the individual effects of each of the elements that contributed to control the spin. It is also important to understand the aerodynamic behavior of Huygens as it may pertain to the design of the future atmospheric probes that would require a controlled spin profile.

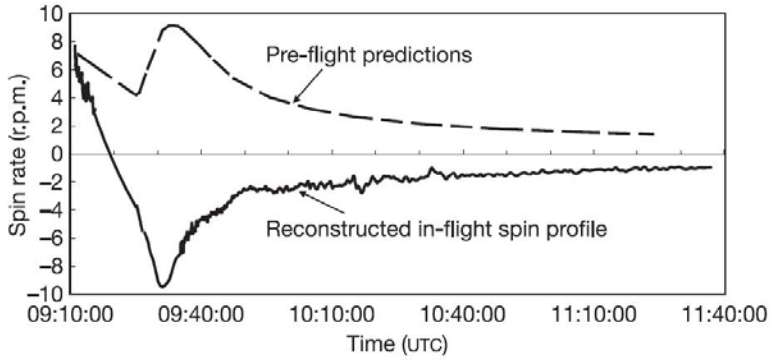

Figure 2.4: Spin rate profile as function of time (reproduced from Lebreton et al. 2005)

Looking at the spin rate profile, it appears that the real spin rate started to deviate from the pre-flight predictions at the very beginning of the descent sequence (t_0: 09:10:21). It decreased more rapidly than predicted and eventually reversed after 10 min under the main parachute. After almost one hour (at 10:10:00), the spin rate reduced and became relatively stable (although reversed) until landing on Titan's surface. The descent in Titan's atmosphere was controlled by the Huygens Descent Control Sub-System, which contained three parachutes: pilot chute, main parachute and stabilizer parachute. The pilot chute deployed immediately at Mach 1.5 at the end of the entry phase, then the main parachute was deployed to decelerate through Mach 1. After 30 seconds, the heat shield meant to protect the probe (Huygens descent module) against atmospheric friction during entry, was released and dropped underneath the probe under parachute. Figure 2.5 below shows an overview of the descent and its events, described in table 1. All deployable devices (the two HASI booms and the DISR cover) on the probe were commanded to deploy within 60 sec under the main parachute (Table 1). The good quality images confirmed that the DISR camera head was properly exposed, confirming the proper deployment of its cover. As there was no direct indicator (in the HK data) that the HASI booms had fully deployed, it relied on scientific measurements to infer their configuration after release.

Important events		
Mission time (s)	Event	Color in the figures
0	t_0 - Start of the descent sequence	
2	Main parachute deployment	
32	Heat shield separation	
50	GCMS inlet cap jettison	
62	HASI boom deployment (latest)	
66	DISR cover jettison	
90	ACP inlet cap jettison	
900	Stabilizer parachute deployment	
8870	Surface impact	

Table 1: Color coding of the events for Figure 2.5 and Figure 2.6

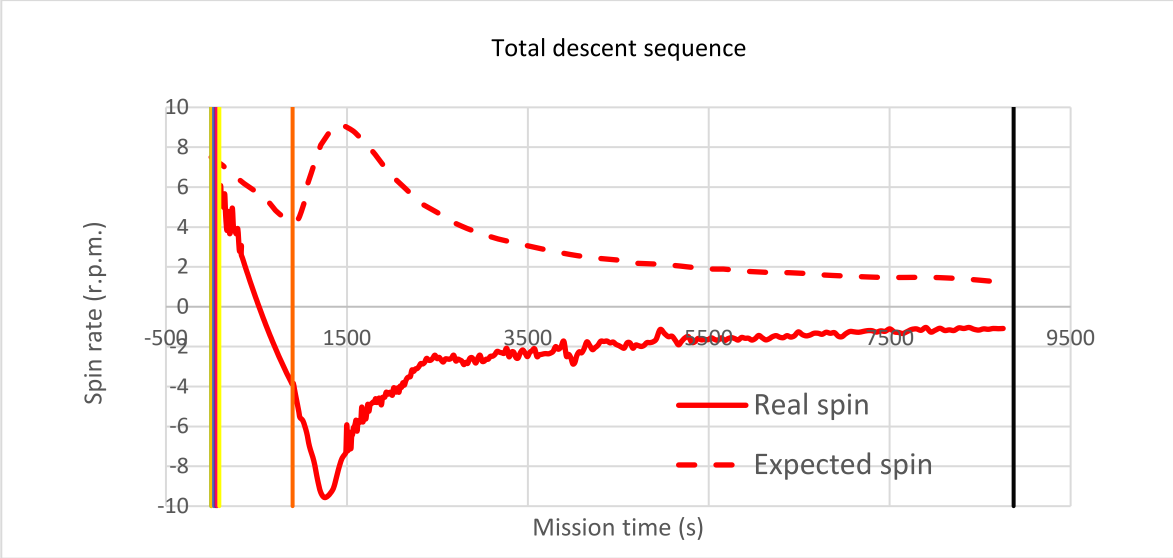

Figure 2.5: Total descent sequence with occuring events

As many of the events occured during the first 90 seconds, Figure 2.6 presents a zoom of this period to provide a better view of the probe behaviour during this mission period and confirms that the spin rate decreased more rapidly than predicted from the start of the descent under parachute.

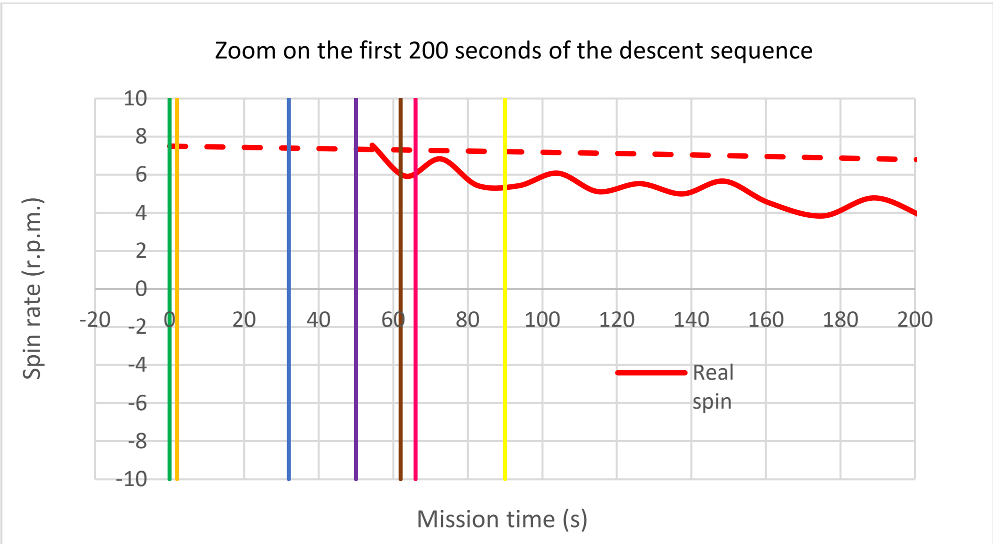

Figure 2.6: Zoom on the first 200 seconds of the descent sequence

Unfortunately, the recovered engineering (House Keeping) data set, that included the early spin information, was not complete (channel A failure, (Lebreton 2005)) and did not contain the first 50 seconds. However, information about the probe trajectory, attitude and spin, was recorded by the HASI instrument during the entry prior to, and during parachute deployment. From the engineering data alone, it is clear that the real spin rate is already varying (this is attributed to probe nutation) and following a slowly decreasing trend. The previous industrial study (Ltd VORTICITY 2015) focused on the effects of the HASI booms that did not deploy properly at the start of the descent, as was found out from the analysis of the science data. It concluded that one possible cause for the reversed spin could be the non-deployment of one of the two HASI booms during the whole descent.

3 Wind tunnel testing

3.1 Test strategy

During the development of the Huygens probe, a mock-up was tested without all the appendages during wind tunnel tests (AEROSPATIALE 1993). Therefore, the 36 spin vanes were the only main torque inducers. The vanes were designed for a specific spin rate, which was verified during the pre-flight tests. However, during the real mission, several appendages were part of the flight probe, but were not systematically included in the pre-flight tests. The test (WT17) initially foreseen with a flight-like mock-up was cancelled, mostly for cost reasons.

A full-size model of the Huygens probe (called SM2) was also tested in the Earth atmosphere in 1995. It was launched from a stratospheric balloon from Kiruna. Its main purpose was to validate the sequencing of the Descent Control Subsystem and the spin profile. Unfortunately it turned out that the SM2 data analysis focused on the spin profile, but not on the spin direction. The spin was also reversed during the SM2 flight but this was only noticed during the re-evaluation of the SM2 performances when analyzing the flight performances of the probe in Titan's atmosphere (Sarlette, et al. 2005). As a result of the evaluation of the SM2 test performance, the inclination of the vanes on the flight probe was increased from 2.2° to 2.8° in order to better fulfill the DISR spin rate requirement during the last 10 km of the descent.

Since the spin rate of Huygens during its descent was very low, we have decided to conduct only static tests for this investigation. Indeed, with a spin rate up to 10 rpm, it is reasonable to assume that friction effects caused by the rotation can be neglected in the face of more predominant geometrical effects. Hence, the mock-up was designed and mounted via a fixed mast to an aerodynamic load balance with its spin axis in a horizontal position in order to investigate on-axis induced torques due to the numerous geometrical protuberances in particular. Considering that any small geometry modification can affect the spin, it was postulated that the appendages may have played a role in the unexpected rotational behavior during the descent. The approach in our project was then to test one by one each appendage mounted on the mock-up, including each of the two HASI booms in different deployment configurations to determine their effect on the spin. Indeed, previous investigations on the subject have shown the substantial impact that the HASI booms could have on the rotational dynamics of the probe. A significant part of this work therefore focused on the HASI booms to characterize the effects they could have on the spin profile. By doing so, we intended to characterize the effect of each appendage during the descent and therefore possibly provide new insights into the causes of the spin anomaly.

During the descent on Titan, it was observed that the probe was subjected to a large pendular movement. It led us to test the mock-up at several sideslip angles (angle of attack) to characterize the behavior of the probe when it is not fully aligned with the main flow direction. This series of tests allowed us to identify a possible effect of the DISR camera head.

3.1.1 The PRISME Lucien Malavard wind tunnel and mock-up dimensions

The facility used for the test campaign is the Lucien Malavard wind tunnel, located at Polytech Orléans. It is mainly used for research purpose by the PRISME laboratory. It is a closed return wind tunnel with a closed test section as shown in Figure 3.1. The tests were performed in the main test section. The main test section is equipped with an external 6-component aerodynamic load balance installed under its floor (see Appendix 1 for more details). It was used to measure the aerodynamic loads experienced by the mock-up under the influence of a flow, whose uniformity had been previously characterized. The values measured are drag, lift, side force, rolling, yawing and pitching moments. In addition to the balance measurements, the flow velocity was measured via a Pitot tube. The measurement of the test section temperature and the atmospheric pressure was also performed to compute the air density. During WP2, a torque meter was added.

Regarding the size of the mock-up, it was chosen by taking account the characteristics of the main test section, the blockage effect condition and the force and moment measurement ranges of the aerodynamic balance (see Appendix 1). A scale of 1/3rd for manufacturing the mock-up was then chosen. The mock-up reference diameter is D = 0.452 m.

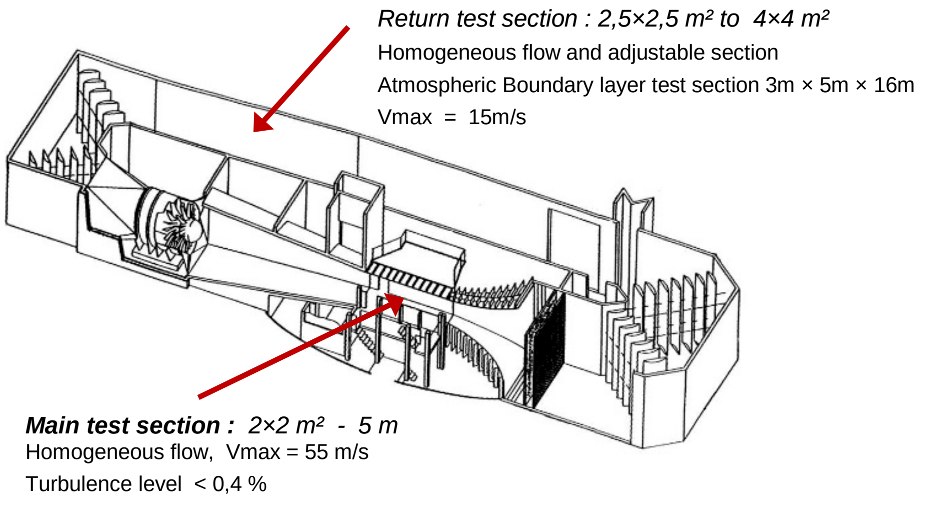

Figure 3.1: Scheme of the Lucien Malavard subsonic wind-tunnel

3.1.2 Reynolds similarity

During its descent to Titan surface, the Huygens probe experienced several variations of the environmental conditions such as viscosity and temperature. A characterization of the analogies between Titan atmosphere and the wind-tunnel conditions was studied to recreate the most appropriate probe environment during the wind tunnel tests. The Reynolds number was calculated for several altitudes of the descent, allowing the determination of the wind-tunnel speed to test the behavior of the probe at different times of the descent.

The data concerning pressure, temperature, density and probe speed depending on the altitude were obtained from data published by the Huygens Descent Trajectory Working Group (DTWG, (Kazeminejad, et al. 2007)), which reconstructed the descent data with the probe instrument measurements. In detail, data is coming from two files that can be found in the ESA archives (https://www.cosmos.esa.int/web/psa/huygens):

- HUY_DTWG_DESCENT_VEL.TAB
- HASI_L4_ATMO_PROFILE_DESCEN.TAB

The Reynolds number Re was used to determine the analogy between Titan atmosphere and wind-tunnel conditions.

$$Re = \frac{\rho V D}{\mu}$$ (density ρ, probe speed V, diameter D, dynamic viscosity μ)

Reynolds conditions in Titan's atmosphere:

The Reynolds number is calculated for several altitudes. The probe speed and the atmosphere density, as a function of the altitude z, are contained in the previous data, and the probe diameter is a constant (1.3 m).

The viscosity is not given in the data and needs to be computed. It can be calculated with Sutherland's formula:

$$\mu(z) = \mu_{ref} \left(\frac{T(z)}{T_{ref}}\right)^{\frac{3}{2}} \frac{T_{ref} + S}{T(z) + S} \quad [Pa.s^{-1}]$$

$T(z)$ is the temperature at the desired altitude. μ_{ref} is the reference viscosity at the reference temperature T_{ref}, and S is the Sutherland constant. These values are constant but depend on the gas composition (only nitrogen was considered).

μ_{ref}	T_{ref}	S
17.81 x 10^{-6} Pa.s^{-1}	300.55 K	111 K

Table 2: Sutherland's constants and reference temperatures for Nitrogen

The computed viscosity fluctuates between 1.09 x 10^{-5} Pa.s^{-1} at an altitude of 146.8 km and 6.22 x 10^{-6} Pa.s^{-1} at the surface of Titan.

Using a diameter of 1.3 meters for the probe, the Reynolds number as a function of the descent altitude on Titan is calculated and allows to determine the test conditions in the wind-tunnel (see Figure 3.2).

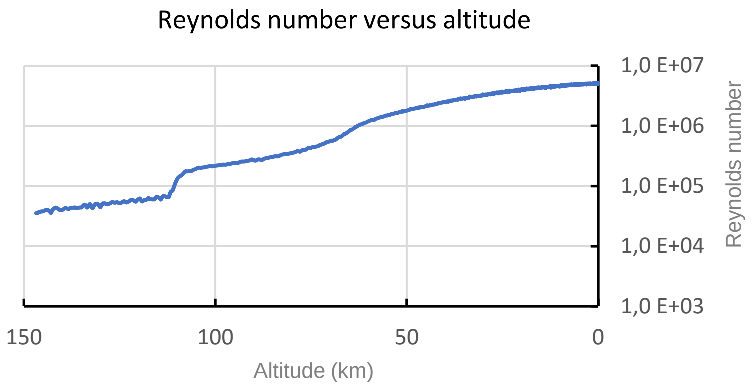

Figure 3.2: Reynolds number as a function of altitude on Titan

Reynolds analogies for wind-tunnel testing conditions

The Reynolds number similarity is then used to determine the wind tunnel air speed to apply in the wind-tunnel for each altitude to test. The conditions for the campaign tests are the following, considering 20°C for the air temperature:

μ_{air}	ρ_{air}	D_{model}
1.85 x 10^{-5} Pa.s^{-1}	1.204 kg.m^{-3}	0.452 m

Table 3: Conditions for an air temperature of 20 °C

The wind tunnel air speed can be computed using Reynolds formula and is plotted in Figure 3.3 as a function of the probe altitude *z*:

$$V_{wind-tunnel} = \frac{Re(z)\mu_{air}}{D_{model}\,\rho_{air}} \quad [m.s^{-1}]$$

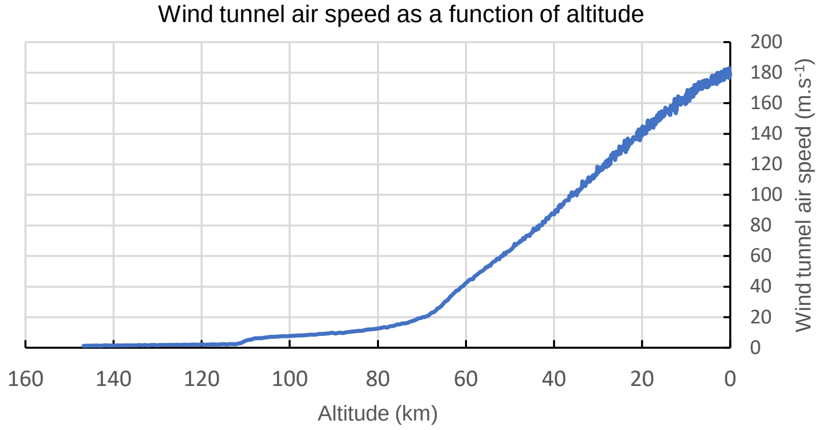

Figure 3.3: Wind tunnel air speed as a function of the descent altitude on Titan to match descent reynolds number

3.1.3 Analysis of the possible test conditions

As said in part 2.3, the spin deviation appeared at the very beginning of the descent sequence, meaning that the relevant tests in wind tunnel should be conducted at low air speeds (lower than 5 $m.s^{-1}$) in order to match the descent Reynolds number (see blue curve in Figure 3.4). However, the range of the available wind-tunnel air velocities goes from 10 to 50 $m.s^{-1}$, making the testing at low speeds (lower than 10 m/s) hard to conduct as they would provide unreliable results. The tests were then conducted in a Reynolds regime corresponding at the highest altitude under the stabilizer parachute as shown in Figure 3.4. The chosen air speed in the wind tunnel was 40 m/s corresponding to the part of the descent under the stabilizer at about 60km altitude.

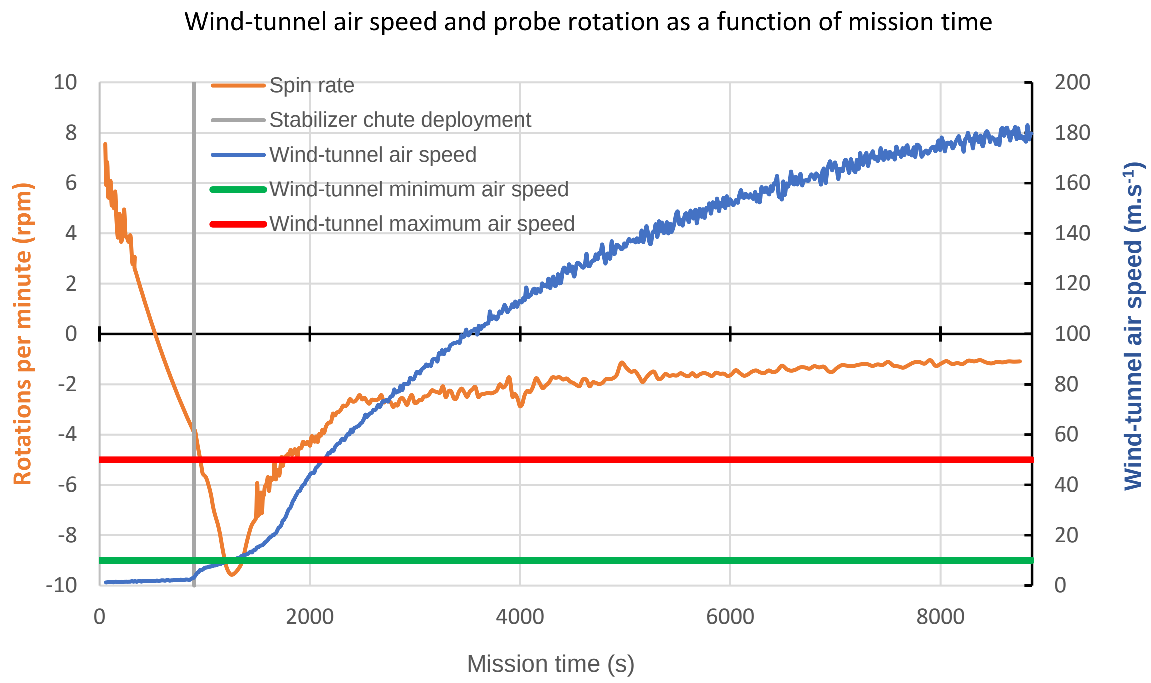

Figure 3.4: Wind-tunnel air speed to match descent Reynolds number and probe rotation as a function of mission time

3.2 Experimental set-up

3.2.1 The 1:3 mock-up and its appendages

From the original full ESA-provided Catia© CAD file, a simplified CAD model of the Huygens probe shown on Figure 3.5 was designed using SolidWorks© software and the dimensions have been chosen to 1/3rd of the original probe. Given the purpose of this work as described in the introduction and given the complexity of the original probe, when scaling to 1/3 scale, we made choices to simplify the CAD in order to facilitate the fabrication of the mock-up.

The mock-up (bare model = model without any appendage, but with the DISR camera head, as shown in Figure 3.5(b)) was fabricated by an external company in three main parts, in polyurethane foam 470 (density of 600kg/m^3), using 3- and 5-axis numerical machining. The mock-up has slots where the vanes can be inserted, and holes to insert the SEPS, the RAA, the HASI booms and the TPP, that allowed to insert or to remove them to test different configurations. The holes designed on the front part of the mock-up modeling SSP inlet, ACP inlet and GCMS inlet, have been filled with 3D-printed plugs for the tests, as it was verified that the effects of these appendages were not significant on the rotational dynamics of the probe. The mock-up was painted, which gave it that smooth look. This surface finish, especially on the front part, is probably not an accurate representation of the original probe. It may influence some phenomena related to the boundary layer nature and thickness of the flow impacting the vanes and consequently their efficiency, (see (AEROSPATIALE 1992) (AEROSPATIALE 1993) and (AEROSPATIALE 1996) for more remarks on this issue). As it was in the real case, at this 1/3 scale, the vane chord based Reynolds number of the flow impacting the vanes is still laminar, leading here to a ≈2 mm thick boundary layer (estimation based on modelling of a flat plate boundary layer). The transition to a turbulent regime, where the boundary layer thickness would be thicker, could actually be due to wall roughness. But for our 1/3 scale mock-up, it can be assumed that the mean roughness is not greater than one fifth of the boundary layer thickness. It is not so easy to perform an experimental characterization of the boundary layer on such a complex model by using hot wire anemometry for example. And, without available data on the surface finish for the original probe and the mock-up (roughness dimensions), it was decided not to conduct specific investigations for this issue and to focus on the modeling of the numerous appendages, sources of flow separation.

As shown in Figure 3.5(b), the DISR head design has been simplified as there was no original CAD file available for this study. This geometrical simplification is justified knowing that this appendage, where it is located, is certainly embeded in the separated wake flow limiting its impact on the torque, as it was already assessed during the Huygens design phase (AEROSPATIALE 1993).

(a) (b) (c)

Figure 3.5: CAD provided by ESA (a), Simplified CAD model (b) and delivered mock-up (c)

During the mock-up development, a focus has been put on the design of the vanes because they were designed to be predominant in the spin control. During the Huygens design, the vanes were initially set to an inclination of 2.2° on the flight model but after a balloon test carried out in the Earth's atmosphere, it has been decided to set them to an inclination of 2.8°. During WP1, the vane slots were designed for a vane inclination of 6.8°, as a result of a mis-specification to the manufacturer. For WP2, a new foredome was constructed with radially oriented slots, in order to implement 1 mm thick 3D-printed vanes (see Figure 3.6) with two available inclinations 2.2° and 2.8°. The use of the previous vanes allowed to test also the 0.0° inclination.

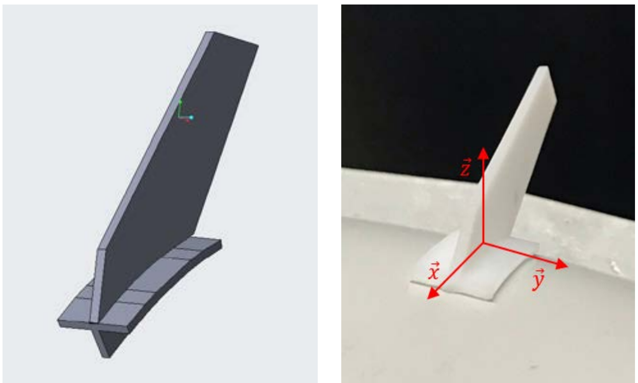

Figure 3.6: CAD for vanes and removable 3D-printed vane in its insert

The appendages of the probe have been 3D-printed as faithfully as possible at the scale 1/3rd as well (except for the HASI booms and their sensors which were machined and assembled) as illustrated on Figure 3.7 and Figure 3.8. They can be mounted and removed for testing different combinations of appendages. At this scale, the overthickness of the junction between the two branches that exists for the flight HASI boom has not been reproduced.

On Figure 3.7 are shown the following appendages:

- 1: RAA, Radar altimeter antennae – x 4
- 2: HASI Instrument deployable booms – x 2
- 3: SEPS, Heat-shield and back-cover separation subsystems (SEPS) – x 3
- 4: TPP, HASI pressure and temperature sensors x 1

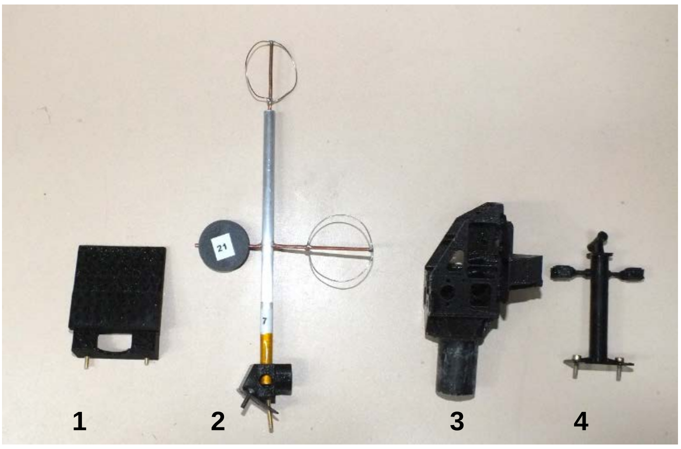

Figure 3.7: 3D printed appendages

On Figure 3.8 are shown two additional 3D printed appendages, namely the SEPS cable support and the electrostatic dischargers b), which have been designed mainly to make the mockup more in line with its original design. The part a) is made to hold a cable next to the SEPS and has been designed to be plugged in the central ring. Instead of 3D printing a replica of the cable, a real cable has been used. However, considering this experimental test at our wind tunnel scale and our available means of measurement, it was not possible to highlight the effects of the SEPS cables and electrostatic dischargers on the aerodynamic behavior of the model beyond measurement uncertainty. Therefore, they were not included in the different configurations studied and presented later in this report.

a) SEPS Cable on the SM2 probe and 3D printed support for cable

b) Electrostatic dischargers

Figure 3.8: Additional 3D printed appendages

The HASI deployable booms can be mounted on the mock-up in three positions: i) fully deployed (open configuration), ii) intermediate and iii) stowed (closed configuration) (see Figure 3.9). These three positions allow to characterize the effects of a possible non-deployment of one of the booms. To avoid any misunderstanding between the two booms, they are labelled B1 and B2 and small marks are placed on the mock-up.

Figure 3.9: Full deployed, stowed and intermediaite configurations of HASI booms.

3.2.2 Mock-up mounting in the main test section

The mock-up is linked to the external balance located under the floor by two perpendicular steel bars as shown in Figure 3.10. A fine-accuracy torquemeter was added on the mounting interface between the mock-up and the horizontal bar for the tests carried out during WP2. This mounting places the mock-up in the center area of the test section, reducing possible wall effects. To reduce the aerodynamic influence of the mounting, a fairing is screwed to the floor and covers the vertical steel bar without touching it. The horizontal part of the mounting is located in the flow recirculation area at the rear of the mock-up therefore its aerodynamic effect can be considered as very low.

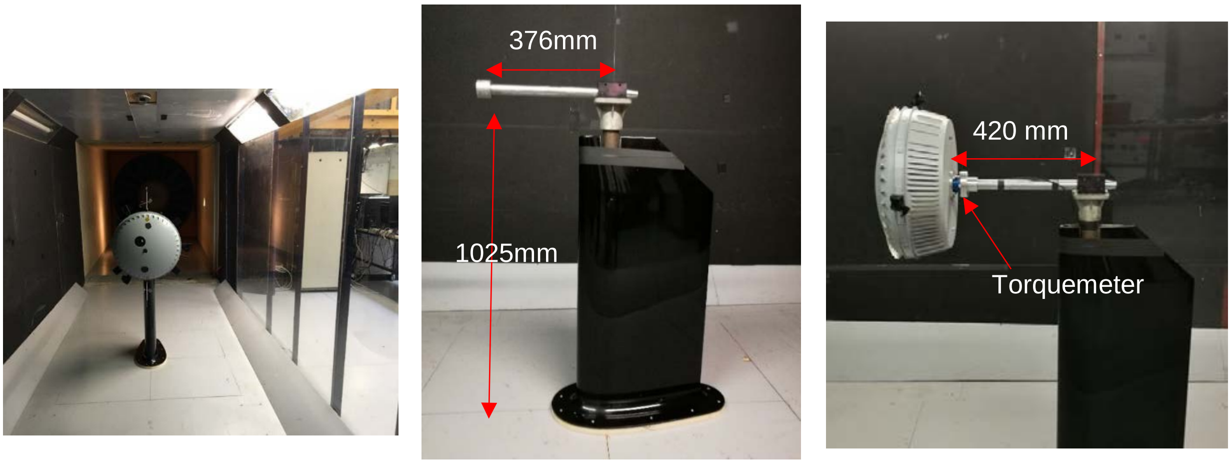

Figure 3.10: Mock-up mounting in the wind tunnel test section

The experiments were performed with many configurations. We decided to place the mock-up in the wind tunnel with its initial position depending on the azimuthal position of the camera DISR, as it turned out, at a zero angle of attack, to show some influence on the measurements. As the wind tunnel flow was previously characterized as uniform, the small azimuthal dependence of the DISR position was suspected to be due to a small misalignment of the mock-up mounting that could not be fully validated. This led us to define a specific “spin” angle as detailed in the following section. It turned out that the DISR influence on the aerodynamic coefficient proved to be strongly dependent on the angle of attack.

3.2.3 Reference frame and sign convention

As a reminder, Figure 3.11 shows the definition of the initial and reversed spin compared to clockwise (c/w) and anti-clockwise (a-c/w) rotation.

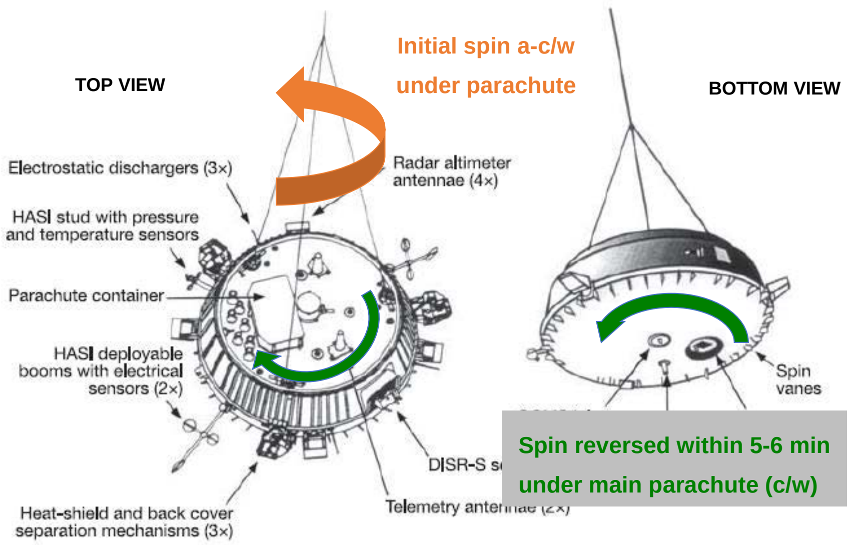

Figure 3.11: Spin direction convention (a-c/w : anti clockwise-positive- ; c/w : clockwise-negative-) as seen in the speed direction (defined as top view)

The technical drawings provided by ESA are shown in Figure 3.12 (left). On the left figure, the SEPS mounting interfaces are shown, but not the SEPS themselves. It allows to define a probe reference frame (with the subscript p) and to identify the location of the appendages and more particularly both HASI booms (B1 and B2). On the right figure, the mock-up is shown, seen from its bottom, in the same orientation around the X axis as on the left figure.

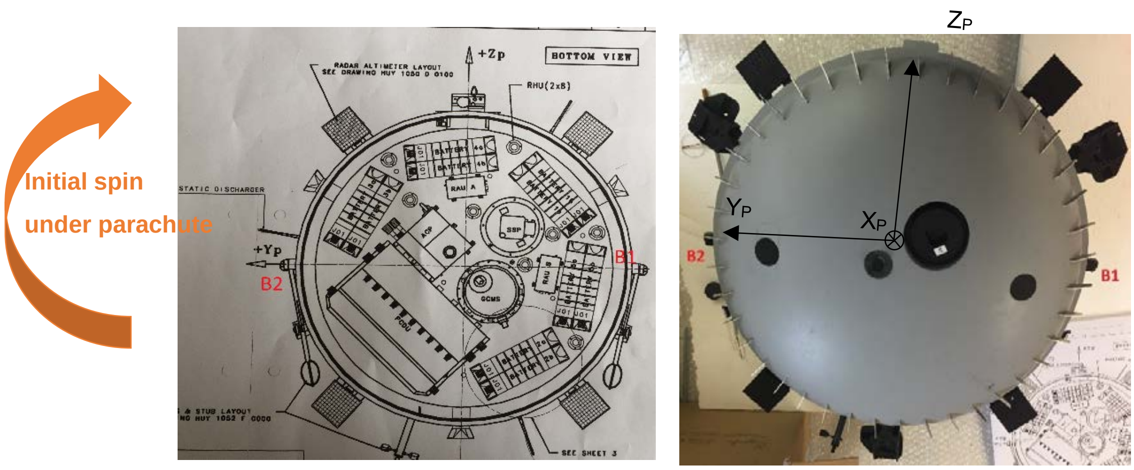

Figure 3.12: Spin direction convention as seen from technical drawings (left) and mock-up (right) in bottom view

According to this technical drawing in bottom view, the probe frame is referenced by:

- The Xp axis is oriented toward the parachute (opposite to the descent velocity direction)
- The Yp axis is oriented to the position of the boom HASI_2 that is the closest HASI boom to the TPP
- The Zp is oriented toward the camera DISR position
- The SEPS_1 is next to the boom HASI_1 (B1)
- The SEPS_2 is next to the boom HASI_2 (B2)
- The SEPS_3 is next to the TPP

As the direction of the spin seen in top view is anti-clockwise, it is clockwise seen from bottom view. According to this drawing, the clockwise direction goes from + Yp to + Zp.

For wind tunnel test analysis, a wind reference frame (subscript w) is defined according to the wind direction as shown in Figure 3.13 with the mock-up installed on its support linked to the load balance from which drag, lift and side forces, roll pitching and yaw moments are measured. Indeed, it corresponds to the probe frame defined above in the case when the wind direction is aligned with the Xp axis (angle of attack is null).

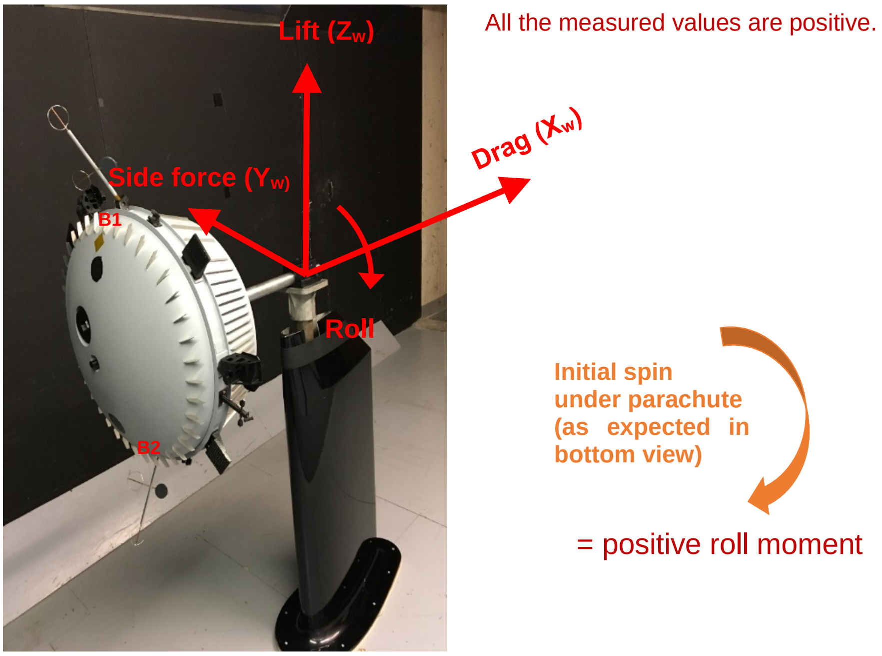

Figure 3.13: Wind reference frame and sign convention

Only one single free axis (rotation around Z_W axis) is available to vary angles of attack of the mock-up. Due to a specific mounting of the mock-up in the wind tunnel, it has then been necessary to define a transitional probe frame with the prime' exponent and two angles of rotation of this frame with respect to the wind reference frame and a reference location for the DISR camera (see Figure 3.14).

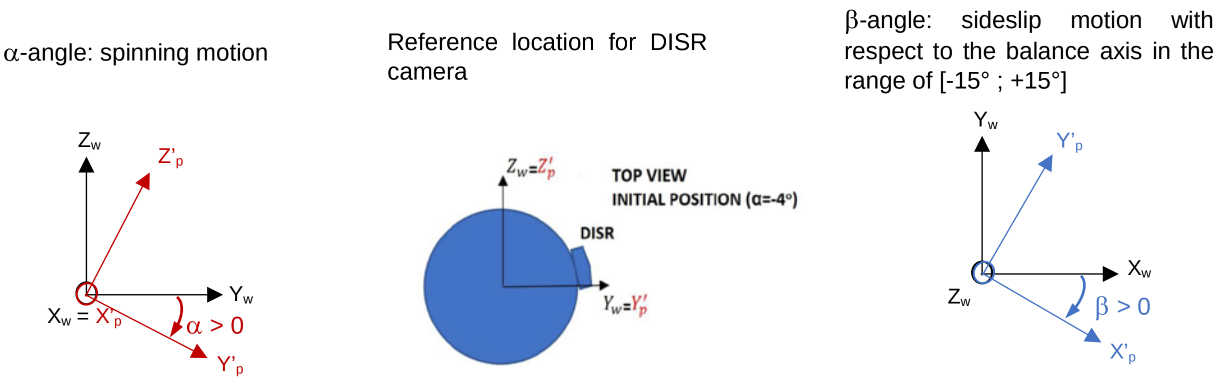

Figure 3.14: Sign convention for rotation angles of the mock-up with respect to the wind reference frame

Loads are measured according to the wind reference frame with respect to a geometrical center of the balance, and consequently, they are post-processed to be referenced in a probe frame at the geometrical center of the mock-up (see Appendix 1). Both α and β angles are defined clockwise positive, therefore negative in the trigonometric direction.

3.3 Experimental protocol for aerodynamic load measurement

3.3.1 Force and moment definitions

Aerodynamic forces and moments experienced by the mock-up are computed in the wind reference frame from the balance measurements. The aerodynamic resultant torsor with respect to the geometrical center of the balance is then composed of

- Three forces: Drag (F_X), Side Force (F_Y), Lift (F_Z)
- Three moments: Roll (M_X), Pitch (M_Y), Yaw (M_Z)

Aerodynamic forces are defined as following:

$$F_X = \frac{1}{2}\rho S V^2 C_D \ \ ; \ F_Y = \frac{1}{2}\rho S V^2 C_Y \ \ ; \ F_Z = \frac{1}{2}\rho S V^2 C_L \ \ ;$$

where C_D, C_Y and C_L are non-dimensional drag, side force and lift coefficients respectively. They depend on the geometry of the body.

Aerodynamic moments are defined as following:

$$M_X = \frac{1}{2}\rho S V^2 L C_{MX} \ ; M_Y = \frac{1}{2}\rho S V^2 L C_{MY} \ \ ; M_Z = \frac{1}{2}\rho S V^2 L C_{MZ}$$

where C_{MX}, C_{MY} and C_{MZ} are respectively roll moment, pitch moment and yaw moment non-dimensional coefficients respectively.

ρ is the air density ($\rho = 1.225 \text{ kg.m}^{-3} \text{ at } 15°C$), S is the reference area without appendages (S = 0.160 m²), V is the wind speed and L is the reference length (mock-up diameter) used to calculate the moment induced by the corresponding force. See Appendix 1 for more details on the post-processing of the final force and moment values expressed in the probe reference frame.

3.3.2 Uncertainties

Considering the aerodynamic balance characteristics (See Appendix 1) and the fact that, for this study, the main relevant parameter is the roll moment, a calibration experiment was made to determine at which values the torque would be measurable and a study of the sensibility of the balance was conducted for low efforts and moments. Indeed, the measured resultant torque was expected to be very low. The result is that any torque value under 0.3 N.m should be considered carefully when measured by the balance. This limitation was remedied by implementing a more sensitive measurement device. A single-axis torquemeter has been added for the WP2 campaign between the mock-up and the horizontal bar in order to measure a roll moment with better accuracy. The chosen device (Scaime DF2553-10N.m) supports a nominal load of 10 N.m and has an uncertainty of 0.01 N.m. With this type of device, it is recommended to avoid axial and radial forces, which could lead to measurement errors and possible degradations of the device. Thus, mechanical parts linked to the torquemeter have to be aligned (axial, radial, angular) as best as possible to avoid interference forces. The torquemeter was also only used for low (in practice zero) angle of attack measurements.

3.3.3 Data acquisition

During the tests, the following measurements were made: 6-axis balance for the aerodynamic loads, the roll moment by the torquemeter, the wind speed with a Pitot tube. The test section temperature and the atmospheric pressure were also acquired to process the wind speed and the Reynolds number. A Pitot tube located at the contraction section of the wind tunnel made the measurement of the wind speed in the test section. Since this is not the exact location of the mock-up, a preliminary test was done by placing a Pitot tube at the location of the mock-up. A correction factor was therefore determined and was applied for computing the correct wind speed at the mock-up location.

The overall acquisition was carried out by a software developed for the processing of the wind tunnel measurements. Data acquisition were based on a 30-second time series (30 000 samples, 1 000 Hz) from which time-averaged values were computed.

Each test configuration was carried out three times to ensure the repeatability of the measurements. For the roll moment, the average of the difference between the three tests over all tests was about 0.2 N.m when measured by the balance, whereas lower than 0.01 N.m when measured by the torquemeter. In some results presented in the next section, all measured data have been plotted.

During the tests, at high speed, the probe and its mounting encountered vibrations that may have disturbed the measurements. Since data acquisition was made using time series, this effect was corrected on average, but the root mean square of certain times series remained substantial.

See Appendix 2 for a list of test cases and the corresponding nomenclature.

3.4 Experimental set-up for PIV measurement

Flow investigation by PIV was performed in order to illustrate the appendage effects on the mock-up wake. Time-averaged velocity fields of the flow around the model were then computed and plotted as vectors and contours of velocity magnitude with respect to the incoming flow. Measurements are performed in the (X,Z) symmetry plane of the mock-up installed in the test section and in a (Y,Z) transverse plane located 10 cm downstream of the mock-up as shown in Figure 3.15.

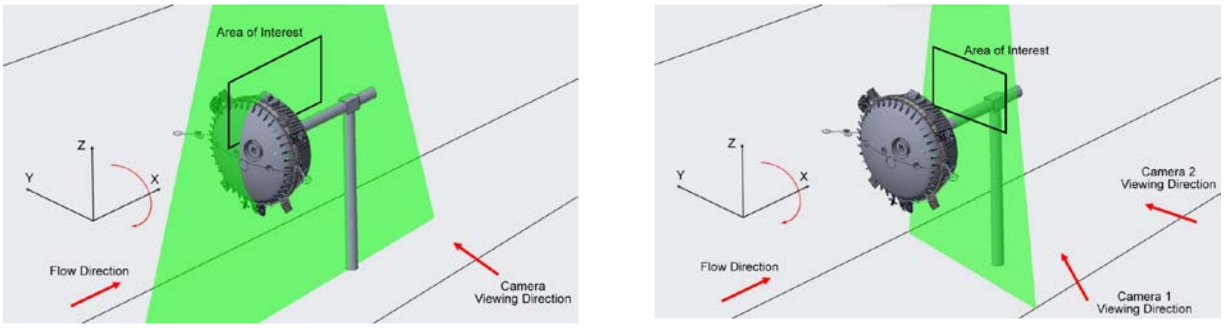

a) Two-dimensional flow field (2D-PIV)
For two-component velocity vectors (X,Z)

b) Two-dimensional flow field (Y,Z)
For three-component velocity vectors (Stereo-PIV)

Figure 3.15: Schemes of the PIV set-up implemented in the test section, a) 2D-PIV and b) Stereo-PIV

PIV system and main testing parameters are summarized below:

- Evergreen 200 Nd:Yag laser emitting 2 pulses (2 x 200 mJ) with wavelength 532 mm and 2.5 Hz emission rate
- Seeding particles are micron-sized olive oil droplets sprayed by a PIVTEC seeding system
- Images are acquired with one or two LaVision Imager LX cameras (4032x2688 px^2) and a 105 mm lens equipped with 532 nm wavelength filter.
- The software used for image processing is DaVis 8.3.1 (LaVision GmbH)

- The time delay between both images is set according to the incoming wind speed: 22µs for 2D-PIV and 30µs for Stereo-PIV.
- The field of view data size is about 300 mm x 200 mm, and the final resolution is one vector every 2.5 mm with a multi pass decreasing size (64x64 px^2, 32x32 px^2) interrogation window with an overlap of 50%
- 400 image pairs are recorded in order to compute the ensemble-averaged velocity statistics

4 Experimental results

4.1 Bluff body

As a result of its shape, the Huygens probe generates separated flow over a substantial part of its surface. It is a bluff body because at large Reynolds numbers the drag is dominated by the pressure losses in the wake. When the flow separates from the surface and the wake is formed, the pressure recovery is not complete. The larger the wake, the smaller is the pressure recovery and the greater the pressure drag.

4.1.1 Airflow visualisation

The Lucien Malavard wind tunnel allows the execution of simple visualisation of the airflow using white smoke. It does not bring a lot of information about the roll moment but it is interesting for looking at the impact of the different appendages, particularly concerning the drag. The following pictures show some screenshots of the visualisation films made around the appendages of the mock-up.

a) SEPS

b) RAA

c) closed HASI boom

d) deployed HASI boom

Figure 4.1: Flow visualisation around the appendages of the mock-up

Figure 4.2 shows contours of velocity magnitude with respect to the incoming flow in the longitudinal 2D-view and in the transverse view of the wake around RAA. Figure 4.3 shows contours of velocity magnitude with respect to the incoming flow in the longitudinal 2D-view of the wake around SEPS. A large recirculation zone in blue can be observed behind the mock-up. It is characterised by a large velocity deficit, bound by the development of a shear layer, which grows from the resulting velocity discontinuity, and it thickens downstream. The wake enlarges downstream the mock-up as can be seen on the transverse view of the flow (c). Adding appendages facing the flow emphasizes the wake as shown here with RAA and SEPS for example. The appendages are evidently intrusive and generates their own wake, which can interact with the one of the mock-up body. In such bluff body near wake, flow instabilities can develop, generating vortices which can induce structure vibrations and noise. Far downstream of the model, viscous effects attenuate these phenomena.

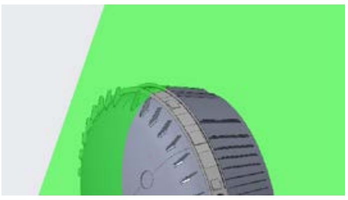

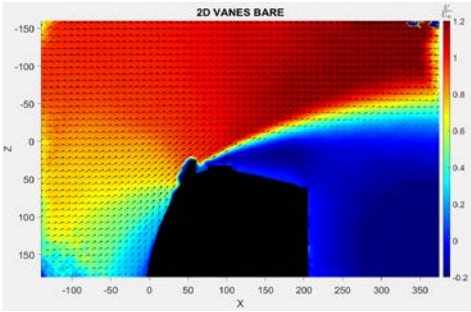

a) 2D-PIV without RAA

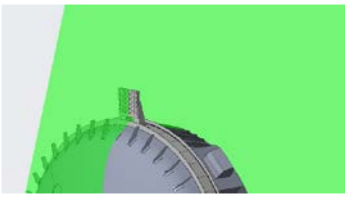

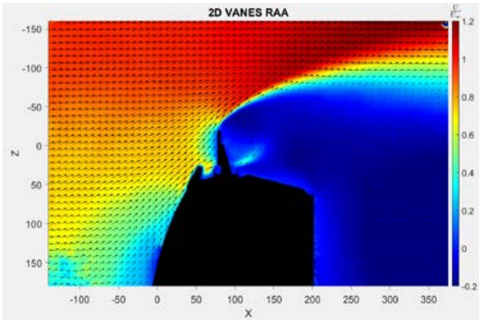

b) 2D-PIV with RAA

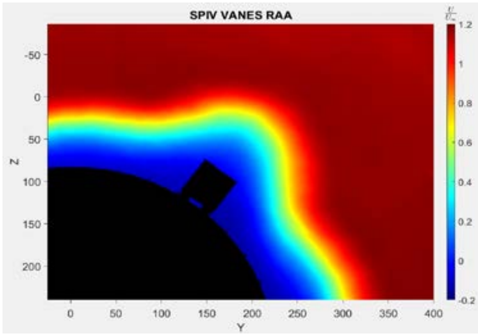

c) Stereo-PIV with RAA

Figure 4.2: Time-averaged velocity fields around RAA, V = 30 m/s

Separation subsystems (SEPS)

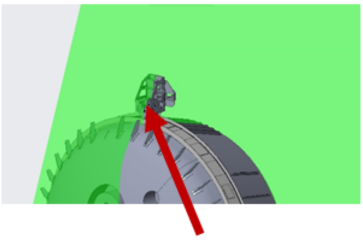

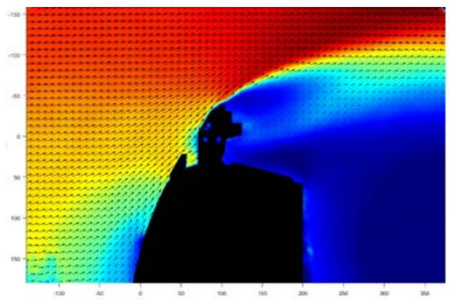

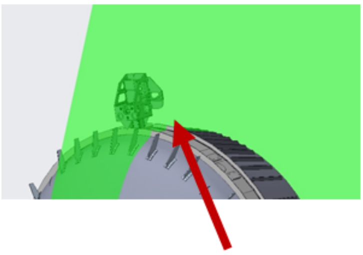

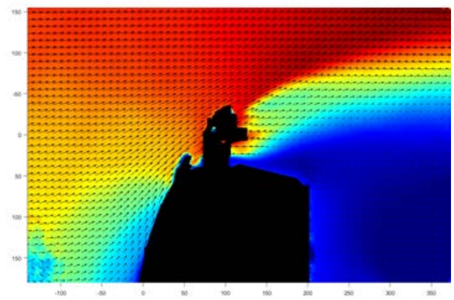

Side plane

Figure 4.3: Time-averaged velocity fields around SEPS, V = 30 m/s

4.1.2 Drag and Reynolds independence

According to the Reynolds similarity study, in order to recreate the conditions of the descent in Titan upper atmosphere, the wind air speed should be set at a value lower than 1 m.s^{-1}. At this speed, it is not possible to measure any aerodynamic forces due to the balance sensitivity limitations. However, many configurations have been tested at higher wind air speed (up to 45 m.s^{-1}). Most of the load measurements were conducted at the wind speed of 40 m/s.

In Figure 4.4, the drag coefficient ($C_D = \frac{2F_X}{\rho S V^2}$) measured for different configurations is plotted against the wind speed. These results were obtained for the first mock-up with vanes at 6.8° of inclination. The reference surface S was kept at $0.160\ m^2$ for the drag coefficient computation. Considering that the increase in the reference area to be taken into account would be a maximum of about 10% for the fully equipped mock-up, this would overestimate the C_D by a maximum of 10%, and less for the mock-up equipped with only SEPS, but without modifying the trends to be deduced.

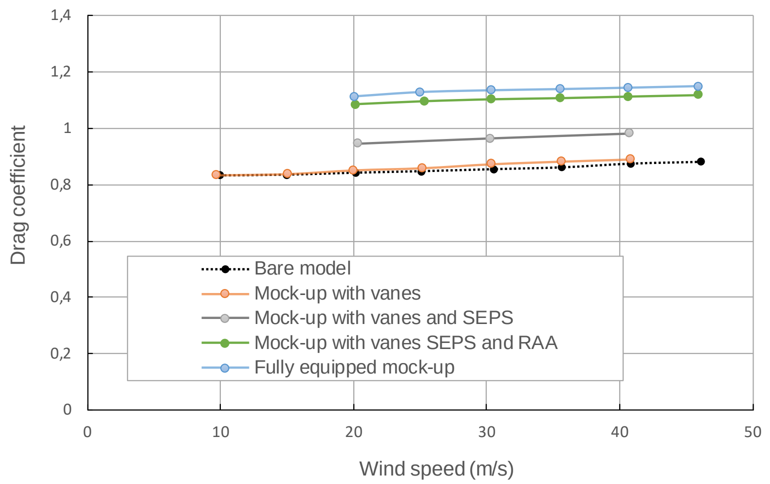

Figure 4.4: Drag coefficient for different configurations against the wind air speed for 6.8° vanes

For a wind air speed of 20 m/s and 40 m/s, the Reynolds numbers are respectively Re = 566 727 and Re = 1 129 883.

It can be observed that the drag is significantly increased by appendages as it might be expected whereas drag increase is under 2% by the vanes only.

Whatever the mock-up configuration, the drag coefficient is nearly constant as the wind air speed increases, which means that Reynolds effects are not so relevant in the range of tested wind air speeds. This trend was expected because the drag here is mainly due to flow separation induced by this typical bluff body geometry and the appendages. Therefore, it is assumed that the flow regime at high speed and low speed should be analogous. Hence, most of the tests were performed at the highest speed of 40 m/s, which has been considered to reduce the measurement uncertainty and to observe the phenomena when they are the most significant.

A comparison with drag coefficient values for the real Huygens probe given by (AEROSPATIALE 1992) in appendix 3 shows that our mock-up may have a slight higher drag coefficient value. The present values seem rather close to CD max, value of 0.9 for a Reynolds number of 1.0e06 as indicated in appendix 3 for the nominal real shape, namely vanes+SEPS+RAA. Considering the reference surface, the measurement uncertainties, and the fact that it is a 1:3 simplified mock-up, this difference is within an acceptable value.

4.2 Bare mock-up characteristics and DISR camera effects

According to the location of the DISR camera around the Huygens model, more downstream than the appendages, it was decided to include it in the design of the bare mock-up, as shown in Figure 3.5 (b). As this camera shows a complex geometrical shape, a simplified shape was chosen to represent it in the CAD model, while respecting the main geometrical dimensions. As expected, without sideslip angle for the coming flow, the DISR camera is embedded in the blue recirculation zone, signature of the large wake behind the model, as depicted on PIV views in Figure 4.5.

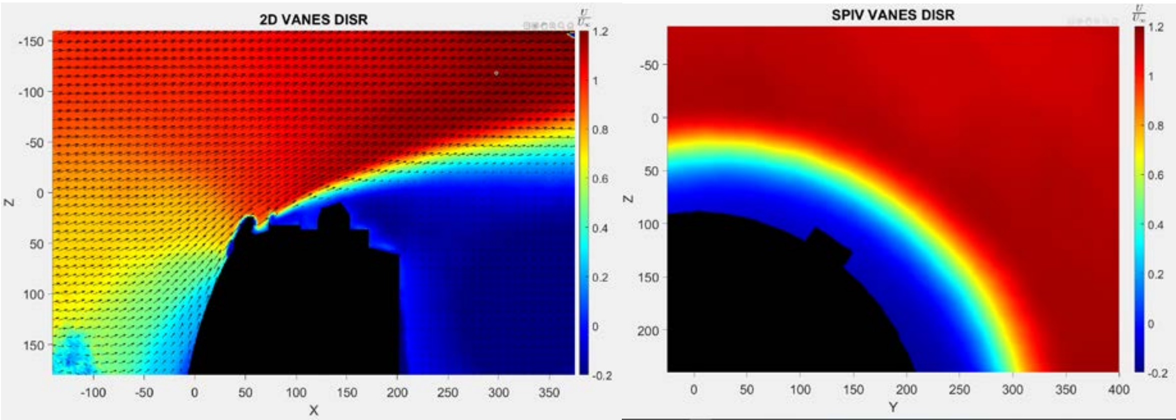

Figure 4.5 : Time averaged velocity fields of the bare mock-up, 2D longitudinal and transverse views.

Nevertheless, the bare mock-up is not symmetric according to its main revolution axis (X). Different orientations of the bare mock-up were then investigated according to the spin α-angle and the sideslip β-angle defined in Figure 3.13 and shown in Figure 4.6.

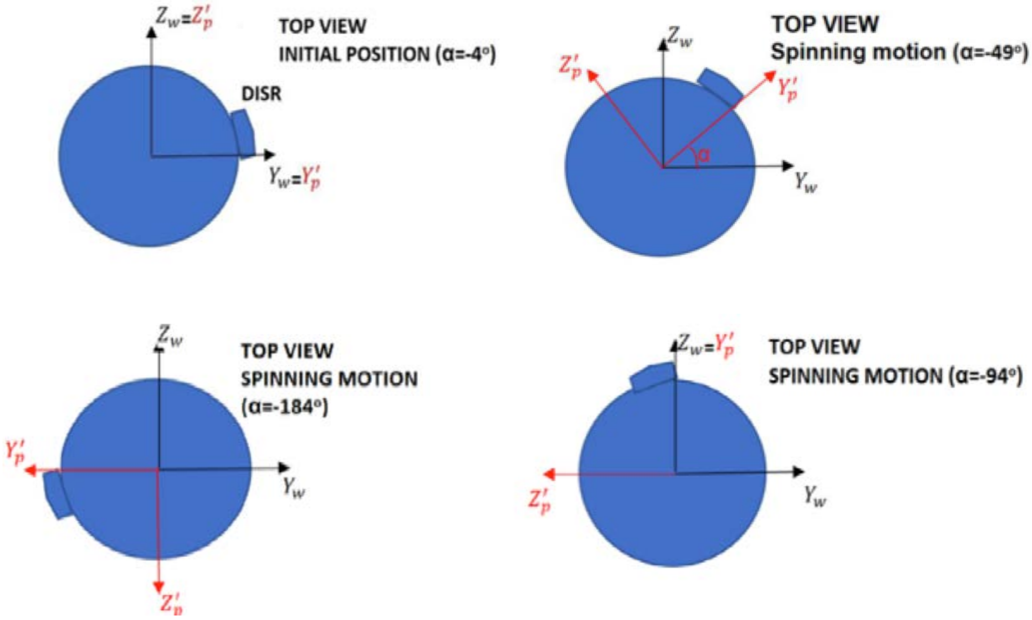

Figure 4.6: Definition of the spin α-angle for different orientations of the camera DISR (β = 0°)

By applying an angle of attack (sideslip β-rotation), the DISR camera is then oriented either downwind or upwind as drawn on sketches in Figure 4.7 more particularly for spin angles of -4° and -184°. Thus it expected that the combined effect of the spin and sideslip angles on the DISR camera's orientation towards the incident wind leads to the observation of variations in aerodynamic forces and moments. Indeed, depending on the DISR camera location, the bare mock-up may not be symmetrical with respect to the (Xw, Zw) plane, reference plane for the β-rotation for example.

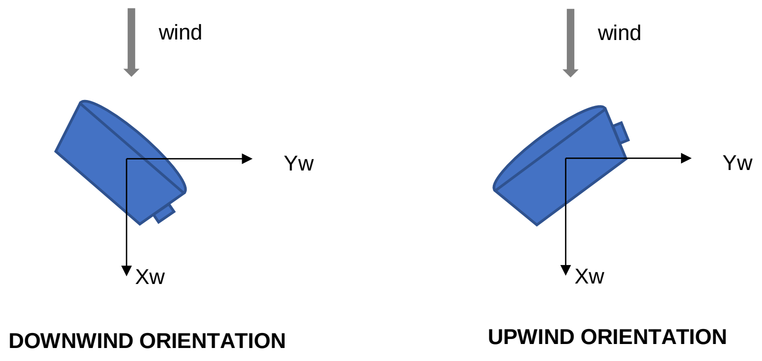

Figure 4.7 : Sketches for DISR orientation : downwind vs upwind for a spining angle of -4°

In Figure 4.8 are plotted non-dimensional side (a) and lift (b) forces of the bare mock-up measured by the aerodynamic load balance as a function of the β-angle in the range from -15° to +15° for different spin angles. First, the variations of these two forces against these two specific angles reveal either a symmetric or a non-symmetric force magnitude variation with respect to β-angle, depending on the spin angle, and secondly, the higher the angle of attack, the greater the force magnitude.

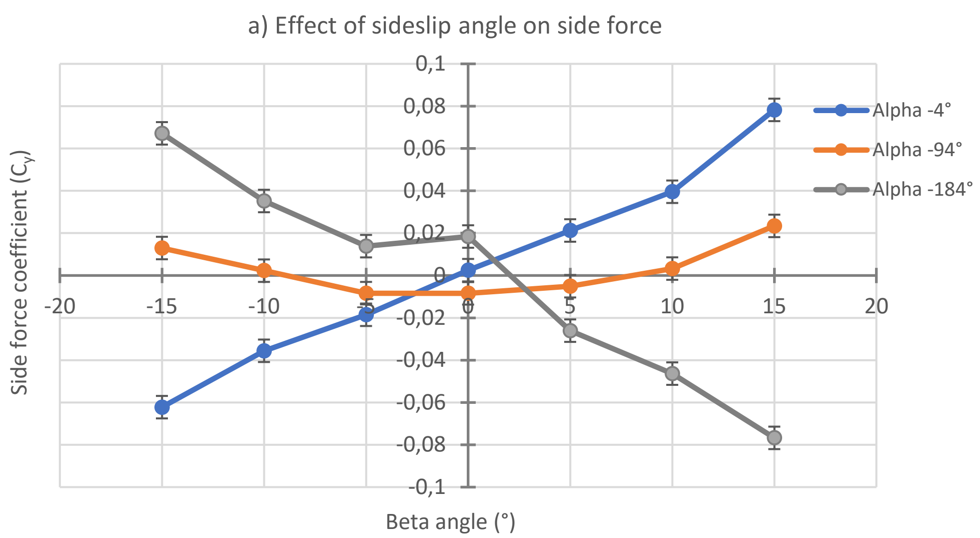

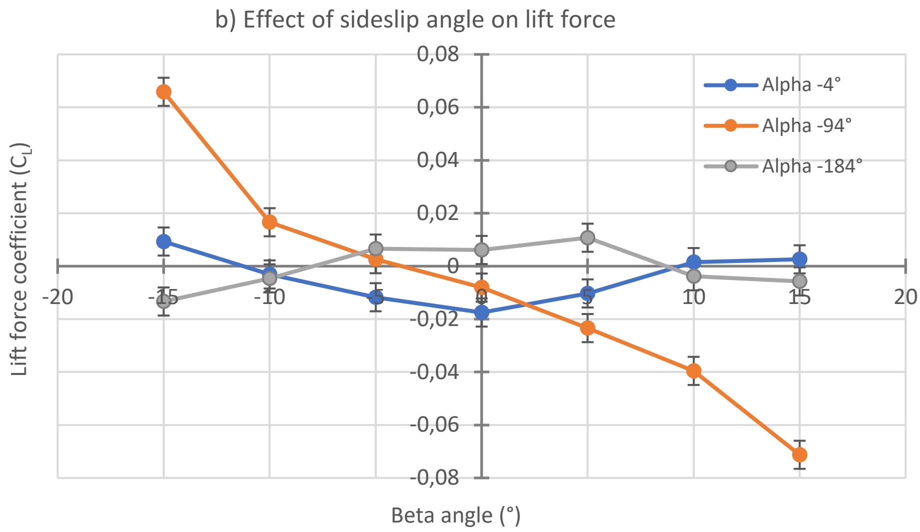

Figure 4.8: Non-dimensional side (a) and lift (b) forces of the bare mock-up as a function of the angle of attack for different spin angles (30 m/s)

These trends are confirmed in the three moments. Their variations against the angle of attack are depicted in Figure 4.9 ((a) roll, (b) pitch and (c) yaw) for different spin angles. Depending on the spin angle, sideslip effects on the three non-dimensional moments measured by the balance are different in evolution and in order of magnitude. The higher the angle of attack, the greater the moment magnitude. It is possible to interpret and extrapolate more finely these effects on the global dynamics of the probe. However, considering that the focus of this study is placed on spin behaviour, what is important to stress here is that the effects measured on roll are about 10 times weaker than those measured on yaw and about 5 times weaker than those measured on pitch (in absolute value). For the spin angle of -94°, it can be observed that a sideslip angle induces roll moments in the positive direction and increasing with the β-angle value, so it confirms that some DISR camera's orientations towards the incident flow may lead to affect the roll moment.

These results suggest that the DISR camera should also be considered as an "appendage" likely to influence the global dynamic behaviour of the probe, in case of pendular motion more specifically. Finally, they highlight angle of attack effects, which have been also investigated for the mock-up with vanes and appendages later in this report.

As a final comment, these results must be interpreted taking into account the following remarks:

- the camera design was simplified

- the alignment uncertainties between the revolution axis of the mock-up and the X-axis of the wind tunnel test section may exist, even if they are estimated at less than half a degree

- very low moment magnitudes must be considered with caution, due to the range of the balance measurement uncertainty (lower than $|\pm 0.3\ \mathrm{N.m}|$) and to a possible uncertainty in resetting sensors. Indeed, for such low moment magnitudes, in case of β = 0° in particular, some disparities in the moment magnitudes have been observed for the same studied configurations, which lead for example to obtain a positive or negative average value of the three acquisitions performed to verify measurement repeatability.

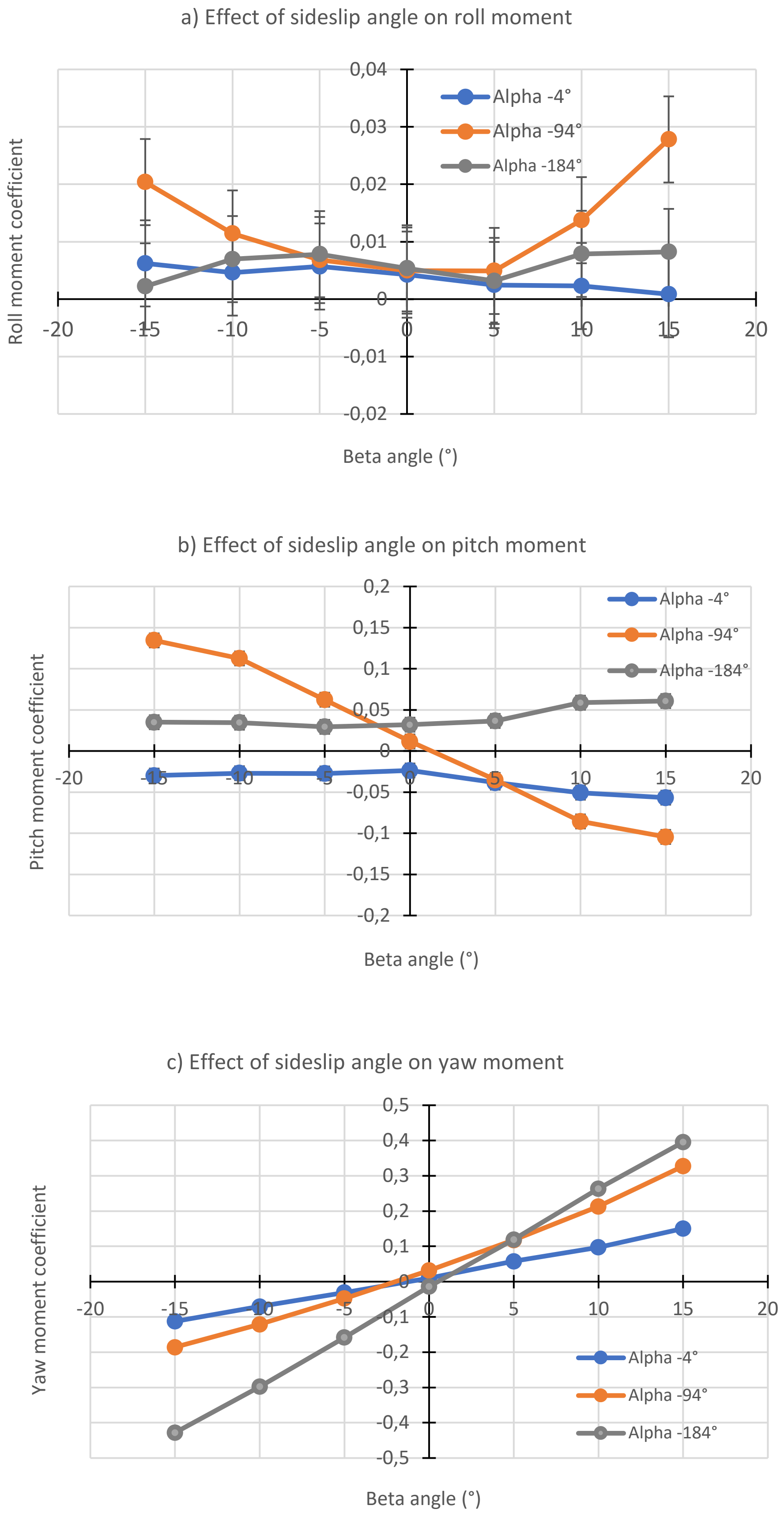

Figure 4.9: Non-dimensional moment coefficients of the bare mock-up as a function of the angle of attack for different spining angles (30 m/s - uncertainty : ±0.0075)

4.3 Effects of the vanes at zero angle of attack

In order to assess the effects of the vanes on the spin direction, different inclinations of vanes have been studied. The 2.2° value corresponds to the one which was implemented for the SM2 probe whereas the 2.8° value was used for the flight probe.

Figure 4.10 shows values of the mean roll moment and roll moment coefficient measured by the balance and the torquemeter as a function of the vane inclination. It can be observed that vanes induce a positive roll moment meaning a correct spin direction, as expected from the design. The roll moment generated by the vanes is increasing quasi linearly with their inclination angle as expected. The moment amplitude produced by the vanes for a 2.8° inclination is indicated in the additional table and can be considered as our reference case.

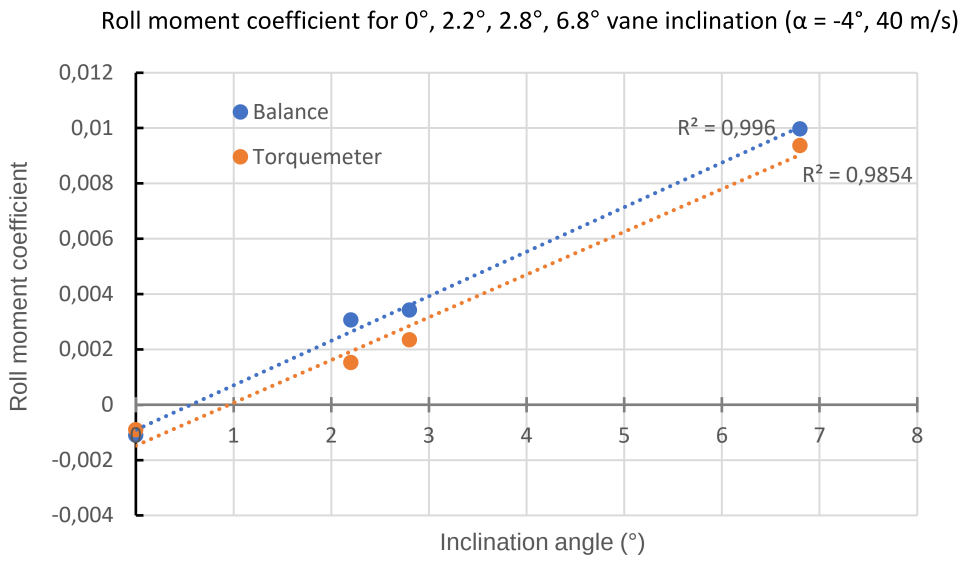

40 m/s - Torquemeter	2.8°	6.8°
Roll Moment (± 1.10^{-2} N.m)	0.17 N.m	0.66 N.m
Roll Moment Coefficient (± 2.10^{-4})	0.0024	0.0094

Figure 4.10: Roll moment and roll moment coefficient measured by balance or torquemeter for different vane inclinations

With no vanes or 0° tilt vanes, the roll moment stays close to zero but is slightly negative. It might be due to the protruding DISR camera head effect as seen previously.

The roll moment measured by the aerodynamic balance during the first test series, and the corresponding roll moment coefficient, are plotted against the wind air speed for the bare model without the vanes and with the 6.8° vanes in Figure 4.11. The roll moment increases linearly with wind air speed. In section 4.2.1, it has been shown that Reynolds number effects are not so relevant in the range of tested wind air speeds. This statement can be verified by plotting the roll moment coefficient. Indeed, it depends slightly on wind air speed for values above 30 m/s. At lower wind speeds, this appears less true, but the measured values are less reliable. This is because the measurement uncertainty is greater for the moment than for the drag force, especially at low wind air speeds. What needs to be noted here is that the SEPS tend to attenuate the effects of the 6.8° vanes, implying that the SEPS induces a torque opposite to that of the vanes.

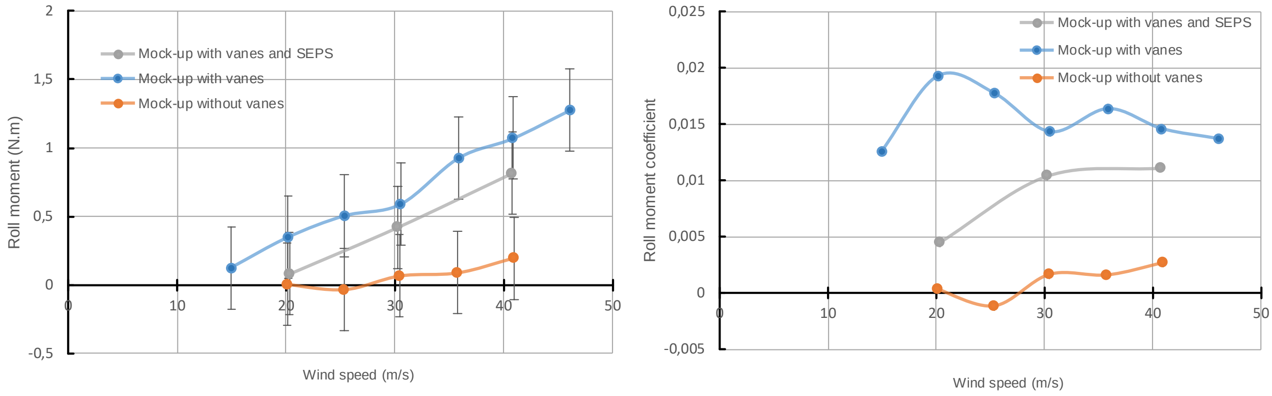

Figure 4.11: Roll moment and roll moement coefficient with and without vanes against the wind speed

Another effect of the vane inclination is observed on the drag coefficient plotted in Figure 4.12. In this histogram, one balance measurement series per colour is depicted in order to show the repeatability level of the measurements. Drag coefficient shows a slight tendency to decrease when the inclination angle of the vanes increases. The test data do not allow local determination of the aerodynamic forces applied to the vanes and the resulting deviation of the induced flow. CFD simulations could help to highlight this possible trend, but were not planned in our study.

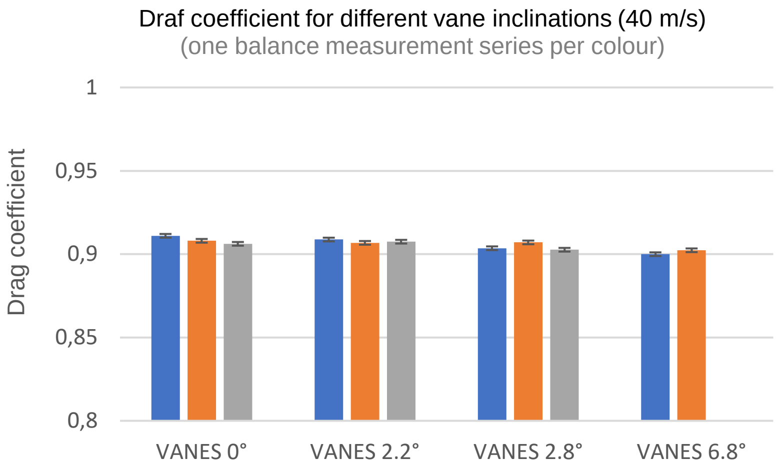

Figure 4.12 : Drag coefficient versus vane inclination angles

4.4 Effects of each appendage at zero angle of attack

Many configurations at zero angle of attack were tested including:

- The vane mock-up with each appendage (the SEPS, the RAA, the TPP, the booms HASI)
- The full mock-up with different positions of the HASI booms
- The full mock-up with different positions of the HASI booms for the different angles of attack of the wind (The HASI booms were vertical with respect to the wind tunnel floor).
- The fully equipped mock-up with different positions of the HASI booms and the reduction of the vane number (in order to reduce the effect of the 6.8° vanes, as a first approach to reducing the vane inclination)

4.4.1 Combined effects of vanes, SEPS and RAA

Many configurations were tested on the mock-up equipped with the vanes by adding each type of appendages, separately or combined, in order to quantify their aerodynamic contribution on the global roll moment. The roll moment coefficient is plotted for each case in Figure 4.13 and in Figure 4.14 for the two vane inclination angles 6.8° and 2.8° respectively at a wind speed of 40 m/s. Each of the 3 balance measurements per series is plotted in different colors in order to illustrate the repeatability level of the measurements.

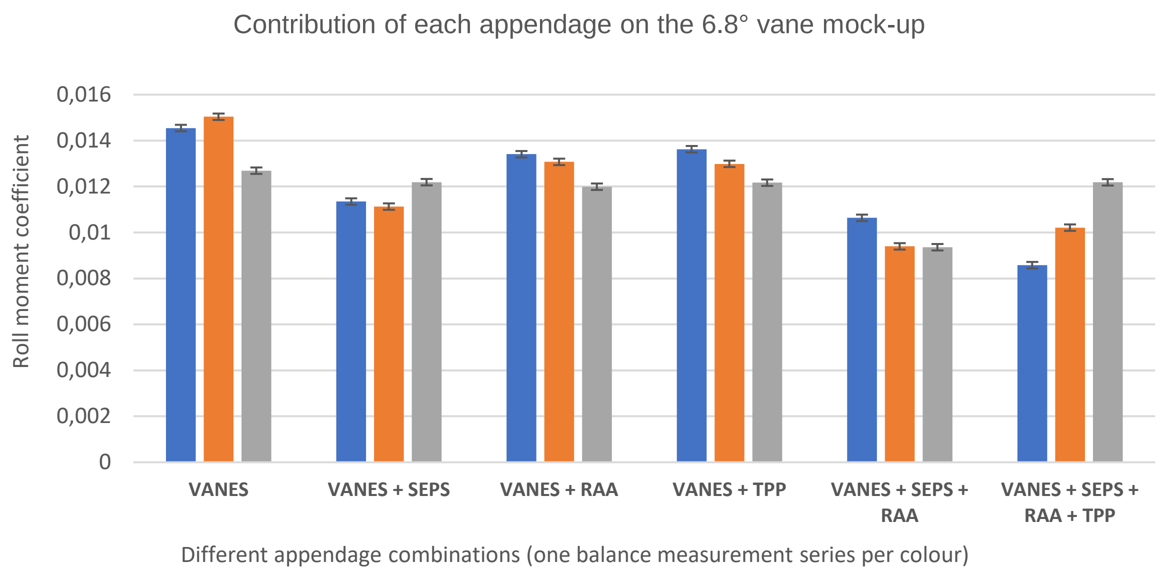

Figure 4.13: Roll moment of 6.8° vane mock-up equipped with each appendage and their combination

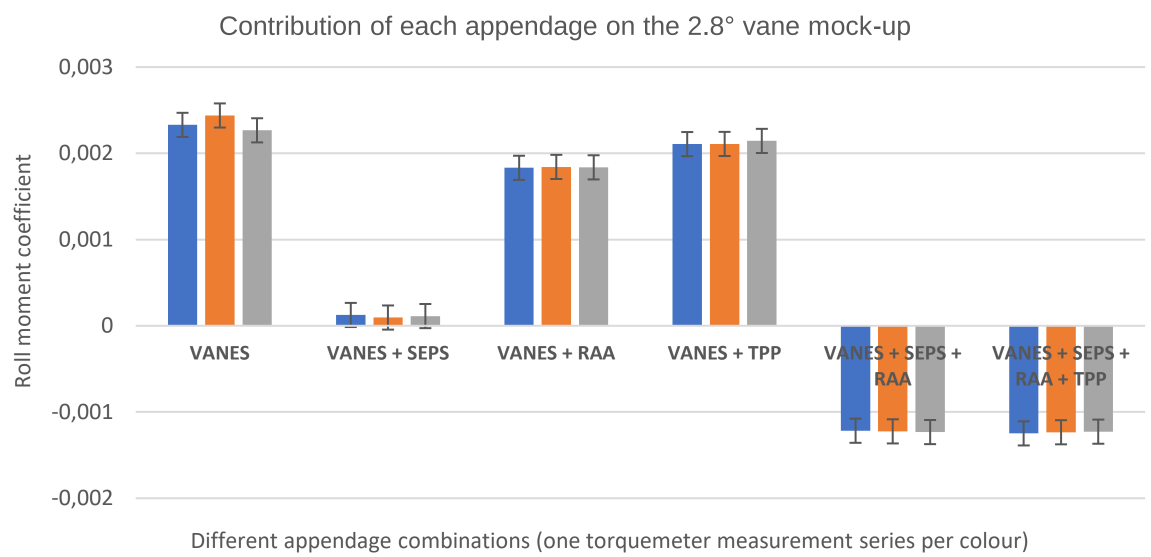

Figure 4.14: Roll moment of 2.8° vane mock-up equipped with each appendage and their combination

According to Figure 4.13, for a 6.8° angle of vane inclination, the tests of each appendage on the vane mock-up show that each appendage reduces slightly the roll moment produced by the vanes. This suggests that each appendage produces a moment in the opposite direction, with however an amplitude smaller than the one produced by the 6.8° vanes. The TPP is a small piece so its effect appears negligible. We can see that the roll moment is reduced most by adding the SEPS as observed on the following three configurations: i)

SEPS, ii) SEPS_RAA and iii) SEPS_RAA_TPP. There are three SEPS and four RAA mounted on the probe. Thus, it is observed that the reduction of the roll moment (on the mock-up equipped with 6.8° vanes) is due to the presence of the SEPS and the RAA. The same data are plotted in Figure 4.14 for a 2.8° angle of vane inclination. The same conclusions can be drawn concerning the effects of the appendages. But, due to a lower induced roll moment by this vane inclination (2.8°), **what is important to note here, is that the reversed roll moment induced by the SEPS and RAA combination leads to a negative roll moment**.

The relative roll moment coefficients with respect to the bare mock-up or the vane-equipped mock-up were calculated for RAA or/and SEPS and are plotted in Figure 4.15. The two zero values, which are different for the bare mock-up and for the vane mock-up, have been plotted at the same level in the figure to better visualize the influence of the appendages. It can be concluded that the presence of the vanes intensifies the reversed roll moment induced by SEPS+RAA. Our interpretation is that the flow deviation induced by the vanes modifies the flow direction experienced by the combination of SEPS+RAA, which consequently modifies the aerodynamic forces exerted on these appendages.

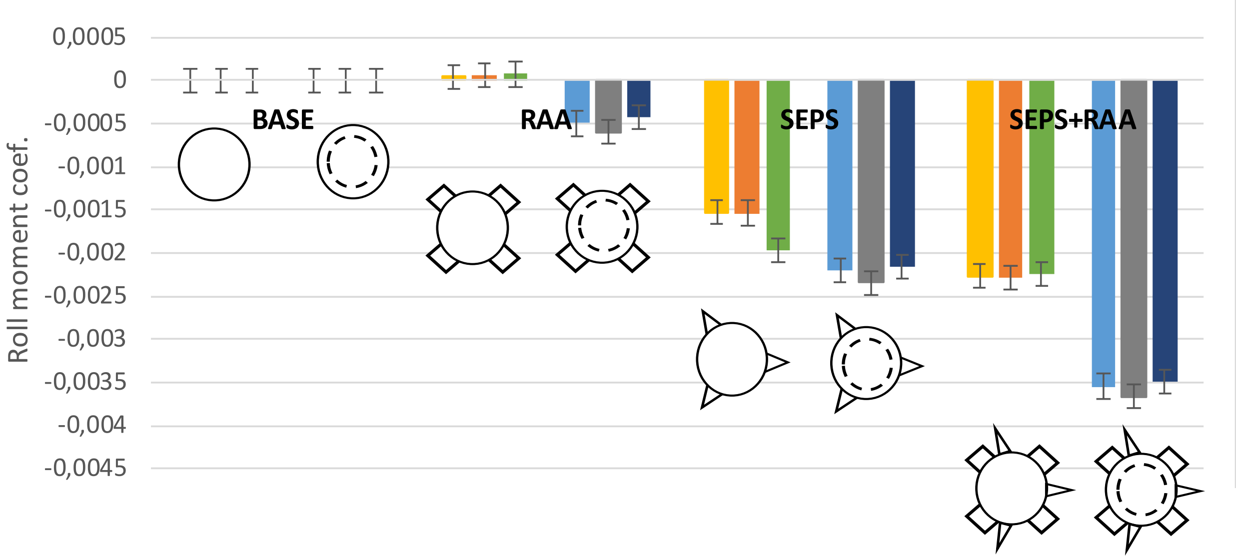

Figure 4.15: Relative roll moment coefficients with respect to the bare mock-up (empty circle) or the vane-equipped mock-up (two circles, one of which is dotted) with each appendage and their combination. Note that, for best visualizing the relative effects of the appendages, the zero values for the bare mock-up and for the vanes mock-up, although different, are plotted at the same level.

The above results suggest non-linear interactions between vanes and appendages, and more particularly for the SEPS and RAA different geometrical combinations. Their respective contribution to the roll moment does not add up in a simple linear way. Indeed, two different close configurations of RAA and SEPS exist on the probe as shown in Figure 4.16. Moreover, it has to be noted that the SEPS cable is not modelled here because it has proved too difficult to represent it accurately at this scale. Finally the flow in the vicinity of the two devices, for the two configurations when they are close together, the gap in the space between the two being different for the two configurations, leading to different contributions to the roll moment. This can be visualized in the PIV results presented in Figure 4.17.

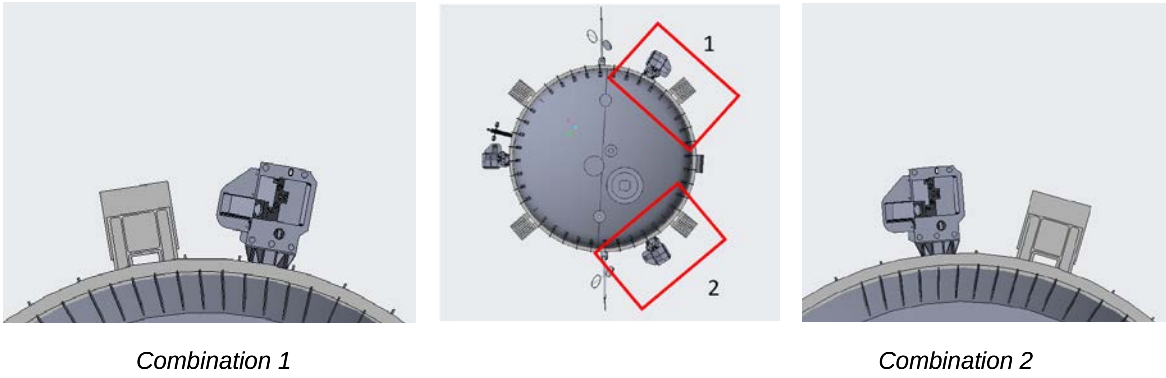

Figure 4.16: The two set-up for RAA and SEPS combination

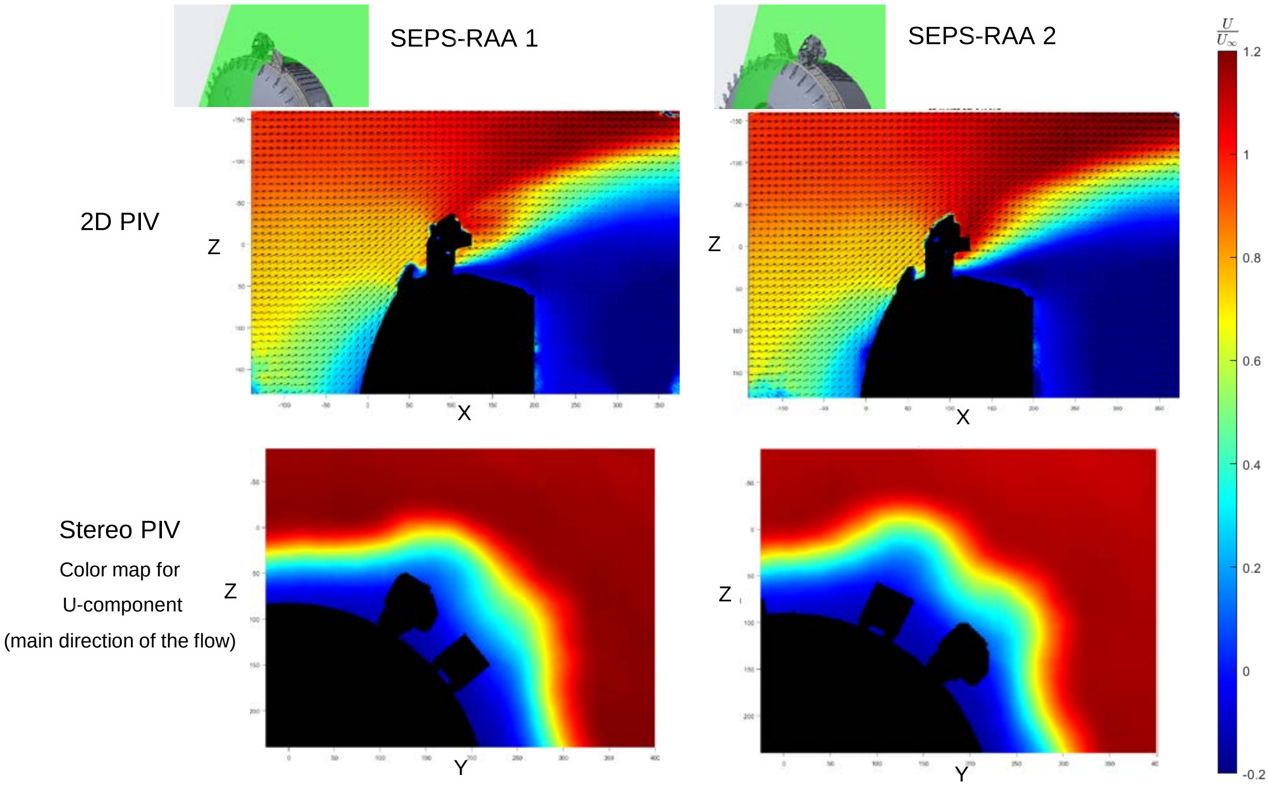

Figure 4.17: Flow visualisation from PIV for the two different combination of SEPS and RAA.

4.4.2 Effects of HASI booms

The roll moment coefficient induced by different HASI boom positions for the mock-up with vanes only and the mock-up equipped with vanes, RAA, SEPS is plotted in Figure 4.18. Two consecutive letters describe the respective position of each boom. The first letter is for the B1 boom and the second one for the B2 boom. C, O and I stand for closed, full open and intermediate positions respectively. Small sketches are also added to illustrate the two different boom configurations.

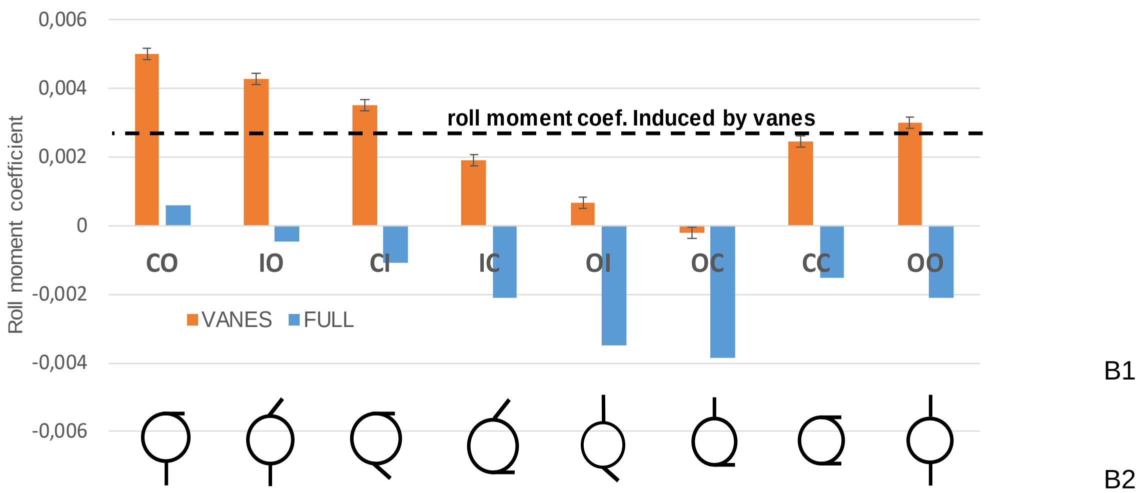

Figure 4.18: Roll moment contribution of 2.8° vane mock-up (orange) and full equipped mock-up (blue) with different configurations of the two HASI booms

When both booms were closed (CC) or open (OO), they have a very small influence on the roll moment, as per design. Assymetric opening of booms increases or decreases the roll moment, depending on which boom is partially or not deployed. When B1 is open and B2 is closed (OC), we can see that the roll moment is reduced, while it is increased when B1 is closed and B2 is open (CO). Configuring both the HASI booms in the same opening leads to induce moments that counter each other. The vanes control the probe spin in the expected direction. This means that one of the booms will induce a moment that will counter that of the vanes. And the other boom will induce a moment that will further add to that of the vanes.

According to this result, whereas the deployed boom B2 produces a moment in the same direction as that of the vanes (positive), the boom B1 produces a moment in the opposite direction (negative).

The intermediate positions of HASI booms affect the roll torque with an intermediate value of the roll moment. As it is suspected, as inferred from the analysis of the science data, that at least one HASI boom did not deploy nominally at the top of the descent, those measurements may help to assess the aerodynamic effects of the non-nominal boom deployment. Indeed, the non-deployment of boom B1, or even its partial deployment, could be an explanation for, or have contributed to, the reversed roll moment at the top of the descent.

The presence of the HASI booms with other appendages (blue bars) does not change significantly these results, regardless their position. The roll moment is then globally lower than the roll moment for the vane mock-up with only vanes, even negative. So, those results also suggest that that the presence of all fixed appendages produces a moment opposite to the one produced by the vanes as well illustrated in Figure 4.15.

4.5 Angles of attack effects for the full-equipped mock-up

In this section, a few results are shown concerning the effects of spin (α-angle) and sideslip (β-angle) angles on aerodynamic loads for the full-equipped 2.8° vane mock-up. They complement those presented previously in the section 4.2 (Bare mock-up characteristics and DISR camera effects).

As the bare mock-up, the fully-equipped mock-up remains not symmetric according to its main revolution axis (X). The main appendages, which causes this asymmetry, are the TPP, the SEPS nearby TPP and the camera DISR. Both HASI booms also introduce asymmetry. Moreover, whereas the full mock-up with two booms deployed vertically with respect to the wind tunnel floor (corresponding to the case α= -4º) is not symmetrical with respect to the (Xw, Zw) plane, the full mock-up with two booms deployed horizontally (corresponding to α= -94º) could appear quasi-symmetrical with respect to β-angle variation.

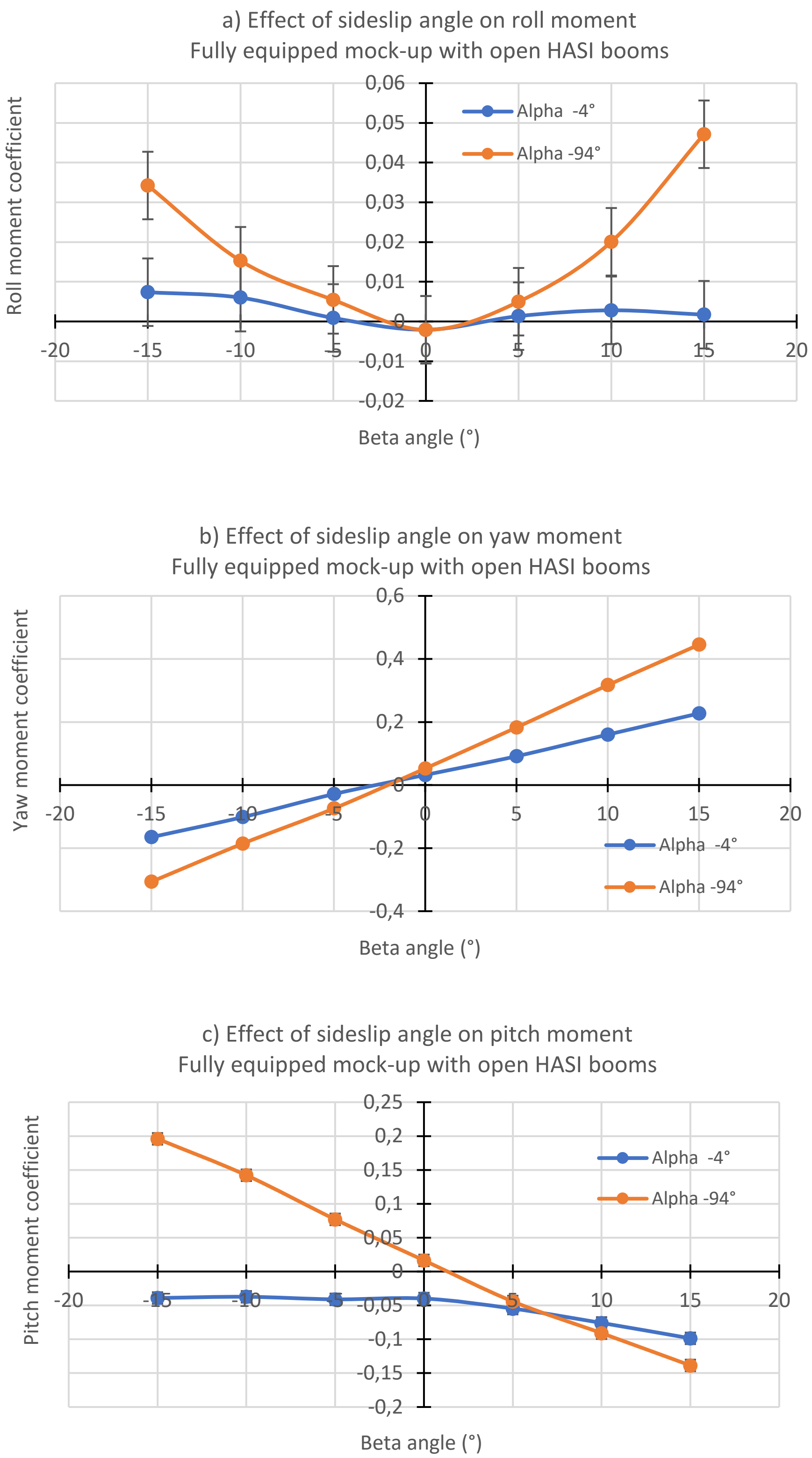

Figure 4.19: Aerodynamic moments of full mock-up with booms deployed vertically (α = -4°) and horizontally (α = -94°) against sideslip angle effect

The three aerodynamic moments measured by the balance are plotted in Figure 4.19. By adding the appendages and the open HASI booms, in comparison with the bare mock-up configuration presented in Figure 4.9, it can be observed that:

- the moment magnitudes are slightly higher than those obtained for the bare mock-up
- the moment variations of the value of the three moments against the sideslip angle for the two spin angles of -4° and -94° are the same as those previously observed for the bare mock-up.

It suggests that the aerodynamic behavior of the fully-equipped mock-up as a function of the angles of attack is quite similar to that of the bare mock-up including a DISR camera head model.

5 Comparison with results from Vorticity Ltd

One task in the present work was to make a comparison between the wind tunnel test results obtained during our study and those obtained by (Ltd VORTICITY 2015). We have selected the most relevant cases for comparison. Details are provided in appendix 4. As the tested specimens (SM2 and our mock-up) are quite different in their relevant details, the comparison focuses on a qualitative interpretation of the only two parameters that can be compared: i) the spin direction: clockwise (c/w) and anti-clockwise (a-c/w) rotation as defined in Figure 3.11; and ii) the HASI boom effects. The Radar Altimeter antennae were omitted on the SM2 configuration, while they were included in our study. They were found to have a significant effect.

The wind tunnel tests in (Ltd VORTICITY 2015) were performed at the Von Karman Institute with the SM2 original model (see Figure 5.1) mounted on a low-friction air bearing. About half of the tests performed included a non-flight item mounted on the SEPS. The comparison confirms that the SEPS produce a negative torque of a magnitude comparable to that created by the 2.2° vanes mounted on the SM2. The 2.8° vanes we used in our work produces a higher negative torque. Each of the HASI booms produces a torque of the same magnitude to that produced by the vanes, but of opposite sign. When both booms are either closed or open, they do not produce a measurable torque (as per design). It should also be noted that in the Vorticity study, the designation of the HASI booms (HASI-2-CON for B1 and HASI-1-PRO for B2) is inverse to the one used in our work; the latter configuration was validated with pre-flight documentation and pictures of the hardware.

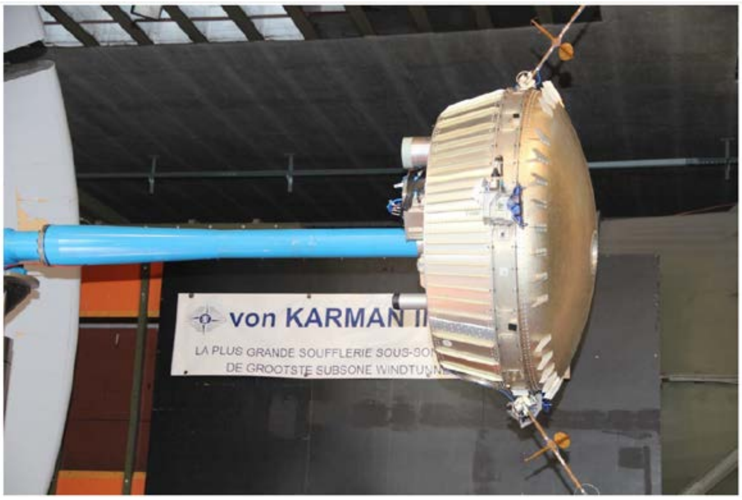

Figure 5.1: SM2 model in the wind tunnel at the Von Karman Institute (from (Ltd VORTICITY 2015)).

The following observations can be drawn from comparing both experimental works:

- The vanes, whether at 2.2° or at 2.8°, produce a torque in the expected direction
- The Separation Subsystem (the 3 SEPS) produce a torque of the same magnitude but opposite to that produced by the vanes
- The effect of the HASI booms in different configurations (closed, open) show clear trends:
  - HASI boom B1 (HASI-2-CON in Vorticity nomenclature) produces a moment opposite to that produced by the vanes.
  - HASI boom B2 (HASI-1-PRO in Vorticity nomenclature) produces a moment of the same sign to that produced by the vanes
  - When both HASI booms are fully deployed, or fully closed, they produce no significant torque
- Our work shows that the RAA, although flat plates, produce a torque opposite to that of the vanes. This is attributed to the fact that the flow impinging of the flat RAA antennae is deviated by the vanes.
- While the SM2 behavior was reproduced in our study, it was not in Vorticity's study, one possible reason being that the RAA were not mounted on the SM2 during the VKI wind tunnel tests.

6 Rotational aerodynamic modeling

Although the main effort of this work was an experimental study, a group of students started to implement and exploit an analytical model of rotational dynamics of the probe in order to bring complementary information to the understanding of this spin anomaly and to decipher the effects of each appendage and of different combinations of them.

The first part of their work, based on experimental results, was to analyze, to study and to implement the main approaches proposed by Aerospatiale (AEROSPATIALE 1993), (EADS report 2005), and Vorticity Ltd (Ltd VORTICITY 2015) in order to retrieve previous modeling results (see reference R5). Some results presented in reference R5 confirm trends and findings presented in (Ltd VORTICITY 2015).

In a second part, another rotational dynamic model has been developed to calculate the roll moment induced by the different appendages without using experimental data to calibrate aerodynamic models of the different appendages. This last approach is based on the decomposition of the appendages (DISR, SEPS, RAA, HASI BOOMS...) into elementary lifting surfaces from their respective CAD drawings (see reference R5). However this approach proved to be too complex to implement and to validate it in the time available and has not been fully completed.

Subsequently an other group of students further looked into the first approach and studied detailed aspects, and the limits, of both Aerospatiale and Vorticity models (see reference R7).

Concerning the first approach, it consists in solving the fundamental principle of dynamics of rotation:

$$\mathrm{I_{xx}}\frac{d\omega}{dt} = \sum_k \mathrm{M_k}\,(\omega)$$

where $\mathrm{I_{xx}}$ is the probe's moment of inertia about its axis of symmetry, ω is the probe's rotational rate about its axis of symmetry and $\mathrm{M_k}$ models the contribution of the protuberances k (vanes and appendages), including also moments induced by aerodynamic damping and swivel friction. In (AEROSPATIALE 1993) and (Ltd VORTICITY 2015), one can find different expressions of the term $\mathrm{M_k}$ depending on the induced torque being modelled. In the above equation, it is assumed that the various torque contributions are additive.

In (Ltd VORTICITY 2015), another approach is based on experimental data to calibrate specific coefficients for each $\mathrm{M_k}$. In this case, for all the protuberances, $\mathrm{M_k}$ is expressed identically as:

$$\mathrm{M_k}(\omega) = \frac{1}{2}\rho V^2 r\left(\alpha_k - \frac{\omega r}{V}\right)(kS)_k$$

where r is the radius of the probe, α_k the incidence angle of the term k and $(kS)_k$ the product of the lift curve slope times the reference area characterizing the aerodynamics and geometry of the term k.

Experimental data obtained during this work (see Figure 4.14 and Figure 4.15 for example) can be used to determine such coefficients related to aerodynamics and geometry of the appendages. With this approach, it is possible to take into account some aerodynamic interactions, between RAA, SEPS and vanes, as illustrated in Figure 4.15. Instead of assuming additive contributions of protuberances to the resulting torque, one single term of $\mathrm{M_k}$ can be calibrated for the configuration studied. For example, in Figure 6.1 are plotted the real and expected spin profile and values of the spin rate obtained by the iterative resolution of the above equation of dynamics of rotation, for an altitude of 60 km corresponding to a descent speed of 25 m/s. $\mathrm{M_k}(\omega)$ has been calculated using either (AEROSPATIALE 1993) and (Ltd VORTICITY 2015) expressions, or using one single term for RAA, SEPS and vanes. Figure 6.1 highlights an important trend, which is that the modelling also shows that taking into account the aerodynamic interactions between the different protuberances makes it possible to better account for the spin rate profile along the descent.

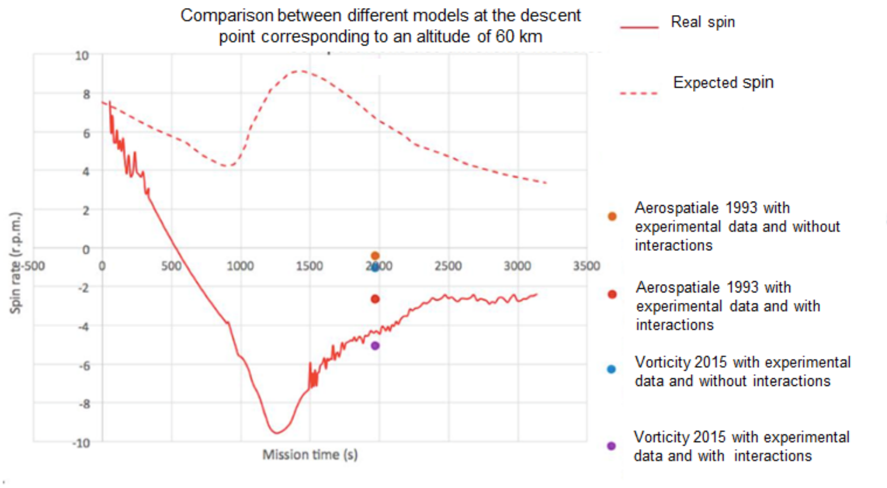

Figure 6.1: Comparison of different models to spin rate prediction by including or not one single term to take into account the interactions between appendages (see reference R7)

7 Discussion

The experimental work performed during our study was based on wind tunnel tests with of a modular 1:3 scale mock-up of the Huygens module that could be equipped in a modular way with fixed appendages and the HASI booms. The modularity allowed to test various configurations of the appendages that proved essential to understand the subtle aerodynamic effects of each of the individual appendages and of different combinations of them.

Our main findings are:

- The spin vanes work as designed (and also, as anticipated, the effect of 2.8° vanes mounted on the flight probe was higher than that of the 2.2° vanes mounted on the SM2 drop test model). We tested a wider range (0° to 6.8 °) in order to best understand their performances. The vanes create, in the range tested, a positive torque proportional to their inclination angle.
- The three SEPS create a negative torque of the same magnitude as that of the vanes.
- The Radar Altimeter Antennae create also a negative torque. This is attributed to the fact that the gas flow impinging on the flat antenna plates is deviated by the vanes.
- Both HASI booms create a torque of the same magnitude, but of opposite sign.
- One of the HASI booms in the deployed configuration creates a positive torque comparable in magnitude to the one created by the vanes, while the other HASI boom creates a positive torque of the same magnitude.
- Both HASI booms in stowed configuration (they are then placed in the separated wake flow) or in the deployed configuration (they are placed in the undisturbed flow) do not create a measurable torque as per design.
- The negative torque created by the SEPS and the RAA combined is higher than the linear sum of the individual torques due to the complex interaction between the SEPS, the RAA, and the airflow deviated by the vanes.
- Although not completely conclusive on that point, our work strongly suggests that the anomalous spin of the SM2 is due to the combined effect of the vanes, the SEPS and of the RAA.
- A limited set of Angle of Attack wind tunnel studies have shown that the DISR camera head produces a noticeable effect of the spin. But it could not be fully characterized, because the camera head design was not fully representative. As this is a finding which was not anticipated, the DISR camera head was designed as a fixed appendage.
- The rapid deviation of the spin profile of Huygens under the main parachute, and its reversal within 10 min of descent, can most likely be attributed to the combined effect of the SEPS, the RAA, and the anomalous deployment of one of the HASI booms. The non-deployment of one HASI boom under the main parachute was postulated by the science team early on during the science data analysis phase, with no possibility to identify which one was not deployed.
- In parallel with experimental wind tunnel tests, modeling work was carried out to replicate the wind tunnel tests results and apply them to the modeling of both the SM2 and Flight probe behavior. This part of the work proved to be more challenging than expected and is not complete.
- As the current understanding of the results of the HASI science data does not support the hypothesis that the non-deployed boom did not deploy for the whole descent, the major reason for the anomalous Huygens spin profile under parachute in Titan's atmosphere of Huygens can most likely be attributed to the combined effect of the SEPS and RAA. However there is evidence in several engineering and science data sets that the aerodynamic configuration of Huygens changed during the descent, in particular around and after parachute exchange at high altitude.
- No firm conclusion can yet be drawn from our work regarding the full deployment history of the HASI booms, but our results provide solid inputs for further studies on this remaining open question. But our results allow to confirm with good confidence the hypothesis that one HASI boom was not deployed nominally at the start of the descent under the main parachute.
- The results of our study provide a good reference to further study the correlation of the various science measurements and the dynamic history of the probe descent attitude and spin. Further analysis is on-going (outside of this contract) to address this issue.

During the development of Huygens, several WT campaigns were carried out with different mock-ups, with an emphasis to validate various designs of the vanes and to characterize their effects on the spin. Part of our work was dedicated to reviewing the relevant Huygens archived documentation. The most representative Huygens development WT tests were the WT11 (1992) and WT13 (1993). WT11 included an early vane design and HASI booms mock-up (unfortunately designed in a way that they would not produce a measurable spin torque). WT13 included the 36 vanes, three SEPS (but whose geometry was not fully representative), the four Radar Altimeter Antenna and more representative mock-ups of the HASI booms than in WT11. The analysis of the WT13 data clearly pointed out to the need for further WT tests with a mock-up more representative of the flight configuration. Such a test (WT17) initially included in the Huygens test plan was unfortunately cancelled, mainly for cost reasons. Unfortunately neither a flight representative SM2 configuration, nor a representative configuration of the Huygens probe were tested prior to flight.

The spin anomaly experienced by the SM2 balloon drop test (1995) was not noticed at the time of the test data analysis and interpretation (1996). It was only identified in 2005 a few months after the Huygens mission was over in the course of a traineeship work whose task was to do a comparative evaluation of the Huygens and SM2 descent performance under parachute.

The evaluation of the Huygens spin anomaly carried out by industry in 2005/2006 explored several possible causes of the spin anomaly, primarily reversed spin vanes and effects of the HASI booms. They also identified that the SEPS could have played a role, but no detailed study was undertaken. No conclusion could be reached as to the reasons of the spin anomaly and it was then recommended to conduct additional WT tests to study further the spin anomaly. As it took 8 years to implement such a study, some of the knowledge of the details of the Huygens design were hard to find.

In 2013, ESA placed an industrial contract to reevaluate the overall Huygens engineering entry and descent performances. This requested work included further investigations of the spin anomaly. The study, led by Vorticity, included WT testing in the Von Karman Wind Tunnel facility near Brussel. Those tests used the SM2 with fixed vanes (2.2° angle), that could be instrumented with the HASI boom engineering units (HASI booms were not part of the SM2 drop test) that could be either stowed or fully deployed. The SEPS could be either un-mounted or mounted. The radar Altimeter Antennae were unfortunately not available for this study. Although most of the WT tests were carried out with non-flight “blue pieces” attached to the SEPS, they allowed to identify that the SEPS induced a torque contrary to the one induced by the vanes. But the SEPS results alone were not sufficient to satisfactorily reproduce both the SM2 and the Huygens spin profiles. The study recommended to perform a more comprehensive wind tunnel test program. Such a detailed study was the object of the contract subject of this report.

8 Conclusion

This report provides a description of the work carried out in the framework of an ESA contract with CNRS Orleans to further study the spin anomaly of Huygens during its descent under parachute to the surface of Titan in January 2005, but also the spin anomaly of the Huygens mock-up (called SM2) that was dropped from a stratospheric balloon in 1995. The experimental work was conducted in the subsonic wind tunnel of the University of Orléans PRISME laboratory. All the wind tunnel tests, the analysis and interpretation of the results were made in the framework of academic projects that involved students primarily from Polytech, the Engineering school of the University of Orleans, but also students from the Universities of Grenoble and Orsay, and from the Ecole de L'Air et de l'Espace in Salon de Provence, France.

Static WT (wind tunnel) tests were carried out on a scale 1:3 mock-up of the Huygens descent module that could be equipped with spin vanes and all appendages that are assumed to have contributed to the overall spin torque. Different configurations of the vanes were used as the Huygens vanes and the SM2 vanes were different (inclination angle respectively of 2.8° and 2.2°). The different vane models used and the appendages were designed to be removable and mounted in different combinations as to allow to study their individual effects, but also their combined effects. A large database of more than 300 Wind Tunnel data was accumulated and archived. The effect of the Angle of Attack was also studied by varying the orientation of the mock-up with respect to the incoming gas flow.

Significant progress has been made in the characterization of the effects of all the appendages and the understanding of the spin anomaly and its possible causes, but no solid conclusion was drawn on the deployment profile of the HASI booms.

Recommendation: In this study, all the wind tunnel tests were carried out as static tests. In order to confirm our results and to go further into the analysis of the boom configuration changes, it is recommended to consider carrying out a dynamic tests of the two flown descent module configurations: i) The SM2 with 2.2° vanes, the SEPS, the RAA; ii) the Huygens flight probe with 2.8° vanes, the SEPS, the RAA, the DISR camera head, and the HASI booms with the capability to partially deploy them, in addition to being is a stowed or fully deployed configuration.

The ONERA vertical wind tunnel in Lille, France, which was approached during the study, has been identified as a suitable facility for such tests. Huygens development tests were carried out in that facility in the early '90s.

Lessons Learned: An excellent compilation of the Huygens lessons learned was published in 2017 (Lorenz, 2017). Our study further contributes to the lessons learned, and show that more lessons can still be learned from the deep analysis of the Huygens engineering and science data set. Our study benefited from a good archiving of the science and engineering data (https:// https://www.cosmos.esa.int/web/psa/huygens), and of the technical documentation, most of it in paper form.

9 References

AEROSPATIALE. «Huygens Program, Phases B2/B3, Aerdoynamic studies.» *Technical report, HUY-AS/m-120-TN-0009*, 1992.

AEROSPATIALE. «Huygens Program, Wind tunnel test (WT12) analysis and spin rate performances.» *Technical report, HUY-AS/m-120-PL-0005*, 1993.

AEROSPATIALE. «Huygens Program: Analysis of the descent module spin rate during SM2 test.» *Technical report, YX/AA N° 119 683*, 1996.

Béghin, C, et al. «A Schumann-like resonance on Titan driven by Saturn's Magnetosphere possibly revealed by the Huygens Probe.» *Icarus* 191 (2007): 251-266.

Couche, Simon, et al. «Further aerodynamic characterization of the ESA huygens probe and its appendages: a combined testing and modeling approach.» *16th annual International Planetary Probe Workshop IPPW-2019, July 8-12.* University of Oxford, Oxford, 2019.

EADS, Huygens Program: Entry and Descent Level 0 Post-Flight Analysis, Technical Report, HUY.EADS.MIS.TN.0006, October 2005

Hamelin, Michel. «Note about the possible effect of HASI-PWA booms on the Huygens rotation during the descent in the atmosphere of Titan and planned wind tunnel tests.» *unpublished*, 2012.

Hamelin, Michel, et al. «Electron conductivity and density profiles derived from the mutual impedance probe measurements performed during the descent of Huygens through the atmosphere of Titan.» *Planet Space Science* 55 (2007): 1964-1977.

Jäkel, E, P Rideau , P.R. Nugteren, et J Underwood . «Drop Testing of the Huygens Probe.» *ESA Bulletin*, 1996.

Kazeminejad, B., D.H. Atkinson , M. Pérez-Ayucar , J.P. Lebreton, et C. Sollazzo. «Huygens entry and descent through Titan's atmosphere - Methodology and results of the trajectory reconstruction.» Édité par DTWG. *Planetary Space Science* 55 (2007): 1845-1876.

Lebreton, Jean-Pierre. «An overview of the descent and landing of the Huygens probe on Titan.» *Nature* 438, n° 90 (2005): 785-791.

Leroy, Annie, et al. «Detailed investigations of the Huygens spin anomaly in a subsonic wind tunnel.» *15th annual International Planetary Probe Workshop IPPW-2018, June 11-15.* University of Colorado, Boulder, 2018.

Leroy, Annie, et al. «ESA Huygens probe spin anomaly: new aerodynamic investigations in wind tunnel.» *Titan after Cassini-Huygens workshop, 23-25 September.* European Space Agency - ESAC, Madrid, 2019.

Leroy, Annie, et Jean-Pierre Lebreton. «Huygens Close-out activities.» *Mid-term Technical Report*, Decembrer 2018.

Lorenz, Ralph, HASI Boom Deployment Anomaly as Possible Explanation for Huygens Spin Behaviour, Presentation to the Huygens Science Working Team, June 2005.

Lorenz, Ralph: Huygens Probe: A Retrospective and Lessons for the Future, 2017, 2017 IEEE Aerospace Conference. **DOI:** 10.1109/AERO.2017.7943716

Ltd VORTICITY. «Huygens flight performance validation.» VOR-RE-1507 (November 2015).

Pérez-Ayucar, Miguel, A. Sarlette, P. Couzin, T. Blancquaert, O. Witasse, et J.-P. Lebreton. «Huygens attitude reconstruction based on flight engineering parameters.» *3rd annual International Planetary Probe Workshop IPPW-2005,.* Athens, Greece, 2005.

Sarlette, A, Miguel Pérez-Ayucar, Olivier Witasse, et Jean-Pierre Lebreton. «Comparison of the Huygens mission and the SM2 test flight for Huygens attitude reconstruction.» *3rd International Planetary Probe Workshop IPPW-2005.* Anavyssos, Greece, 2005.

Thébault, Guillaume, Julien Simier, Annie Leroy, Philippe Devinant, Stéphane Loyer, et Jean-Pierre Lebreton. «Testing of an instrumented Huygens mock-up in a subsonic wind tunnel: 1st campaign and preliminary results.» *15th annual International Planetary Probe Workshop IPPW-2018, June 11-15.* University of Colorado, Boulder, 2018.

Tran, Ph, G Pinaud, et S Perez. «Huygens Program - Entry and descent, level 0, Post-flight analysis.» EADS Report, HUY.EADS.MIS.TN.0006, 2005.

Additional references under restricted dissemination conditions are the students ‘internship reports or academic projects:

R1 - Lucas METHIVIER from the University of Grenoble, *Design of the mock-up (Analysis of the possible test conditions, CAD model, 3D-printed appendages)*, May-July 2017.

R2 - Guillaume THEBAULT and Julien SIMIER from POLYTECH Orléans engineering school, *Aerodynamic characterization of the model with and without appendages at zero angle of attack*, January-March 2018.

R3 - Trong Binh VU from the University of Orsay, *Aerodynamic characterization of the model with and without appendages at different angles of attack*, May-July 2018.

R4 - Armand BERAUD, Simon COUCHE and César DE TIENDA from POLYTECH Orléans engineering school, *Further aerodynamic characterization of the 1/3rd mock-up of the ESA HUYGENS probe and its appendages*, January-March 2019.

R5 - Léo KOVACS and Rémy JOCHMANS from POLYTECH Orléans engineering school, *Development of a dynamic simulation for the study of the ESA HUYGENS probe*, January-February 2019.

R6 - Maxime BOYER from POLYTECH Orléans engineering school, *Aerodynamic study of a HUYGENS probe mock-up by PIV testing*, April-June 2019.

R7 - Thomas MORDEC and Guillaume SERMET from the Ecole de l’Air (French Air force Academy), Investigations sur l’anomalie de rotation détectée lors de la descente sous parachute de la sonde Huygens, December 2019.

10 Acknowledgments

This work was carried out under ESA contract under the responsability of Nicolas Altobelli. Continuous support from Miguel Perez-Ayucar on all aspects of the project is heartfully acknowledged.

Many people contributed or provided support to the study. First, we would like to acknowledge all the students that did a fantastic work: Armand Beraud, Maxime Boyer, Simon Couche, Cesar De Tienda, Remy Jochmans, Leo Kovacs, Lucas Methivier, Thomas Mordec, Guillaume Sermet, Julien Simier, Guillaume Thebault, Trong Binh Vu. Thanks for your great work. We enjoyed working with you all.

It's a real pleasure to acknowledge Stéphane Loyer, who operates the wind tunnel facility, for his continuous support and tutoring of the students during the experimental work. Academic advice provided to the students by Philippe Devinant, especially for the modeling work is gratefully acknowledged.

We expressed our thanks to Ralph Lorenz for his dedication to the project and for his various advices on many technical issues, including on aerodynamics, and for his contribution to the interpretation of various Huygens science measurements of relevance to the spin issue.

We acknowledge the active participation to the study of the following members of the HASI team: Francesca Ferri, Michel Hamelin, and Christian Béghin, for their help to progress in the understanding of the HASI booms deployment scenarii.

Thanks to John Underwood and Aurélien Hugon from Vorticity for their participation to the mid-term review, who provided useful comments and advices, and to Sébastien Paris, from the Von Karman Institute, for his help to dig out information on the vane design and on the tests carried out at VKI.

Thanks also to the following members of the Huygens industrial team who always responded kindly to various requests on the 25+ years old Huygens design: Patrice Couzin, Michel Pastorino, Eric Blanc, Anne-Marie Schippers, all now from Thales Alenia Space, Cannes.

Finally, we want to recognize the friendly and continuous support of Olivier Witasse who provided advices all along the study and who helped us to go through the 25-30 years old Huygens archived documentation at ESTEC.

Appendix 1

Details for experimental set-up and load measurement protocol

1 Aerodynamic load balance

Measurement ranges:

Lift (vertical Z-axis):	0-150DaN	(measured from a combination of three strain gauges)
Drag (longitudinal X-axis):	0-50DaN	(measured from one main strain gauges)
Side force (transverse Y-axis):	0-50DaN	
Moments:	0-30DaN.m	

Load measurement errors for the set-up are estimated as follows:

- Drag force maximum uncertainty: ±0.16 N
- Lift force maximum uncertainty: ±0.47 N
- Uncertainty of the differential pressure sensor (Pitot probe located upstream of the modeled to calculate the free-stream velocity): ±1Pa
- Uncertainty on the test-section temperature: negligible
- Uncertainty on the atmospheric pressure: negligible

Drag

For test dimensioning, the main force to be considered is the drag. It is therefore important to estimate it considering the balance limitations. The drag force is defined by:

$$F_X = \frac{C_D\, \rho\, V^2 S}{2}$$

- 1/3rd mock-up surface $S = 0.16\, m^2\ without\ appendages$
- Air density $\rho = 1.225\, kg.m^{-3}$ at $T = 15°C$
- Wind tunnel maximum velocity V: $55\ m/s$
- Drag coefficient C_D

The geometry of the probe can be compared as a first approximation to a semi-spherical ($C_D = 0.42$) or a disk ($C_D = 1.1$) geometry. Consequently, the drag force is calculated with multiple C_D values.

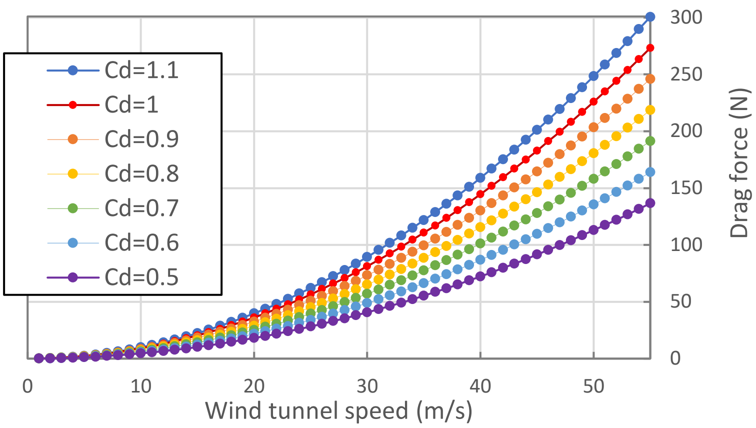

Figure 1: Drag force according to wind tunnel speed

In the worst case, this shows a maximum drag force of 301 N, which is largely below the 500 N limit not to exceed. Consequently, even with appendages, the mock up should not have any test restrictions regarding to the drag force during the wind tunnel campaign.

The aerodynamic load balance will measure the moment induced by the drag at the base of the mast holding the mock-up. This moment must not exceed 300 N.m. The drag moment depends on the height of the mast

$(H = 1.175m)$ and the drag force calculated above as shown in Figure 2 and is plotted in Figure 3. A maximum moment value of 353 N.m is obtained with $C_D = 1.1$ at 55 m/s. Considering the balance specifications, the tests have to be conducted below 50 m/s.

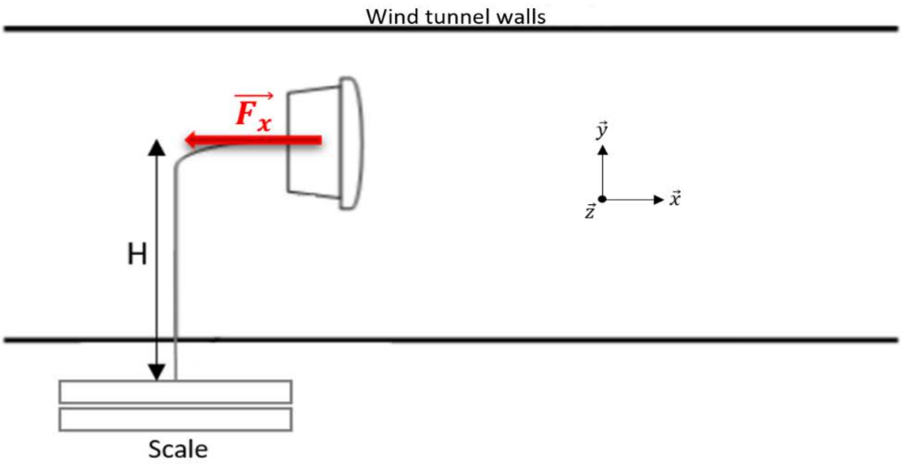

Figure 2: Mock-up in the wind tunnel

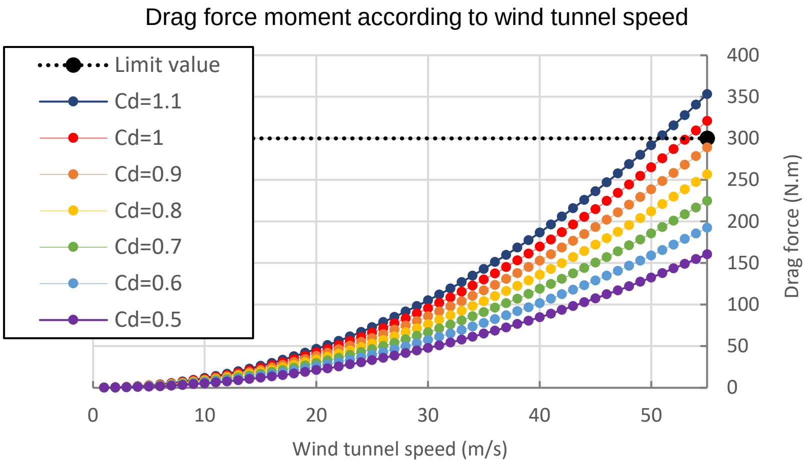

Figure 3: Drag force moment according to wind tunnel speed

2 Blockage effects

In order to determine the diameter of the mock-up, blockage effects in the test section have been considered. The blockage effect is commonly defined by calculating the ratio between the frontal surface of the mock-up and the section test area. For a 1/3 mockup of the probe, the mockup has a resulting diameter of about 0.45 m. The blockage ratio value obtained is of 4%. As the blockage ratio is lower than 5%, we can consider that there is no blockage effect, meaning that it is not necessary to apply any specific corrections on measurement.

$$S_{mock-up} = \pi \left(\frac{0.45}{2}\right)^2 = 0.160\ m^2 \qquad \rightarrow \qquad \frac{S_{mock-up}}{S_{test\ section}} = \frac{0.16}{4} = 4\ \%$$

3 Wind and body frames

The probe motion during its descent under parachute experienced at the same time a pendular motion and a spin motion. To express forces and moments in the probe frame from those measured by the balance, two rotations have to be taken in account. The first one is a pendular motion which expresses the angles of attack of the wind impacting the probe: β-angle (yaw or sideslip angle). The second is a spin motion defined by α-angle. The β and α angles were chosen in the indirect direction for convenience. *See Figure 3.14: Sign convention for rotation angles of the mock-up with respect to the wind reference frame*

The wind frame (subscript w):

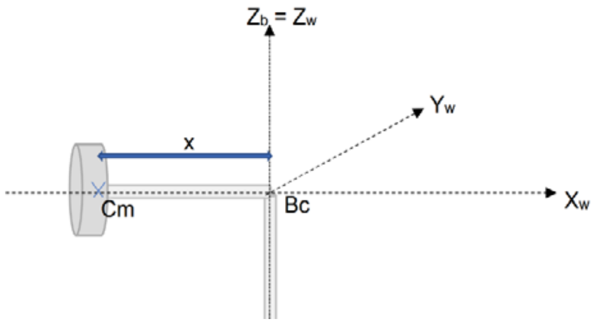

Figure 4: Wind reference frame

In the wind frame, we noted the 6 components of the aerodynamic loads (force and moment):

- The three aerodynamic forces consist of Drag (D), Crosswind force (C) and Lift (L)

$$\vec{F} = \begin{pmatrix} D \\ C \\ L \end{pmatrix}$$

- The three force moments consist of Roll moment (RM), Pitching moment (PM) and Yaw moment (YM) with respect to the geometrical center of the balance (Bc)

$$\vec{M} = \begin{pmatrix} RM \\ PM \\ YM \end{pmatrix}$$

The probe frame (subscript p):

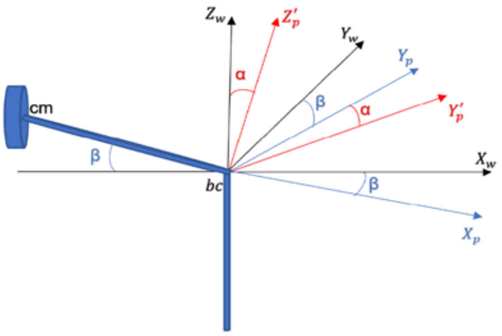

Figure 5: Body reference frame

In the body frame, we get the 6 projected components of aerodynamic loads (force and moment):

- The three forces consist of Axial force (A), Side force (S) and Normal force (N)

$$\vec{F} = \begin{pmatrix} A \\ S \\ N \end{pmatrix}$$

- The three moments consist of Axial force Moment (AM), Side force Moment (SM) and Normal force Moment (NM) with respect to the mass center of the mock-up (cm)

$$\vec{M} = \begin{pmatrix} AM \\ SM \\ NM \end{pmatrix}$$

The mass center of the mock-up has been approximated with the geometrical center of the bare mock-up without considering the DISR camera in a first approach.

Moments are initially measured with respect to the geometrical center of the balance (bc). In order to calculate them with respect to the mock-up geometrical center (cm) in the body frame, two sucessive operations are necessary. The first operation consists in converting the wind frame to the body frame with two rotations.

$$(X_w; Y_w; Z_w) \xrightarrow{\beta \text{ rotation around } Z_w \text{ axis}} (X_p; Y_p; Z_w) \xrightarrow{\alpha \text{ rotation around } X_p \text{ axis}} (X_p; Y'_p; Z'_p)$$

Transformation β rotation matrix : $P_\beta = \begin{pmatrix} cos\beta & -sin\beta & 0 \\ sin\beta & cos\beta & 0 \\ 0 & 0 & 1 \end{pmatrix}$

Transformation α rotation matrix : $P_{\beta\alpha} = \begin{pmatrix} \cos(\beta) & -\sin(\beta) & 0 \\ \cos(\alpha)\sin(\beta) & \cos(\alpha)\cos(\beta) & -\sin(\alpha) \\ \sin(\alpha)\sin(\beta) & \sin(\alpha)\cos(\beta) & \cos(\alpha) \end{pmatrix}$

With the transformation matrix $P_{\beta\alpha}$, the force and moment components in the body frame can be calculated:

$$\begin{pmatrix} A \\ S \\ N \end{pmatrix} = P_{\beta\alpha} * \begin{pmatrix} D \\ C \\ L \end{pmatrix} = \begin{pmatrix} Dcos(\beta) - Csin(\beta) \\ Dcos(\alpha)\sin(\beta) + Ccos(\alpha)cos(\beta) - Lsin(\alpha) \\ Dsin(\alpha)\sin(\beta) + Ccos(\alpha)cos(\beta) + Lcos(\alpha) \end{pmatrix}$$

$$\begin{pmatrix} AM \\ SM \\ NM \end{pmatrix}_{bc} = P_{\beta\alpha} * \begin{pmatrix} RM \\ PM \\ YM \end{pmatrix} = \begin{pmatrix} RMcos(\beta) - PMsin(\beta) \\ RMcos(\alpha)\sin(\beta) + PMcos(\alpha)cos(\beta) - YMsin(\alpha) \\ RMsin(\alpha)\sin(\beta) + PMcos(\alpha)cos(\beta) + YMcos(\alpha) \end{pmatrix}$$

The second operation 2 consists in calculating moments on the mass center of the mock-up (cm):

Finally, the moment components at the mock-up mass center are :

$$\begin{pmatrix} AM \\ SM \\ NM \end{pmatrix}_{cm} = \begin{pmatrix} AM \\ SM \\ NM \end{pmatrix}_{bc} + \begin{pmatrix} xcos(\beta) \\ -xsin(\beta) \\ 0 \end{pmatrix} \wedge \begin{pmatrix} A \\ S \\ N \end{pmatrix}$$

$$\begin{pmatrix} AM \\ SM \\ NM \end{pmatrix}_{cm} = \begin{pmatrix} AM \\ SM \\ NM \end{pmatrix}_{bc} + \begin{pmatrix} -xNsin(\beta) \\ -xNcos(\beta) \\ xScos(\beta) + xAsin(\beta) \end{pmatrix}$$

Appendix 2

Test nomenclature and list of test cases

In this appendix, a non-exhaustive list of test cases are summarized. When performing a test, the wind-tunnel rotor spin rate is regulated to impose a wind speed which is measured by using a pressure sensor. The data acquisition results in **format txt files** containing either the mean values or all the samples. In most cases, in the corresponding database, data file names are chosen with respect to the following nomenclature.

1 Nomenclature

The nomenclature of the different tests is globally based on a set of different codes as follows:

- Type of test:
  - **PT:** Preparatory tests which were performed prior to the wind tunnel campaign to verify the proper functioning of the experience.
  - **CAL_TM**: Torquemeter Calibration tests.
  - **WRONG**: First tests done with wrong vane angle design (see 4.3.2).

- Layout of the mock-up:
  - **FULL**: All appendages installed, including SEPS + RAA + TPP + HASI booms.
  - **VANES**: With vanes. The vane angle is specified right behind. If not specified, the regular 2.8° set of vanes is used.
  - **BARE**: No vanes installed.

- Angle of attack:
  - **A--**: The letter A followed by a number gives the angle alpha for the current test.
  - **B--**: The letter B followed by a number gives the angle beta for the current test, if it is not specified, beta = 0°.

- Appendages used:
  - **SEPS**: 3 SEPS installed.
  - **RAA**: 4 RAA installed.
  - **TPP**: TPP installed.
  - **OO/OI/OC/IC/II/IO/CO/CI/CC**: If HASI booms are installed, 2 consecutive letters describe the position of each boom. The first letter corresponds to the B1 boom and the 2nd letter corresponds to the B2 boom.
    O stands for "**Open**" position, **I** for "**Intermediate**" position and **C** for "**Closed**" position.
  - **NSSP**: stands for "No SSP", meaning that SSP is not installed. If not specified, SSP is installed.

2 First test campaign (see reference R2)

During this first compaign, the mock-up was aligned with the wind direction in the main test section of the wind-tunnel, consequently with a sideslip angle of $\beta = 0°$. The reference position if for a spin angle of $\alpha = -4°$. If not, two spin angles were tested, -4°or -94° to have a configuration where the full deployed booms are either vertical or horizontal to the test section floor. The vanes available were those with an inclination of 6.8°.

2.1 Model with no appendages

The delivered 1:3 probe model is a bare mockup with no appendages and no vanes. The Surface Science Package (SSP) is equipped before any test, because this appendage is always present in the same configuration. Two sets of experiments were performed to measure the roll moment with and without the vanes with an inclination of 6.8°. For each of these tests, several Reynolds number have been chosen to determine if this latter has an influence on the flow characteristics. For each case, three different acquisition are repeated to verify the repeatability of measurement.

Test reference	**Model configuration**	**Wiind Tunnel Rotor spin rate**
Bare_model_1	Model as delivered + SSP	From 50 r.p.m to 450 r.p.m, with increment of 50 r.p.m
Bare_model_2	Model as delivered + SSP	
Bare_model_3	Model as delivered + SSP	
Vanes_model_1	Model with vanes + SSP	
Vanes_model_2	Model with vanes + SSP	
Vanes_model_3	Model with vanes + SSP	
Vanes_model_4	Model with vanes + SSP	

2.2 Influence of the appendages

Four types of appendages are tested during this campaign:

- Separation subsystems (3) - SEPS
- Radio-altimeter antennas (4) - RAA
- Temperature and pressure probe (1) - TPP
- HASI booms (2)

The HASI booms (named B1 and B2) have two possible positions (initially open or closed, later in the study intermediate) and are tested in four different configurations.

Test reference	**Model configuration**	**Wind Tunnel Rotor spin rate**
SEPS_1	Model with 3 SEPS	From 200 r.p.m to 450 r.p.m, with increment of 50 r.p.m
SEPS_2	Model with 3 SEPS	
SEPS_3	Model with 3 SEPS	
RAA_1	Model with 4 RAA	
RAA_2	Model with 4 RAA	
RAA_3	Model with 4 RAA	
RAA_4	Model with 4 RAA	
HASI_OO_1	Model with B1 and B2 open	
HASI_OO_2	Model with B1 and B2 open	
HASI_OO_3	Model with B1 and B2 open	

HASI_OC_1	Model with B1 open and B2 closed	
HASI_OC_2	Model with B1 open and B2 closed	
HASI_OC_3	Model with B1 open and B2 closed	
HASI_CO_1	Model with B1 closed and B2 open	
HASI_CO_2	Model with B1 closed and B2 open	
HASI_CO_3	Model with B1 closed and B2 open	
HASI_CC_1	Model with B1 and B2 closed	
HASI_CC_2	Model with B1 and B2 closed	
HASI_CC_3	Model with B1 and B2 closed	
TPP_1	Model with TPP	
TPP_2	Model with TPP	
TPP_3	Model with TPP	

Some tests were also conducted with appendage combinations:

Test reference	Model configuration	Wind Tunnel Rotor spin rate
SEPS_RAA_1	Model with 3 SEPS and 4 RAA	From 200 r.p.m to 450 r.p.m, with increment of 50 r.p.m
SEPS_RAA_2	Model with 3 SEPS and 4 RAA	
SEPS_RAA_3	Model with 3 SEPS and 4 RAA	
SEPS_RAA_TPP_1	Model with 3 SEPS, 4 RAA and TPP	
SEPS_RAA_TPP_2	Model with 3 SEPS, 4 RAA and TPP	
SEPS_RAA_TPP_3	Model with 3 SEPS, 4 RAA and TPP	

2.3 Tests with full mock-up

This part of the test campaign concerned the following configurations:

- Tests with all appendages and vanes, mock-up facing the flow
- Tests with all appendages and removed vanes, mock-up facing the flow

2.3.1 Vanes and all appendages

Two positions of the mock-up are tested with reference to the spin. If the test reference contains a “0 (zero)”, the mock-up position on the wind-tunnel is related to α = - 4°, both booms are quasi perpendicular to the floor, and if the test reference contains the letter “B”, the mock-up position corresponds to α = - 94°, both booms are quasi horizontal to the floor.

Test reference	Model configuration	Wind Tunnel Rotor spin rate
Full_CC_0.1	Full model with both booms closed	From 200 r.p.m to 450 r.p.m, with increment of 50 r.p.m
Full_CC_0.2	Full model with both booms closed	
Full_CC_0.3	Full model with both booms closed	
Full_OC_0.1	Full model with B1 open and B2 closed	

Full_OC_0.2	Full model with B1 open and B2 closed	
Full_OC_0.3	Full model with B1 open and B2 closed	
Full_CO_0.1	Full model with B1 closed and B2 open	
Full_CO_0.2	Full model with B1 closed and B2 open	
Full_CO_0.3	Full model with B1 closed and B2 open	
Full_OO_0.1	Full model with both booms open	
Full_OO_0.2	Full model with both booms open	
Full_OO_0.3	Full model with both booms open	

Test reference	**Model configuration**	**Wind Tunnel Rotor spin rate**
Full_CC_B.1	Full model with both booms closed	From 200 r.p.m to 450 r.p.m, with increment of 50 r.p.m
Full_CC_B.2	Full model with both booms closed	
Full_CC_B.3	Full model with both booms closed	
Full_CC_B.4	Full model with both booms closed	
Full_OC_B.1	Full model with B1 open and B2 closed	
Full_OC_B.2	Full model with B1 open and B2 closed	
Full_OC_B.3	Full model with B1 open and B2 closed	
Full_OC_B.4	Full model with B1 open and B2 closed	
Full_CO_B.1	Full model with B1 closed and B2 open	
Full_CO_B.2	Full model with B1 closed and B2 open	
Full_CO_B.3	Full model with B1 closed and B2 open	
Full_OO_B.1	Full model with both booms open	
Full_OO_B.2	Full model with both booms open	
Full_OO_B.3	Full model with both booms open	

2.3.2 All appendages and removed vanes, mock-up facing the flow

A few series of tests are performed with different numbers of vanes (all the other appendages being present), with the following names:

- A1: The four vanes in front of the RAA are removed
- A2: two thirds of the vanes
- A3: half of the vanes
- A4: There are no vanes on the model

Test reference	**Model configuration**	**Wind Tunnel Rotor spin rate**
Full_CC_A1.1	Full model with both booms closed	From 200 r.p.m to 450 r.p.m, with increment of 50 r.p.m
Full_CC_A1.2	Full model with both booms closed	
Full_CC_A1.3	Full model with both booms closed	
Full_OC_A1.1	Full model with B1 open and B2 closed	
Full_OC_A1.2	Full model with B1 open and B2 closed	

Full_OC_A1.3	Full model with B1 open and B2 closed	
Full_CO_A1.1	Full model with B1 closed and B2 open	
Full_CO_A1.2	Full model with B1 closed and B2 open	
Full_CO_A1.3	Full model with B1 closed and B2 open	
Full_OO_A1.1	Full model with both booms open	
Full_OO_A1.2	Full model with both booms open	
Full_OO_A1.3	Full model with both booms open	

Test reference	**Model configuration**	**Wind Tunnel Rotor spin rate**
Full_CC_A2.1	Full model with both booms closed	From 200 r.p.m to 450 r.p.m, with increment of 50 r.p.m
Full_OC_A2.1	Full model with B1 open and B2 closed	
Full_CO_A2.1	Full model with B1 closed and B2 open	
Full_OO_A2.1	Full model with both booms open	

Test reference	**Model configuration**	**Wind Tunnel Rotor spin rate**
Full_CC_A3.1	Full model with both booms closed	From 200 r.p.m to 450 r.p.m, with increment of 50 r.p.m
Full_OC_A3.1	Full model with B1 open and B2 closed	
Full_OC_A3.2	Full model with B1 open and B2 closed	
Full_OC_A3.3	Full model with B1 open and B2 closed	
Full_OC_A3.4	Full model with B1 open and B2 closed	
Full_OC_A3.5	Full model with B1 open and B2 closed	
Full_CO_A3.1	Full model with B1 closed and B2 open	
Full_CO_A3.2	Full model with B1 closed and B2 open	
Full_CO_A3.3	Full model with B1 closed and B2 open	
Full_OO_A3.1	Full model with both booms open	
Full_OO_A3.2	Full model with both booms open	
Full_OO_A3.3	Full model with both booms open	

Test reference	**Model configuration**	**Wind Tunnel Rotor spin rate**
Full_CC_A4.1	Full model with both booms closed	From 200 r.p.m to 450 r.p.m, with increment of 50 r.p.m
Full_CC_A4.2	Full model with both booms closed	
Full_CC_A4.3	Full model with both booms closed	
Full_OC_A4.1	Full model with B1 open and B2 closed	
Full_OC_A4.2	Full model with B1 open and B2 closed	
Full_OC_A4.3	Full model with B1 open and B2 closed	
Full_CO_A4.1	Full model with B1 closed and B2 open	
Full_CO_A4.2	Full model with B1 closed and B2 open	

Full_CO_A4.3	Full model with B1 closed and B2 open	
Full_OO_A4.1	Full model with both booms open	
Full_OO_A4.2	Full model with both booms open	
Full_OO_A4.3	Full model with both booms open	

2.4 Tests without vanes and not all appendages mounted

Series of tests were performed for a configuration of the mock-up with no vanes but with some appendages mounted on the mock-up.

Test reference	Model configuration	Wind Tunnel Rotor spin rate
HASI_OO_A4.1	Model with B1 and B2 open	
HASI_OO_ A4.2	Model with B1 and B2 open	
HASI_OO_ A4.3	Model with B1 and B2 open	
HASI_OC_ A4.1	Model with B1 open and B2 closed	
HASI_OC_ A4.2	Model with B1 open and B2 closed	
HASI_OC_ A4.3	Model with B1 open and B2 closed	
HASI_CO_ A4.1	Model with B1 closed and B2 open	
HASI_CO_ A4.2	Model with B1 closed and B2 open	
HASI_CO_ A4.3	Model with B1 closed and B2 open	
HASI_CC_ A4.1	Model with B1 and B2 closed	
HASI_CC_ A4.2	Model with B1 and B2 closed	
HASI_CC_ A4.3	Model with B1 and B2 closed	
SEPS_RAA_TPP_A4.1	Model with TPP	
SEPS_RAA_TPP_A4.2	Model with TPP	
SEPS_RAA_TPP_A4.3	Model with TPP	

3 Second test campaign (See reference R3)

For this second compaign, the main objective was to test the mock-up with a sideslip angle of attack. The vanes available were those with an inclination of 6.8°.

3.1 Influence of each appendages

Test reference	Model configuration
SEPS_A4	Bare mock-up with only the SEPS
RAA_A4	Bare mock-up with only the RAA
SEPS_RAA_A4	Bare mock-up with only the SEPS and the RAA
HASI_CC_A4	Bare mock-up with two booms closed
HASI_OO_A4	Bare mock-up with two booms open
HASI_CO_A4	Bare mock-up with boom 1 closed, boom 2 open
HASI_OC_A4	Bare mock-up with boom 1 open, boom 2 closed

SEPS_CC	Vane mock-up with two booms closed
SEPS_OO	Vane mock-up with two booms open
SEPS_CO	Vane mock-up with boom 1 closed, boom 2 open
SEPS_OC	Vane mock-up with boom 1 open, boom 2 closed
SEPS_RAA_CO	Vane mock-up with the SEPS, the RAA and boom 1 closed, boom 2 open
SEPS_RAA_OC	Vane mock-up with the SEPS, the RAA and boom 1 open, boom 2 closed

3.2 Bare mock-up and vane mock-up for different angle of attacks (β angles) and different positions of the camera DISR (α angles)

Test reference	Model configuration
DISR_A4_-4_0	Bare mock-up for α=-4º, β=0º
DISR_A4_-4_5	Bare mock-up for α=-4º, β=5º
DISR_A4_-4_10	Bare mock-up for α=-4º, β=10º
DISR_A4_-4_15	Bare mock-up for α=-4º, β=15º
DISR_A4_-4_-5	Bare mock-up for α=-4º, β=-5º
DISR_A4_-4_-10	Bare mock-up for α=-4º, β=-10º
DISR_A4_-4_-15	Bare mock-up for α=-4º, β=-15º
DISR_A4_-49_0	Bare mock-up for α=-49º, β=0º
DISR_A4_-49_5	Bare mock-up for α=-49º, β=5º
DISR_A4_-49_10	Bare mock-up for α=-49º, β=10º
DISR_A4_-49_15	Bare mock-up for α=-49º, β=15º
DISR_A4_-49_-5	Bare mock-up for α=-49º, β=-5º
DISR_A4_-49_-10	Bare mock-up for α=-49º, β=-10º
DISR_A4_-49_-15	Bare mock-up for α=-49º, β=-15º
DISR_A4_-94_0	Bare mock-up for α=-94º, β=0º
DISR_A4_-94_5	Bare mock-up for α=-94º, β=5º
DISR_A4_-94_10	Bare mock-up for α=-94º, β=10º
DISR_A4_-94_15	Bare mock-up for α=-94º, β=15º
DISR_A4_-94_-5	Bare mock-up for α=-94º, β=-5º
DISR_A4_-94_-10	Bare mock-up for α=-94º, β=-10º
DISR_A4_-94_-15	Bare mock-up for α=-94º, β=-15º
DISR_A4_-184_0	Bare mock-up for α=-184º, β=0º
DISR_A4_-184_5	Bare mock-up for α=-184º, β=5º
DISR_A4_-184_10	Bare mock-up for α=-184º, β=10º
DISR_A4_-184_15	Bare mock-up for α=-184º, β=15º
DISR_A4_-184_-5	Bare mock-up for α=-184º, β=-5º
DISR_A4_-184_-10	Bare mock-up for α=-184º, β=-10º
DISR_A4_-184_-15	Bare mock-up for α=-184º, β=-15º
DISR_-4_0	Vane mock-up for α=-4º, β=0º
DISR_-4_5	Vane mock-up for α=-4º, β=5º
DISR_-4_10	Vane mock-up for α=-4º, β=10º
DISR_-4_11	Vane mock-up for α=-4º, β=11º
DISR_-4_12	Vane mock-up for α=-4º, β=12º
DISR_-4_13	Vane mock-up for α=-4º, β=13º
DISR_-4_14	Vane mock-up for α=-4º, β=14º
DISR_-4_15	Vane mock-up for α=-4º, β=15º
DISR_-4_-5	Vane mock-up for α=-4º, β=-5º
DISR_-4_-10	Vane mock-up for α=-4º, β=-10º
DISR_-4_-11	Vane mock-up for α=-4º, β=-11º
DISR_-4_-12	Vane mock-up for α=-4º, β=-12º
DISR_-4_-13	Vane mock-up for α=-4º, β=-13º

DISR_-4_-14	Vane mock-up for α=-4º, β=-14º
DISR_-4_-15	Vane mock-up for α=-4º, β=-15º
DISR_-49_0	Vane mock-up for α=-49º, β=0º
DISR_-49_5	Vane mock-up for α=-49º, β=5º
DISR_-49_10	Vane mock-up for α=-49º, β=10º
DISR_-49_15	Vane mock-up for α=-49º, β=15º
DISR_-49_-5	Vane mock-up for α=-49º, β=-5º
DISR_-49_-10	Vane mock-up for α=-49º, β=-10º
DISR_-49_-15	Vane mock-up for α=-49º, β=-15º
DISR_-94_0	Vane mock-up for α=-94º, β=0º
DISR_-94_5	Vane mock-up for α=-94º, β=5º
DISR_-94_10	Vane mock-up for α=-94º, β=10º
DISR_-94_11	Vane mock-up for α=-94º, β=11º
DISR_-94_12	Vane mock-up for α=-94º, β=12º
DISR_-94_13	Vane mock-up for α=-94º, β=13º
DISR_-94_14	Vane mock-up for α=-94º, β=14º
DISR_-94_15	Vane mock-up for α=-94º, β=15º
DISR_-94_-5	Vane mock-up for α=-94º, β=-5º
DISR_-94_-10	Vane mock-up for α=-94º, β=-10º
DISR_-94_-11	Vane mock-up for α=-94º, β=-11º
DISR_-94_-12	Vane mock-up for α=-94º, β=-12º
DISR_-94_-13	Vane mock-up for α=-94º, β=-13º
DISR_-94_-14	Vane mock-up for α=-94º, β=-14º
DISR_-94_-15	Vane mock-up for α=-94º, β=-15º
DISR_-184_0	Vane mock-up for α=-184º, β=0º
DISR_-184_5	Vane mock-up for α=-184º, β=5º
DISR_-184_10	Vane mock-up for α=-184º, β=10º
DISR_-184_15	Vane mock-up for α=-184º, β=15º
DISR_-184_-5	Vane mock-up for α=-184º, β=-5º
DISR_-184_-10	Vane mock-up for α=-184º, β=-10º
DISR_-184_-15	Vane mock-up for α=-184º, β=-15º

3.3 Full mock-up deployed horizontally for different β angles and some complementary test for full mock-up deployed vertically for different β angles

Test reference	Model configuration
Full_OO_10	Full mock-up deployed vertically for β=10º
Full_OO_11	Full mock-up deployed vertically for β=11º
Full_OO_12	Full mock-up deployed vertically for β=12º
Full_OO_13	Full mock-up deployed vertically for β=13º
Full_OO_14	Full mock-up deployed vertically for β=14º
Full_OO_15	Full mock-up deployed vertically for β=15º
Full_OO_-5	Full mock-up deployed vertically for β=-5º
Full_OO_-10	Full mock-up deployed vertically for β=-10º
Full_OO_-11	Full mock-up deployed vertically for β=-11º
Full_OO_-12	Full mock-up deployed vertically for β=-12º
Full_OO_-13	Full mock-up deployed vertically for β=-13º
Full_OO_-14	Full mock-up deployed vertically for β=-14º
Full_OO_-15	Full mock-up deployed vertically for β=-15º
Full_OO_B0	Full mock-up deployed horizontally for β=0º
Full_OO_B5	Full mock-up deployed horizontally for β=5º
Full_OO_B10	Full mock-up deployed horizontally for β=10º
Full_OO_B11	Full mock-up deployed horizontally for β=11º
Full_OO_B12	Full mock-up deployed horizontally for β=12º
Full_OO_B13	Full mock-up deployed horizontally for β=13º

Full_OO_B14	Full mock-up deployed horizontally for β=14º
Full_OO_B15	Full mock-up deployed horizontally for β=15º
Full_OO_B-5	Full mock-up deployed horizontally for β=-5º
Full_OO_B-10	Full mock-up deployed horizontally for β=-10º
Full_OO_B-11	Full mock-up deployed horizontally for β=-11º
Full_OO_B-12	Full mock-up deployed horizontally for β=-12º
Full_OO_B-13	Full mock-up deployed horizontally for β=-13º
Full_OO_B-14	Full mock-up deployed horizontally for β=-14º
Full_OO_B-15	Full mock-up deployed horizontally for β=-15º

4 Third test campaign (see reference R4)

For this third compaign, the torquemeter and the vanes with two possible inclinations (2.2° and 2.8°) were available. Below is the guidelines for the tests that were conducted in this campaign.

Problematic	Tests	Results
Preliminary tests		
Are previous results repeatable?	Roll moment of each appendages	Study of the quality of previous year results
	Fully equipped model sideslip and angle of attack -4°	
	Bare model with sideslip and angle of attack -4°	
	Bare model with sideslip and angle of attack -184°	
What is the influence of the intermediate position of HASI booms	HASI booms positions (B1/B2) with vanes	Identify the influence of a not fully deployed HASI booms
	Fully equipped sideslip β = 15° to -15° and α = -49°	
	Fully equipped sideslip β = 15° to -15° Vertical (and α=-4°)	
	Fully equipped sideslip β = 15° to -15° Horizontal (and α=-94°)	
What is the influence of the upgrading of the mock-up?	SEPS cable tests with vanes	Characterization of the influence of upgrading on the roll moment
	Fully equipped vanes inclination + (B1/B2)	
	Bare model vanes inclination	
Supplementary tests	Wind tunnel symmetry test	
	Data gathering for other Huygens group	
	SM2 tests	

4.1 Preparatory tests

Before delivering results, some preparatory tests have been performed to verify the well-functioning of the wind tunnel and the calibration of measurement devices. Tests have also been performed on different configuration of appendages after calibrations to compare the measurements performed by the torquemeter and by the aerodynamic balance.

Test reference
PT_CAL_TM
PT_FULL_VANES_6.8_A-4_OO
PT_VANES_A-4
PT_VANES_A-4_SEPS_RAA
PT_VANES_6.8_A-4
PT_VANES_6.8_A-4_SEPS

4.2 Repeatability of previous results

Tests in this part have already been performed in the previous campaign. Besides giving more accurate torque data using the torquemeter, they gave us some data to compare with that of the previous campaigns.

4.2.1 Roll moment of each appendages

Test reference	Model configuration and Wind Tunnel rotor spin rate
VANES_A-4	With vanes from 200 to 400 rpm with increment of 100 rpm
VANES_A-4_SEPS	
VANES_A-4_TPP	
VANES_A-4_RAA	
VANES_A-4_SEPS_RAA	
VANES_A-4_SEPS_RAA_TPP	
FULL_A-4_OO	
FULL_A-4_IO	
FULL_A-4_IC	
FULL_A-4_CI	
FULL_A-4_OI	
FULL_A-4_OC	
FULL_A-4_CO	

Test reference	Model configuration and Wind Tunnel rotor spin rate
BARE_A-4_FULL_OO	Without vanes from 200 to 400 rpm with increment of 100 rpm
BARE_A-4_SEPS_RAA	
BARE_A-4_RAA	
BARE_A-4_SEPS	
BARE_A-4_TPP	
BARE_A-4_OO	

BARE_A-4_CO	
BARE_A-4_OC	
BARE_A-4_CC	
BARE_A-4	
BARE_A-4_IO	
BARE_A-4_IC	
BARE_A-4_OI	
BARE_A-4_CI	

4.2.2 Fully equipped model sideslip and angle of attack -4°

The objective was to look for any influence of the appendages with high sideslip angles

Test reference	Model configuration
FULL_A-4_B-15_OO	Full model with sideslip angle from -15° to -10° with increment of 1°, -5°, 0°, 5, and from 10° to 15° with increment of 1°. HASI booms are open.
FULL_A-4_B-14_OO	
FULL_A-4_B-13_OO	
FULL_A-4_B-12_OO	
FULL_A-4_B-11_OO	
FULL_A-4_B-10_OO	
FULL_A-4_B-5_OO	
FULL_A-4_B0_OO	
FULL_A-4_B5_OO	
FULL_A-4_B10_OO	
FULL_A-4_B11_OO	
FULL_A-4_B12_OO	
FULL_A-4_B13_OO	
FULL_A-4_B14_OO	
FULL_A-4_B15_OO	

4.2.3 Bare model with sideslip and angle of attack -4°

The objective was to study the influence of the position of the DISR camera at $\alpha = -4°$.

Test reference	Model configuration
BARE_A-4_B-15	Bare model with sideslip angles from -15° to 15° with increment of 5°
BARE_A-4_B-10	
BARE_A-4_B-5	
BARE_A-4_B0	
BARE_A-4_B5	
BARE_A-4_B10	
BARE_A-4_B15	

4.2.4 Bare model with sideslip and angle of attack -184°

The objective was to study the influence of the position of the DISR camera at α = -184°.

Test reference	Model configuration
BARE_A-184_B15	Bare model with sideslip angles from -15° to 15° with increment of 5°
BARE_A-184_B10	
BARE_A-184_B5	
BARE_A-184_B-5	
BARE_A-184_B-10	
BARE_A-184_B-15	

4.3 Study of the influence of the intermediate position of HASI booms

We tested in this section the influence of the intermediate position of HASI booms compared to open and closed positions.

4.3.1 HASI booms positions (B1/B2) with vanes

The objective of the following tests was to study the behaviour of different HASI booms positions with vanes.

Test reference	Model configuration and Wind Tunnel rotor spin rate
VANES_A-4_CC	Vanes model from 200 to 400 rpm with increment of 100 rpm
VANES_A-4_CO	
VANES_A-4_OO	
VANES_A-4_OC	
VANES_A-4_OI	
VANES_A-4_CI	
VANES_A-4_II	
VANES_A-4_IC	
VANES_A-4_IO	

4.3.2 Fully equipped sideslip β = 15° to -15° Vertical (and α=-4°)

The following tests were done with full configuration and different sideslip angles at α = -4°.

Test reference	Model configuration and Wind Tunnel rotor spin rate
FULL_A-4_B10_CI	Full model at with sideslip angle increments of 5° between -15° and 10° at 200, 300 and 400 rpm.
FULL_A-4_B5_CI	
FULL_A-4_B-5_CI	
FULL_A-4_B-10_CI	
FULL_A-4_B-15_CI	
FULL_A-4_B-15_OI	
FULL_A-4_B-10_OI	
FULL_A-4_B-5_OI	
FULL_A-4_B5_OI	
FULL_A-4_B10_OI	
FULL_A-4_B10_IO	
FULL_A-4_B5_IO	
FULL_A-4_B-5_IO	
FULL_A-4_B-10_IO	
FULL_A-4_B-15_IO	
FULL_A-4_B-15_IC	
FULL_A-4_B-10_IC	
FULL_A-4_B-5_IC	
FULL_A-4_B5_IC	
FULL_A-4_B10_IC	

Test reference	Model configuration and Wind Tunnel rotor spin rate
FULL_A-4_B15_OC	Full model with sideslip angle of 15° from 200 to 400 rpm with increment of 100 rpm.
FULL_A-4_B15_CO	
FULL_A-4_B15_IO	
FULL_A-4_B15_IC	
FULL_A-4_B15_II	
FULL_A-4_B15_CI	
FULL_A-4_B15_OI	

4.3.3 Fully equipped sideslip β = 15° to -15° Horizontal (and α=-94°)

The following tests were performed with full configuration and different sideslip angles at α = -94°.

Test reference	Model configuration and Wind Tunnel rotor spin rate
FULL_A-94_B10_IC	Full model with sideslip angle increments of 5° between -15° and 10° at 200, 300 and 400 rpm.
FULL_A-94_B15_IC	
FULL_A-94_B5_IC	
FULL_A-94_B0_IC	
FULL_A-94_B-5_IC	
FULL_A-94_B-10_IC	
FULL_A-94_B-15_IC	
FULL_A-94_B-15_IO	
FULL_A-94_B-10_IO	
FULL_A-94_B-5_IO	
FULL_A-94_B0_IO	
FULL_A-94_B5_IO	
FULL_A-94_B10_IO	
FULL_A-94_B15_IO	
FULL_A-94_B15_OI	
FULL_A-94_B10_OI	
FULL_A-94_B5_OI	
FULL_A-94_B0_OI	
FULL_A-94_B-5_OI	
FULL_A-94_B-10_OI	
FULL_A-94_B-15_OI	
FULL_A-94_B-15_CI	
FULL_A-94_B-10_CI	
FULL_A-94_B-5_CI	
FULL_A-94_B0_CI	
FULL_A-94_B5_CI	
FULL_A-94_B10_CI	
FULL_A-94_B15_CI	

4.4 Influence of the upgrading of the mock-up

4.4.1 Bare model vane inclination

Some tests were done to compare the effect of different sets of vanes to study their influence on the roll moment. Note that preparatory tests with 6.8° vanes have been retained for the consistency of the results.

Test reference	Model configuration
VANES_0_A-4	Vanes model and full model with 0° vanes
FULL_VANES_0_A-4_OO	

4.5 Supplementary tests

4.5.1 Wind tunnel symmetry test

After quickly post processing some results during the wind tunnel campaign, it was noticed that the bare model seemed to have a negative roll on his own. Thus, it was decided to check the aerodynamic zero of the wind tunnel. The mock-up without the SSP hole in front and covered the holes instead with scotch (NSSP) was also tested.

Test reference	Model configuration and rotor spin rate
BARE_A-86_B-10	Bare model with sideslip angles at -10°, -6° and 10° and from -5° to 5° with increment of 1° at 300 rpm
BARE_A-86_B-6	
BARE_A-86_B-5	
BARE_A-86_B-4	
BARE_A-86_B-3	
BARE_A-86_B-2	
BARE_A-86_B-1	
BARE_A-86_B0	
BARE_A-86_B1	
BARE_A-86_B2	
BARE_A-86_B3	
BARE_A-86_B4	
BARE_A-86_B5	
BARE_A-86_B10	
BARE_A-86_NSSP	
BARE_A-4_NSSP	
BARE_A-184	

4.5.2 Data collected by the student modelling group

The following tests have been requested by the modelling group aimed at studying numerically the descent of the Huygens probe to validate their model.

Test reference	Model configuration and rotor spin rate
VANES_22_A-4_B-15	Vanes model with sideslip angle increments of 5° between -15° and 15° at 300 and 400 rpm
VANES_22_A-4_B-10	
VANES_22_A-4_B-5	
VANES_22_A-4_B0	
VANES_22_A-4_B5	
VANES_22_A-4_B10	
VANES_22_A-4_B15	
VANES_22_A-94_B-15	
VANES_22_A-94_B-10	
VANES_22_A-94_B-5	
VANES_22_A-94_B0	
VANES_22_A-94_B5	
VANES_22_A-94_B10	
VANES_22_A-94_B15	

Test reference	Model configuration and rotor spin rate
VANES_22_A-4_B-15	Vanes model with sideslip angle increments of 5° between -15° and 15° at 300 and 400 rpm
VANES_22_A-4_B-10	
VANES_22_A-4_B-5	
VANES_22_A-4_B0	
VANES_22_A-4_B5	
VANES_22_A-4_B10	
VANES_22_A-4_B15	
VANES_22_A-94_B-15	
VANES_22_A-94_B-10	
VANES_22_A-94_B-5	
VANES_22_A-94_B0	
VANES_22_A-94_B5	
VANES_22_A-94_B10	
VANES_22_A-94_B15	

4.5.3 Test with the SM2 configuration of the Mock-up.

Some new tests have been introduced at the end of the wind tunnel campaign to reproduce the configuration of the SM2 configuration of the Huygens probe, but with the HASI booms added. The idea behind these new tests was to study the behaviour of our model in this configuration and compare our results with those from the SM2 study at VKI.

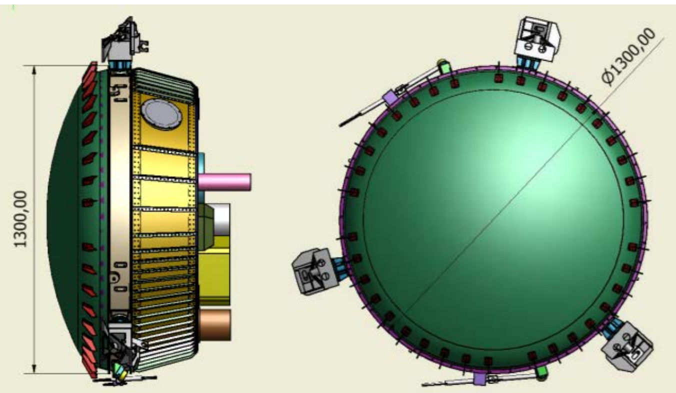

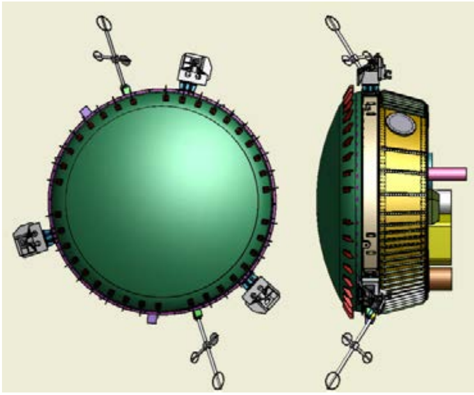

The configuration for the SM2 mock-up configuration uses HASI booms and SEPS. RAA and TPP are not used. However, the DISR camera is also absent from SM2 but we could not separate it from our model. The vanes used for the SM2 probe are angled at 2.2°. Thus, a new set of vanes has been 3D-printed specifically for these tests..

Test reference	Model configuration
SM2_A-4	SM2 configuration at 300 and 400 rpm

5 Fourth test campaign (see reference R6)

This last test campaign concerns PIV measurement. The mock-up was aligned with the wind direction in the main test section of the wind-tunnel, consequently with a sideslip angle of $\beta = 0°$. The mock-up was adjusted around its axis (sipning angle) in function of the desired PIV measuring plane.

TYPE	MODEL	APPENDAGES	FILE NAME
STEREO	VANES	BARE	SPIV_VANES_BARE
		DISR	SPIV_VANES_DISR
		HASI	SPIV_VANES_HASI
		RAA	SPIV_VANES_RAA
		SEPS	SPIV_VANES_SEPS
		SEPS+RAA 1	SPIV_VANES_SEPS_RAA_1
		SEPS+RAA 2	SPIV_VANES_SEPS_RAA_2
		SEPS+RAA 2 with hole	SPIV_VANES_SEPS_RAA_2_HOLE
	BARE	BARE	SPIV_BARE_BARE
		DISR	SPIV_BARE_DISR
		SEPS	SPIV_BARE_SEPS
		SEPS+RAA 1	SPIV_BARE_SEPS_RAA_1
		SEPS+RAA 2	SPIV_BARE_SEPS_RAA_2
		SEPS+RAA 2 with hole	SPIV_BARE_SEPS_RAA_2_HOLE
2D	VANES	COUPOLLE	2D_VANES_BARE
		COUPOLLE HOLE	2D_VANES_BARE_HOLE
		DISR	2D_VANES_DISR
		HASI	2D_VANES_HASI
		RAA	2D_VANES_RAA
		SEPS	2D_VANES_SEPS
		SIDE SEPS	2D_VANES_SIDE_SEPS
		SEPS+RAA 1	2D_VANES_SEPS_RAA_1
		SEPS+RAA 2	2D_VANES_SEPS_RAA_2
	BARE	BARE	2D_BARE_BARE

Appendix 3

Huygens probe drag coefficient from AEROSPATIALE (1992)

TABLE n° 4

HUYGENS DESCENT MODULE (nominal real shape)

with 36 spin vanes, 3 SEPS fittings, and 4 radar antennas

dispersion of CA, CN and Cm against Reynolds number

Reynolds number	ΔCA/CA	ΔCN/CN	ΔCm/Cm
4.00e+04	- 15 %/ + 25 %	- 15 % /+ 15 %	- 30 %/+ 30 %
2.00e+05	- 15%/+ 25 %	- 15 %/+ 15 %	- 30 %/+ 30 %
2.00e+05	- 15 %/+ 15 %	- 15 %/+ 15 %	- 30 %/+ 30 %
1.00e+06	- 15 %/+ 15 %	- 15 %/+ 15 %	- 30 %/+ 30 %
1.50e+06	- 13 %/+ 15 %	- 15 %/+ 15 %	- 30 %/+ 30 %
2.00e+06	- 10 %/+ 15 %	- 15 %/+ 15 %	- 30 %/+ 30 %
5.00e+06	- 10 %/+ 15 %	- 15 %/+ 15 %	- 30 %/+ 30 %

Lref = 1.304 m   Sref = π . (Lref/2)²

Values of CD at zero angle of attack

Reynolds number	cd min	CD	CD max
4.0e04	0.730	0.86200	1.075
1.0e05	0.730	0.86200	1.075
1.5e05	0.725	0.85400	1.075
2.0e05	0.720	0.84600	1.075
2.0e05	0.720	0.84600	0.960
2.6e05	0.713	0.839	0.950
5.0e05	0.685	0.810	0.930
8.0e05	0.665	0.784	0.900
1.0e06	0.660	0.780	0.900
1.3e06	0.670	0.782	0.900
1.6e06	0.696	0.786	0.900
1.8e06	0.700	0.790	0.905
2.0e06	0.710	0.791	0.910
5.0e06	0.720	0.800	0.920

Appendix 4

Comparison between VORTICITY Ltd and selected PRISME test cases

In this appendix we compare the results of a selection of tests performed by PRISME and a selection of those performed by VORTICITY Ltd. The Vorticity tests focussed on the effects of the HASI booms, and the RAA were never mounted. Furthermore, the SEPS configuration, for about half of the Vorticity tests performed, were not identical to their flight configuration as a so-called “blue piece”, a non-flight item, was mounted. Although the “blue pieces” have a significant effect, tests performed with the blue piece still inform about the boom effects. Several Vorticity tests were performed with the SEPS removed. They allow comparing vanes only effects.

In both studies a positive torque (as the one produced by the vanes) creates an anti-clockwise (a-c/w) rotation, while a negative torque creates a clockwise (c/w) rotation. Configurations with both HASI booms open (OO) or closed (CC) and either closed or open (CO and OC) are studied. The boom identifications are different for both studies. In our study we call them B1 (which produces a negative torque) and B2 (which produces a positive torque). In the Vorticity study they are called HASI-B1-PRO, (equivalent to our B2), and HASI-B2-CON, (equivalent to our B1).

Case 1	**PRISME** **Vanes at 2.8°**	**VORTICITY** **SM2 2.2° vanes**	
Test	Vanes_OO	Test1	Test2
AoA (º)	0	0	3
CoG (mm)	0	0	0
Booms	B1:Open; B2:Open	HASI-1-PRO:Open; HASI-2-CON:Open	
Speed (m/s)	40	40	40
Configuration	Full mock-up (Vanes, SEPS, RAA, HASI booms deployed vertically)	HASI, SEPS with the Blue pieces	HASI, SEPS with the Blue pieces
Spin direction (Roll Coeff)	a-c/w (Positive torque: +0.0028);	a-c/w (Alpha=0.95) Positive torque	a-c/w (Alpha=1.1) Positive torque
Remarks	Fig 4.18 (OO orange bar). Vanes control the torque	Table 30 (Vorticity report). Effect of SEPS with blue piece uncertain (but most likely small). Vanes positive torque predominent; No measurable boom effect.	

Case 2	**PRISME** **Vanes at 2.8°**	**VORTICITY** **SM2 2.2° vanes**
Test	Vanes_CC	Test7
AoA (º)	0	0
CoG (mm)	0	0
Booms	B1:Open; B2:Open	HASI-1-PRO:Open; HASI-2-CON:Open
Speed (m/s)	40	40
Configuration	Vanes mock-up, HASI booms closed	SEPS with the Blue pieces, both HASI booms closed
Spin direction (Roll Coeff)	a-c/w (Positive torque: +0.0025);	a-c/w (Alpha=0.95) Positive torque
Remarks	Fig 4.18 (CC orange bar). Vanes control the torque	Table 30 (Vorticity report). Effect of SEPS with blue piece uncertain (but most likely small). Vanes positive torque predominent; No measurable boom effect.

Case 3	PRISME Vanes at 2.8°		VORTICITY SM2 2.2° vanes		
Test	Vanes_OC	Vanes CO	Test3	Test4	Test6
AoA (º)	0		3	3	6
CoG (mm)	0		0	0	0
Speed (m/s)	B1:Open; B2:Closed	B1:Closed; B2:Open	HASI-1-PRO:Open; HASI-2-CON:Closed		
Speed (m/s)	40		40	40	40
Configuration	Vane mock-up with HASI booms		HASI booms, SEPS with blue pieces		
Spin direction	c/w (Small negative torque: -0.0002)	a-c/w. Positive torque (0.005)	No rotation	No rotation	No rotation
Remarks	Fig 4.18 (OC, orange bar). Vane torque almost compensated by negative B1 torque.	Fig 4.18 CO. Positive B2 torque added to vane torque.	SEPS with blue piece effect small. Vanes effect countered by HASI-2-CON negative torque No significant effect of AA. Case compares well with PRISME OC configuration. Boom notation uncertain.		

Comparison case 2 and case 3: Each boom is creating an opposite torque of similar magnitude and of similar magnitude to that created by the vanes. When only the boom that creates a positive torque is open, the torque is doubled compared to that created by the vanes alone. When the other boom is open the boom torque compensates that of the vanes.

Case 4	PRISME Vanes at 2.8°		VORTICITY SM2 2.2° vanes
Test	Vanes_OC	Vanes CO	Test5
AoA (º)	0		3
CoG (mm)	0		0
Booms	B1:Open; B2:Closed	B1:Closed; B2:Open	HASI-1-PRO:Closed; HASI-2-CON:Open
Speed (m/s)	40		40
Configuration	Vane mock-up with HASI booms		HASI booms, SEPS with blue pieces
Spin direction	a-c/w (Small negative torque: -0.0002)	a-c/w. Positive torque (0.005)	a-c/w
Remarks	Fig 4.18 (OC, orange bar). Vane torque compensated by negative B1 torque.	Fig 4.18 CO. Positive B2 torque added to vane torque.	SEPS with blue piece effect small. HASI-1-PRO boom torque adds to Vanes torque. Case compares well with PRISME Vane CO configuration..

<table>
<tr><th>Case 5</th><th>PRISME
Vanes at 2.8°</th><th colspan="2">VORTICITY
SM2 2.2° vanes</th></tr>
<tr><td>Test</td><td>HASI_CC</td><td colspan="2">Test 8, Test 10</td></tr>
<tr><td>AoA (º)</td><td>0</td><td colspan="2">0</td></tr>
<tr><td>CoG (mm)</td><td>0</td><td>0</td><td>0.6</td></tr>
<tr><td>Booms</td><td>B1:Closed; B2:Closed</td><td colspan="2">HASI-2-CON:Closed; HASI-1-PRO:Closed</td></tr>
<tr><td>Speed (m/s)</td><td>40</td><td colspan="2">40</td></tr>
<tr><td>Configuration</td><td>Vanes mock-up with only HASI booms</td><td colspan="2">Vanes, No SEPS, HASI booms</td></tr>
<tr><td>Spin direction</td><td>a-c/w (+0.0025)</td><td>a-c/w (Alpha i=+1.1)</td><td>a-c/w (Alpha i=+1.1)</td></tr>
<tr><td>Remarks</td><td>Fig 4.18 (CC, Orange bar). Positive torque due to vanes. No significant torque applied by both booms closed.</td><td colspan="2">Positive torque due to vanes. No significant torque applied by both booms closed.

No noticeable effect due to CoG shift</td></tr>
<tr><td></td><td colspan="3">The vanes provide (qualitatively) the required positive torque. Confirms vane design. Quantitative comparison not possible..

The SEPS torque compensates the SM2 2.2° vane torque, but not quite the 2.8° vane torque. Very consistent finding. The 3 SEPS induce a negative torque of similar magnitude to that of the vanes. Both boom closed do not provide a torque.</td></tr>
</table>

Case 6	PRISME Vanes at 2.8°	VORTICITY SM2 2.2° vanes
Test	VANES+SEPS (Fig 4.14) FULL_CC (Fig 4.18)	Test13
AoA (º)	0	0
CoG (mm)	0	0.6
Booms	B1:Closed; B2:Closed	HASI-2-CON:Closed; HASI-1-PRO:Closed
Speed (m/s)	40	40
Configuration	Vanes + SEPS (no boom) Full CC (booms closed)	Vanes, SEPS (no blue pieces), HASI booms,
Spin direction	a-c/w (+0.0002). Small positive torque c/w (-0.0015). Negative torque	No rotation
Remarks	Assuming that the CC booms do not create a torque. SEPS negative torque compensates entirely the 2.8° vane positive torque. Addition of RAA, creates an additional negative torque.	Negative SEPS torque compensates 2.2° vane positive torque Absence of RAA does not allow a direct comparison with PRISME result.
	The SEPS torque compensates the SM2 2.2° vane torque, but not quite the 2.8° vane torque. Very consistent finding. The 3 SEPS induce a negative torque of similar magnitude to that of the vanes. Both booms closed do not create a torque.	

Case 7	PRISME Vanes at 2.8°	VORTICITY SM2 2.2° vanes
Test	VANES+SEPS (Fig 4.14) FULL_OO (Fig 4.18)	Test14
AoA (º)	0	0
CoG (mm)	0	0.6
Booms	B1:Open; B2:Open	HASI-2-CON:Open; HASI-1-PRO:Open
Speed (m/s)	40	40
Configuration	Vanes + SEPS (no boom) Full OO (booms open)	Vanes, SEPS (no blue pieces), HASI booms,
Spin direction	a-c/w (+0.0002). Small positive torque c/w (+0.0021). Negative torque	No rotation
Remarks	Assuming that the OO booms do not create a torque. SEPS negative torque compensates entirely the 2.8° vane positive torque. Addition of RAA, creates an additional negative torque.	Negative SEPS torque compensates 2.2° vane positive torque No boom effect when both open Absence of RAA does not allow a direct comparison with PRISME result.

Case 8	PRISME Vanes at 2.8°	VORTICITY SM2 2.2° vanes	
Test	Vanes OC, Vanes CO	Test9	Test 11
AoA (º)	0	0	
CoG (mm)	0	0	6
Booms	B1:Closed B2:Open B1:Closed B2:Open	HASI-1-PRO:Open;HASI-2-CON:Closed;	
Speed (m/s)	40	40	
Configuration	Vanes mock-up with only HASI booms	Vanes, No SEPS, HASI booms	
Spin direction	(Fig 4.18 orange bar OC) : No significant torque (-0.0001). (Fig. 4.18 orange bar: c/w (+0.005)	a-c/w (Alpha i=-0.83)	No rotation (Alpha i=0)
Remarks	Figure 4.18, (OC, Orange bar). Small negative torque due to B1 open. Figure 4.18 (CO, Orange bar). Large positive torque due to B2 open torque on top of vanes torque.	Results show significant effects of CoG shift. Uncertainty in boom configuration. Hard to interpret.	

Appendix 5

Wind tunnel tests for the Separation mechanisms (SEPS) full scale model

This appendix presents the results of a wind tunnel test for the SEPS full scale model which was performed in 2013 at the PRISME Laboratory. The main objective was to measure aerodynamic forces and moments using the aerodynamic balance available under the main test section for stable and no sideslip incoming wind conditions.

The pictures below show the test set-up in the wind tunnel (left with, right without support plate). Let's recall that the positive rotation induced by the vanes is counter-clockwise as seen in the flow direction. The aerodynamic frame in which the aerodynamic loads are measured is indicated. Tests were performed with and without the SEPS support plate and have shown the same trends, albeit values are lower without than with the support plate. In the bottom figure, the measured aerodynamic loads are plotted against the wind velocity for both test configurations. It can be observed that the roll moment is negative (purple curve) meaning that the SEPS induces a torque opposite to the one induced by the vanes.

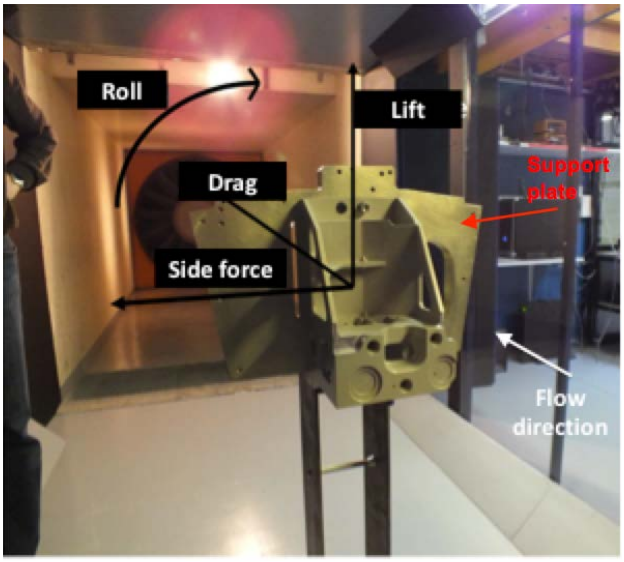

Set-up without the support plate